INFORMATION TO USERS

This manuscript has been reproduced from the microfilm master. UMI films the text directly from the original or copy submitted. Thus, some thesis and dissertation copies are in typewriter face, while others may be from any type of computer printer.

The quality of this reproduction is dependent upon the quality of the copy submitted. Broken or indistinct print, colored or poor quality illustrations and photographs, print bleedthrough, substandard margins, and improper alignment can adversely affect reproduction.

In the unlikely event that the author did not send UMI a complete manuscript and there are missing pages, these will be noted. Also, if unauthorized copyright material had to be removed, a note will indicate the deletion.

Oversize materials (e.g., maps, drawings, charts) are reproduced by sectioning the original, beginning at the upper left-hand corner and continuing from left to right in equal sections with small overlaps.

Photographs included in the original manuscript have been reproduced xerographically in this copy. Higher quality 6" x 9" black and white photographic prints are available for any photographs or illustrations appearing in this copy for an additional charge. Contact UMI directly to order.

ProQuest Information and Learning
300 North Zeeb Road, Ann Arbor, MI 48106-1346 USA
800-521-0600

MEASURING THE SURFACE DILATATIONAL VISCOSITIES OF SURFACTANT MONOLAYERS AT THE AIR-WATER INTERFACE BY THE SHAPE ANALYSIS OF DEFORMING PENDANT DROPS

by

JOSE LORENZO

A dissertation submitted to the Graduate Faculty in Engineering in partial fulfillment of the requirements for the degree of Doctor of Philosophy, The City University of New York

2001

This manuscript has been read and accepted for the Graduate Faculty in Engineering in satisfaction of the dissertation requirement for the degree of Doctor of Philosophy.

5/14/2001
Date

Alexander Couzis
Professor Alexander Couzis
Chair of Examining Committee

5/14/2001
Date

Charles Maldarelli
Professor Charles Maldarelli
Co-Chair of Examining Committee

5-14-2001
Date

Mumtaz K. Kassir
Professor Mumtaz Kassir
Executive Officer

Dr. Lane Gilchrist
Dr. Demetrius Papageorgiou
Dr. Gabriel Tardos
Supervisory Committee

THE CITY UNIVERSITY OF NEW YORK

Abstract

MEASURING THE SURFACE DILATATIONAL VISCOSITIES OF SURFACTANT MONOLAYERS AT THE AIR-WATER INTERFACE BY THE SHAPE ANALYSIS OF DEFORMING PENDANT DROPS

by

Jose Lorenzo

Advisors: Professor Alexander Couzis and Professor Charles Maldarelli

At rest, a surfactant fluid interface is under a state of isotropic stress that is given by the compositional surface tension as a function of the surfactant surface concentration. When the surfactant fluid interface is set in motion, surface flow can induce surfactant interactions and generate interfacial stresses apart from the compositional surface tension. A surface flow can be surface shear, dilatational, or shear-dilatational. The Boussinesq-Scriven constitutive equation completely characterized by the compositional surface tension and surface shear and dilatational viscosities is the simplest relationship between the surface strain rate and surface stress. Compositional surface tension and shear viscosity measurements are very well established. On the other hand, surface dilatational viscosity measurements are difficult because a flow which changes the surface area also changes the surface concentration creating changes in the equilibrium interfacial tension that must be also taken into account.

In this research, we investigate how Langmuir surfactant monolayers subjected to a dilatational strain rate behave and focus on developing a new technique for measuring their surface dilatational viscosities. To fulfill our research goals, we built a pendant drop apparatus with a fast motion analyzer to deform and video record a pendant water drop

with a surfactant monolayer at the air-water interface, developed a hydrodynamic surfactant model to obtain the surface dilatational viscosity from the recorded images, and measured the surface dilatational viscosities employing constant as well as sinusoidal volumetric flow rates. We also developed a correction that allows us to partially account for bulk hydrodynamic effects for pendant drops oscillating at high frequencies. We measured that the surface dilatational viscosity of the expanded phase of the phospholipid L-α-dipalmitoyl phosphatidylcholine (DPPC) is approximately 1.3 mNs/m from the compression experiments and 2.3 mNs/m at 0.2 Hz and 0.8 mNs/m at 1 Hz. We also measured from the oscillatory experiments that the surface dilatational viscosity of tripalmitin is 1.0 mNs/m at 1 Hz. In addition, we measured the surface viscoelasticities of mixed binary monolayers of DPPC and octadecanol in mole ratios 1:1 and 3:1 and found that the surface viscoelasticities of DPPC are twice with the addition of octadecanol.

Acknowledgements

I highly value the support and love to share knowledge of my mentors, Profs. Alexander Couzis and Charles Maldarelli, their energy and time made this learning experience possible. They have the ability to teach to anyone a difficult subject easily. I want to thank for helping supervising my doctoral dissertation Profs. Gilchrist, Papageorgiou, and Tardos. I also want to thank Profs. Acrivos and Weinstein. I have learned a lot from the chemical engineering faculty of CCNY and to a great extent I owe them my chemical engineering education. I would like to thank Mary Wright, Andy Eng, and Zhen Xu.

The financial support from CASI, NYC Louis Stokes Alliance (LSAMP) (NSF-9703600), Pfitzer, and NASA (NAG-3-2167) permitted us to fully concentrate on developing and implementing some good ideas during the course of this work. Finally, I want to thank my family, the PRESS office, and the other graduate students in our group especially the following friends for always showing interest in my work Rajeev Subramanyam, Ravichandra Palaparthi, and Nitin Kumar.

Table of Contents

List of Tables

List of Figures

and 2.7 % change in area: experimental and fitted (A) areas versus time and (B) compositional-dilatational surface tensions versus time.

Chapter 1

Introduction

1.1 Boussinesq-Scriven Surface Dilatational Viscosity of a Surfactant Monolayer

When a liquid interface with a surfactant monolayer is a rest, the interfacial stress is isotropic and given by the compositional interfacial tension as a function of the surfactant surface concentration. When this surfactant fluid interface is set in motion, interfacial flow can induce surfactant interactions and generate interfacial viscous stresses apart from the compositional interfacial tension. The Boussinesq-Scriven constitutive equation is the simplest and most commonly used relationship between the surface stress and surface strain rate. The Boussinesq-Scriven surface stress consists of an isotropic term (the sum of the compositional surface tension and the product of the surface dilatational viscosity and surface dilatational strain rate), and a shear term (the product of the surface shear viscosity and surface shear strain rate)[1]. Fig. 1.1 shows a surface shear flow and a surface dilatational flow. The surface viscosities also depend on the surfactant surface concentration and vanish as the surfactant surface concentration approaches zero. Measuring the interfacial shear viscosity is easy since an interfacial shear flow can be setup without changing the interfacial surfactant concentration. On the other hand, measuring the interfacial dilatational viscosity is difficult because an interfacial dilatational flow always changes the interfacial surfactant concentration creating changes in the interfacial compositional tension that must be also taken into account.

The surface shear rheological techniques currently available are very well established, provide useful information about the phases of surfactant monolayers and their transitions, and constitute the subject of several extensive review articles found elsewhere[2-6]. The surface shear viscosities at low surfactant surface concentrations are very low to be measured whereas the surface shear viscosities at intermediate surfactant surface concentrations are larger and measurable, of the order of 1 μNs/m for the long-chain saturated fatty acids[7-9]. Interestingly, surface shear viscosity studies revealed that alcohols form highly ordered phases, emulsions become more stable as their shear viscosities increase, and small chain alcohols considerably increase the surface shear viscosities of surfactant solutions[10-13].

To understand how the surface viscosities depend on the surfactant surface concentration, it is mandatory to describe the phases of a simple surfactant monolayer. The phases of a surfactant monolayer are established using the thermodynamic phase rule and measurements of surface tension versus area per molecule performed using a Langmuir trough surface balance. The surfactant phase behavior is governed by the intermolecular interactions in the monolayer; the van der Waals attractive or cohesive forces among the hydrocarbon chains composing the non-polar part and the repulsive interactions such as dipolar and electrostatic forces among the polar head. These phases are observed directly using several techniques based on the nature and propagation of light such as x-ray diffraction, Brewster angle microscopy, and fluorescence microscopy[14,15]. Fig. 1.2 illustrates the microscopic differences among the phases of a Langmuir monolayer

as a function of surface pressure (the difference between the clean liquid surface tension and the compositional surface tension) versus area per molecule. The surface tension decreases as the surfactant surface concentration increases within a phase, remains constant as the surfactant surface concentration changes during a first order phase transition, and shows a kink as a function of area per molecule during a second order phase transition. Monolayers exist at high area per molecules in a gaseous (G) state in which the surfactants are floating at the interface very far apart experiencing minimal forces among them. At intermediate area per molecules monolayers exist in an amorphous loosely cohered liquid expanded (LE) state characterized by random orientations of the hydrophobic chains with only the polar functional groups on the polar subphase. At lower area per molecules monolayers exist in a liquid condensed (LC) state, and at the lowest area per molecule in a liquid solid (LS) state. In the LC state the hydrophobic chains are tilted slightly with respect to the surface normal whereas in the LS state molecules are arranged in a two dimensional crystalline structure.

1.2 Research Scope

Interfacial dilatational rheology has many scientific and practical applications, as we briefly discussed in Section 1.3. The objectives of this study are to investigate how surfactant monolayers behave depending on applied area strain rates and to develop a new technique for measuring the surface dilatational viscosity by adding new technology to the classical pendant drop apparatus, convenient for performing studies requiring small amounts of surfactants. From the same research group and for the same surfactant

system, surface dilatational viscosities measured using spatially damped surface waves and rapidly expanding bubbles differ by five orders of magnitude, as shown in Table 2.1. Unfortunately the only two commercially available instruments for measuring the surface dilatational viscosity, the surface invasive version of the longitudinal wave technique and the pressure transducer bubble oscillating technique, have severe limitations as described in Chapter 2. Many studies of soluble surfactants capable of forming only the G and LE phases explain wave damping in terms of a diffusion mass transfer and monolayer elasticity and consequently do not yield surface dilatational viscosities. Only the studies of Wasan and coworkers are able to differentiate elasticity from surface dilatational viscosity[5]. The pendant drop geometry allows to independently study dilatational viscous effects because the area strain rates are larger than the shear strain rates and generally rheological measurements indicate that the surface dilatational viscosity is at least two orders of magnitude larger than the surface shear viscosity [3,5,10,16,17].

To fulfill the research goals of this study, we develop a theory to measure the surface dilatational viscosity by the shape analysis of a deforming pendant drop valid for arbitrary types of area strain rates. To complete this task, we formulated a hydrodynamic surfactant model which describes an incompressible Newtonian axisymmetric unsteady two-dimensional free surface flow with a Boussinesq-Scriven surfactant monolayer since the shape and position of the air-water interface are unknown a priori. The kinematic flow on the drop surface produced by changing its volume leads to an area strain rate distribution and consequently a surface concentration distribution requiring an equation of

state relating the compositional surface tension and surfactant surface concentration. We obtain a solution of the model valid when bulk hydrodynamic effects are substantially less than capillarity as we observe experimentally in Sections 4.3 and 5.3. At low flow rates inertia and viscous normal stresses exerted by the drop liquid on the surface are small compared to capillarity, and we analytically show that the dynamic tension is uniform along the drop surface and that a relation similar to the Young-Laplace equation governs the drop shape. The surface tension is the sum of the compositional surface tension and the dilatational surface tension. By comparing experimental drop shapes to solutions of the new version of the Young-Laplace equation the surface tension is computed. Foremost, we integrate the compositional-dilatational surface tension over the drop surface applying tensor analysis leading to a general equation for measuring the surface dilatational viscosity for arbitrary types of area strain rates.

To conduct the experiments, we built a pendant drop apparatus with a linear micro-syringe pump, an oscillatory piezoelectric micro-syringe pump, and a fast motion analyzer to deform and video record a pendant water drop with an insoluble surfactant monolayer at the air-water interface. We started this study using a pendant drop apparatus capable of recording only 25 f/s, the highest reported recording rate for directly measuring the surface tension from a drop shape without a pressure transducer[18,19]. But, very soon we realized that a higher recording rate was needed to capture accurately the interfaces of a rapidly deforming pendant drop and we decided to add a fast motion analyzer to the pendant drop apparatus. To improve the pendant drop apparatus, we added a fast motion analyzer, capable of recording up to 12,000 f/s and two micro-syringe

pumps for generating constant and oscillatory volumetric flow rates. We designed and built the piezoelectric oscillatory syringe pump.

To experimentally verify our new equation for constant volumetric flow rates, we use to test surfactants OD and DPPC and measure that the surface dilatational viscosity of the LE phase of DPPC is approximately 1.3 mNs/m as reported in Table 4.1. We do not measure the surface dilatational viscosity of OD because it behaves like a solid instead of a liquid and locally collapses at the air-water interface of a pendant drop. Then, from oscillatory experiments, we measure that the surface dilatational viscosity of DPPC is 2.3 mNs/m at 0.2 Hz and 0.8 mNs/m at 1 Hz, and that the surface dilatational viscosity of TP is 1 mNs/m at 1 Hz as reported in Table 5.2. We also measured from oscillatory experiments that the surface dilatational viscosity of a mixed DPPC/OD in mole ratio 1:1 is 1.6 mNs/m as given in Table 5.3. We develop a correction which allows the oscillatory pendant technique based on the Young-Laplace equation to substantially account for bulk hydrodynamic effects permitting to impose frequencies higher than 2 Hz for measuring the surface dilatational viscosity of surfactants with high viscoelastic coefficients.

The values that we obtain for DPPC from compression and oscillatory experiments agree and reasonably comply with the upper limit reported by Snik and collaborators listed in Table 2.1. We can not make a comparison for TP or for the mixed DPPC/OD monolayers because their dilatational viscosities are not reported in the literature. We found good agreement between the Langmuir trough and pendant drop elasticities. Our results on the mixed monolayers indicate that the surface viscoelasticities of DPPC increase by the addition of octadecanol as shown in Table 5.3.

The thesis is divided into 6 chapters. In Chapter 2, we briefly review the existing techniques for measuring the surface dilatational viscosity. Then, in Chapter 3 we introduce a new surfactant hydrodynamic model for measuring the surface dilatational viscosity and in Chapters 4 and 5 present the surface dilatational viscosity measurements. Lastly, in Chapter 6 we share our conclusions and recommendations for future research.

1.3 Scientific and Practical Applications of Measuring the Surface Dilatational Viscosity

In what follows, we briefly describe two of the many applications of measuring the surface dilatational viscosity involving almost pure dilatational flows the expansion and contraction of the alveoli and the impact of surfactant laden drops on hydrophobic solid surfaces, shown in Fig. 1.3. It is true that both systems are complex and required measuring many physical coefficients yet surface dilatational viscosity measurements can help on the design of synthetic surfactants to mimic the function of lung surfactants [20] and to dissipate the kinetic energies of drops at the moment of impact to avoid rebound. The lungs consist of millions of interconnecting microscopic sacks known as the alveoli. This configuration minimizes volume and maximizes surface area for mass transfer processes. The alveoli are lined with a thin layer of a liquid surfactant mixture of low molecular weight phospholipids and proteins. DPPC is the main component of the lung surfactant mixture. During breathing the lung surfactant film should spread rapidly at the alveolar interface in order to stabilize the alveoli. The lack of lung surfactant in a premature infant or adult results in a respiratory distress syndrome. The area strain rate

of breathing is approximately $\pi/6$ rad/s^{-1}. Moreover, recent surfactant protein studies undertaken using the longitudinal wave technique suggested that the surface dilatational modulus may explain the role of protein subunits in imparting mechanical stability to biological membranes and other cellular structures associated with them[21,22].

The impact of water drops laden with surfactants on solid hydrophobic surfaces is relevant to crop protection. Chemicals are applied to foliage by spraying aqueous preparations onto leaf surfaces but because of the hydrophobic nature of the foliate surface impacting drops do not spread but rebound and reflect off the surface creating an environmental hazard, and reducing the efficiency of the spray application. The agrochemical industry has always sought to increase the retention by using surfactants that adsorb onto the drop and leaf surface, and thereby lower the contact angle and enhance spreading. Because leaf surfaces are very hydrophobic, surfactant adsorption is limited on their surfaces, and this approach has only proved partially successful. In recent work from our group, a new method was proposed for enhancing drop retention that acts only at the air-aqueous interface of the impacting drop based on energy dissipation due to the surface dilatational viscosity of a surfactant monolayer. The surface dilatational viscosity is a pure viscous loss coefficient, because it is directly proportional to the amount of mechanical energy dissipated as heat[23]. Bulk soluble surfactants that assemble rapidly into a condensed monolayer at the air-water interface form states known to have high surface shear viscosity and may also have high surface dilatational viscosity. Such surfactant mixture can be used to dissipate the kinetic energy

at the moment of impact and retain the drop on the leaf surface. We can measure the area strain rate of an impacting drop directly by video recording it during impact. In agrochemical spraying a typical drop is 2.7 mm, travels at 1.58 m/sec, and takes 10 ms to expand to its maximum splat diameter an thus it can be shown that the expansion strain rate of the drop on a hydrophobic solid surface is approximately 225 s^{-1}. To determine the amount of kinetic energy that can be dissipated as heat due to the surface dilatational viscosity, the surface dilatational viscosity must be measured independently.

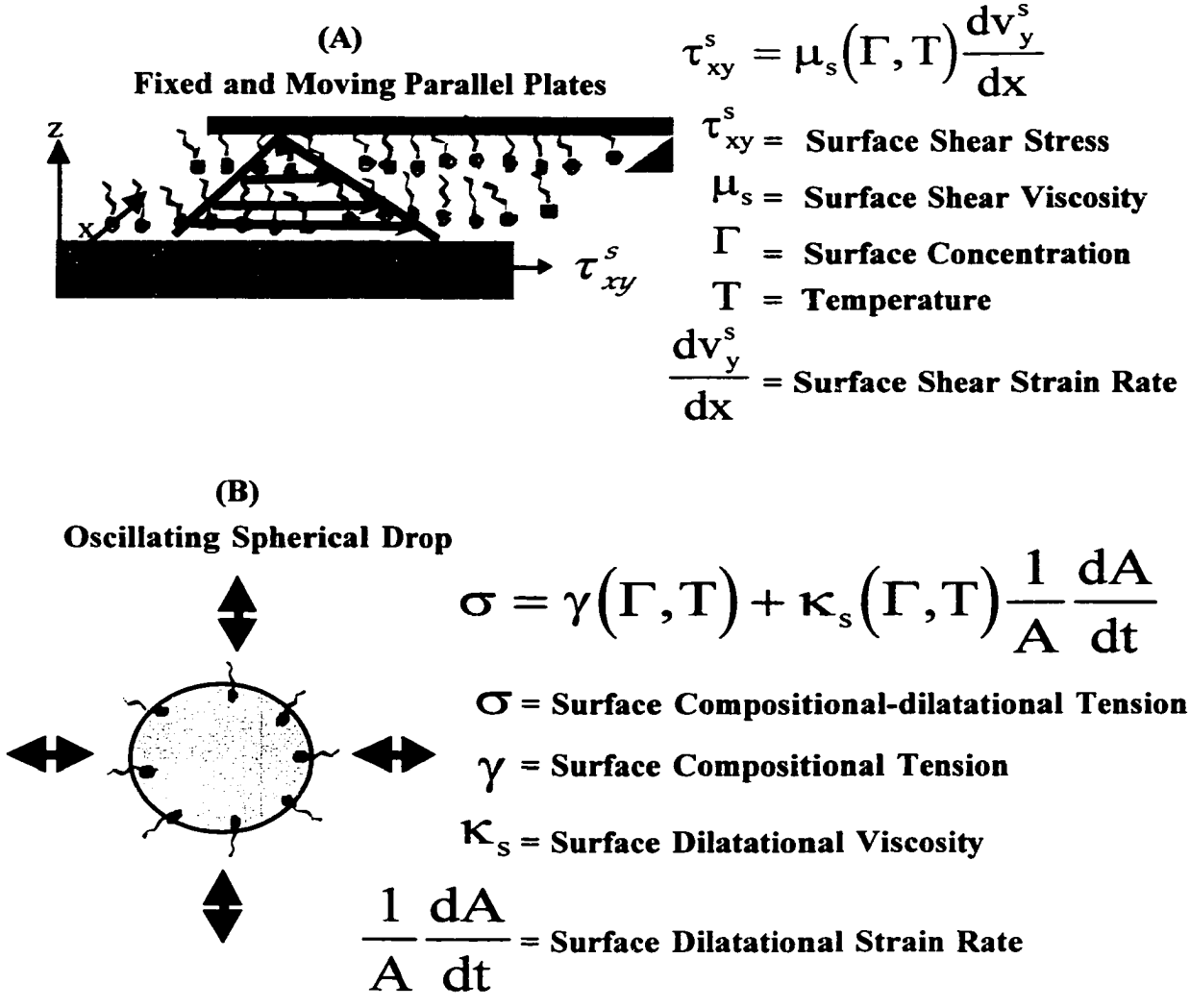

Fig. 1.1 Boussinesq-Scriven surface shear and dilatational viscosities of a surfactant monolayer: (A) surface shear flow and (B) surface dilatational flow.

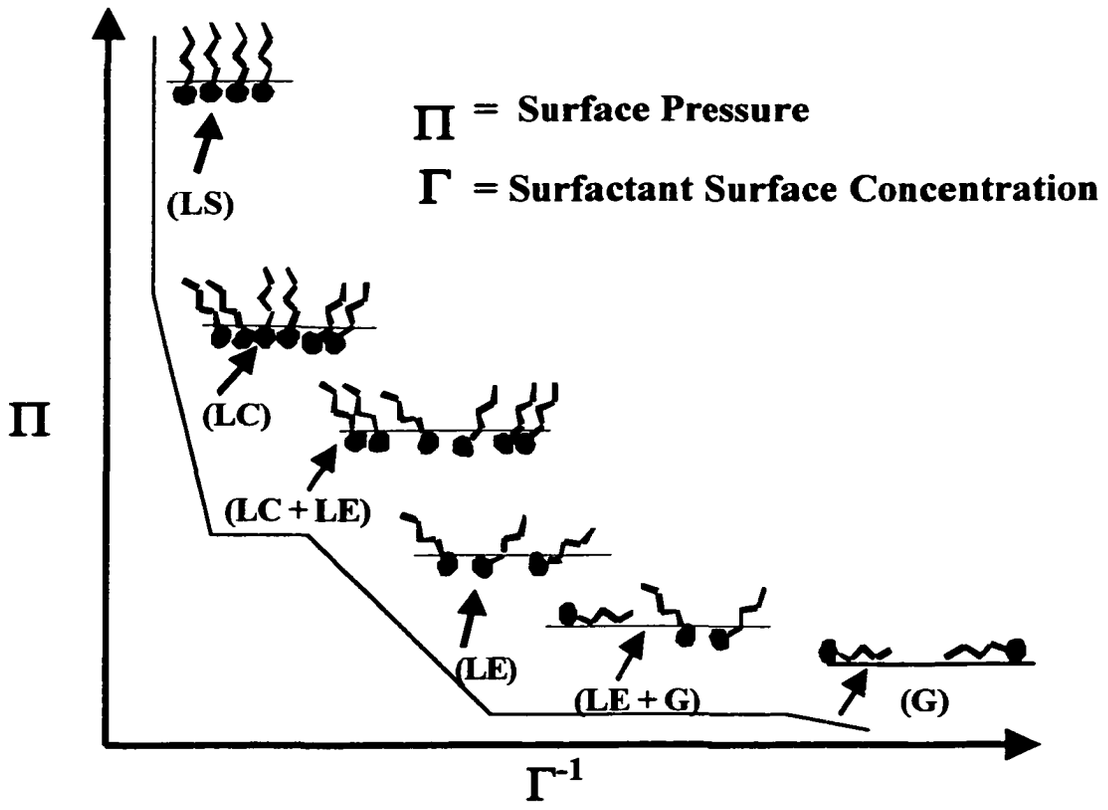

Fig. 1.2 Compositional surface tension and phases of a Langmuir monolayer: (G) gaseous, (LE) liquid expanded, (LC) liquid condensed, and (LS) liquid solid.

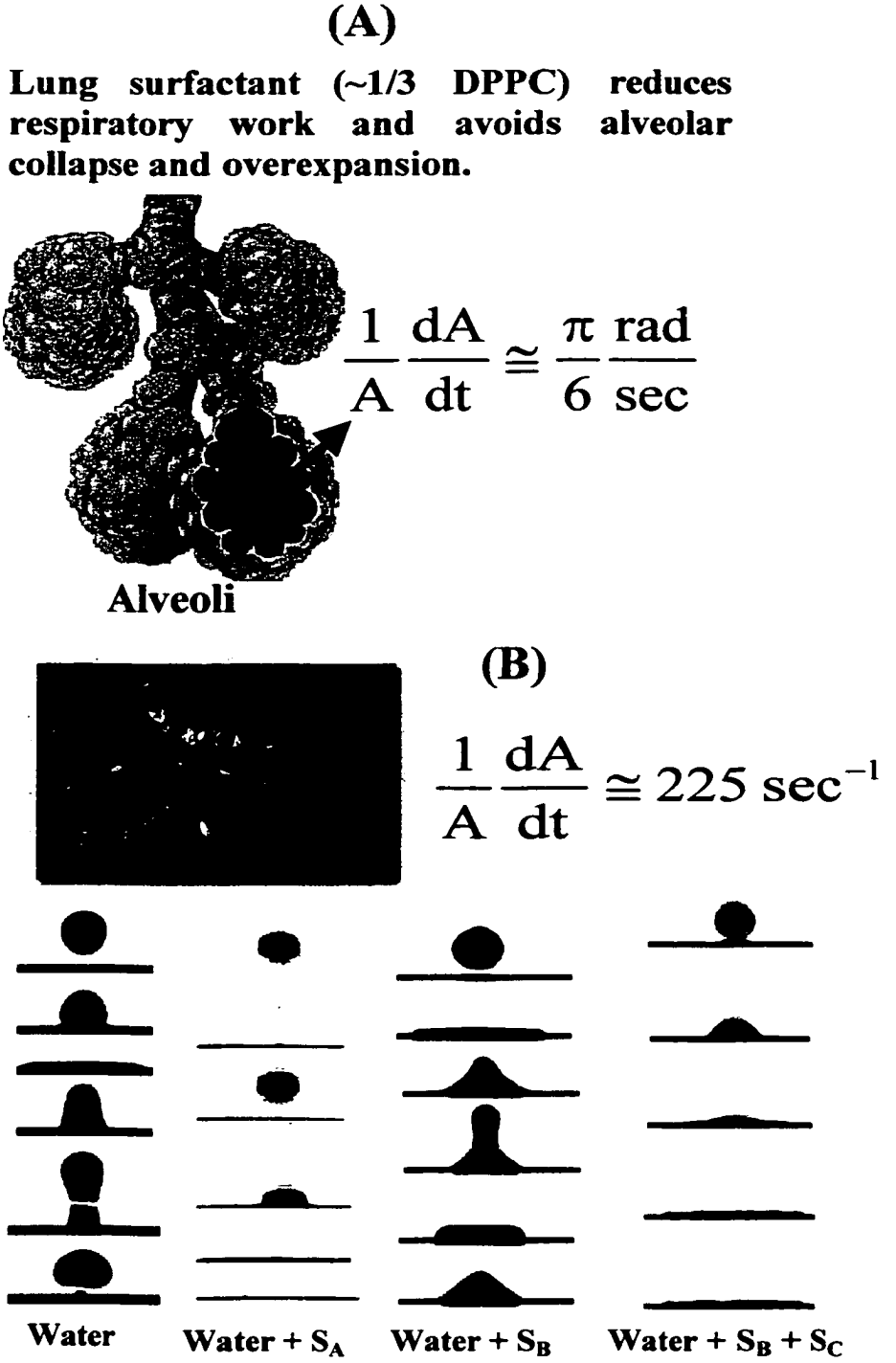

Fig. 1.3 Scientific and practical applications of measuring the surface dilatational viscosity: (A) understanding of the lung mechanics and (B) dissipating kinetic energy of a surfactant laden drop impacting on a hydrophobic solid surface.

Chapter 2

Literature Review of Previous Techniques for Measuring the Surface Dilatational Viscosity

2.1 Introduction

The surface dilatational viscosity has been measured using spatially damped small amplitude surface waves, expanding and oscillating pendant bubbles, and levitated oscillating drops. In the capillary wave technique, transversal waves are generated by normal disturbances to the interface (as for example electrocapillarity) and propagate over long distances. The decay of the amplitude of the capillary wave is measured optically using specular reflection and by comparison with the dispersion equation the surface viscosity is measured. Although capillary waves extend over long distances and their decay constant can be accurately measured, they create small area strain rate and thus the decay is not sensitive to the dilatational viscosity. In the longitudinal wave technique, waves are generated by oscillating in the plane of the interface a very thin wire extending over an entire trough width and detected by transversal waves or invasively using Wilhelmy plate surface balances or surface tracer particles [16,24-27]. While the damping is sensitive to the dilatational viscosity, longitudinal waves are damped over short distances making the accurate measurement of the decay difficult and the resulting measurement possibly less accurate. At the air-water interface, these wave propagation techniques are suitable for spread as well as adsorbed surfactant monolayers. These

longitudinal wave studies at the air-water interface have establish values as shown in Table 2.1 mainly for fatty acids, sodium dodecyl sulfate (SDS), and the insoluble phospholipids DPPC and L-α-dimyristoyl phosphatidyl ethanolamine (DMPE).

The second general class of methods for measuring the surface dilatational viscosity involves setting up interfacial area strain rates accompanied (at least ideally) by uniform changes in the surfactant surface concentration. Lucassen and coworkers [28] first arranged for this type of flow by oscillating opposing barriers on an air-water interface while measuring the surface tension using a Wilhelmy plate balance. For several soluble surfactants, they were only able to measure changes in the compositional surface tension due to diffusion exchange between the bulk phase and the surface. However, the realizable area strain rates with this system are limited and they did not observe surface dilatational viscous effects. Larger dilatational effects can be achieved on the surface of oscillating bubbles and drops. In the oscillating bubble technique, a spherical bubble or drop undergoes small amplitude oscillations. The surface tension is obtained by measuring the bubble pressure using a pressure transducer. The oscillation rates are assumed to be small enough as compare to capillarity so that from the pressure measurements and the Young-Laplace equation the tension can be measured. The area strain rate can be obtained by measuring the bubble radius as a function of time either by monitoring the displacement of the actuating driver or directly by video recording the bubble shape. For the most part these techniques has been used for soluble surfactants presumably having a negligible surface dilatational viscosity. For the soluble case the surface tension variation

is due to compositional changes in tension from which surfactant transport coefficients as for example diffusion coefficients and kinetic rate constants can be obtained. The exceptions are the studies of palmitic acid and DPPC of Palmer and coworkers as listed in Table 2.1. In addition to oscillating spherical bubbles other studies expand bubbles as in the maximum bubble pressure method or grow drops as in the growing drop technique. Also, these techniques have for the most part been used for soluble surfactants and small area strain rate to measure transport coefficients. Kao and et al. [29] are the only group that have used the maximum bubble pressure method to measure the dilatational viscosity by rapidly inflating a bubble while assuming negligible surfactant exchange. At the instant of maximum pressure the bubble is hemispherical and the normal components of the surface stress balance relates the maximum pressure, tube radius, compositional surface tension, surface dilatational viscosity, and gas volumetric flow rate. Then, the surface dilatational viscosity is measured as the gradient of the maximum pressure with respect to the gas volumetric flow rate. They used two soluble surfactants SDS and octanoic acid and found values for the viscosity several orders of magnitude smaller than that reported in Table 2.1 using the longitudinal wave technique. The authors attributed the discrepancy to the inaccuracy on measuring the gas volumetric flow rate at the moment of maximum pressure.

2.2 Trough Techniques for Measuring the Surface Dilatational Viscosity

This section includes the surface wave techniques as well as the rubber band and the laminar vortex pair techniques. The analysis of the surface wave technique starts with

the derivation of the dispersion equation relating wave parameters, bulk transport coefficients, and monolayer properties. Before describing how to generate and measure wave properties a brief review of the hydrodynamic theory of waves is appropriate. Consider a wave generated continuously at $x = 0$, propagating in the positive x-direction, damped spatially by a Boussinesq-Scriven aqueous insoluble surfactant monolayer at the air-water interface, and creating a two-dimensional incompressible water flow obeying Navier-Stokes equation

$$\rho\left[\frac{\partial u}{\partial t} + (u \bullet \nabla u)\right] = -\nabla p + \mu\nabla^2 u + \rho g. \qquad [2.1]$$

Where ∇ is the gradient operator, u is the velocity, ρ is the density, p is the pressure, μ is the shear bulk viscosity, and g is gravity. When the initial wave amplitude (δ) is very small compare to the wavelength (λ), the liquid velocity is small and the quadratic term of the Navier-Stokes equation $(u \bullet \nabla u)$ can be neglected. Then, a first order solution for velocity and pressure in powers of δ of Eq.2.1 is

$$u_x = \delta\left[\frac{Ake^{-kz} + Bqe^{-qz}}{ki}\right]e^{ikx+st}, \qquad [2.2a]$$

$$u_z = \delta\left[Ae^{-kz} + Be^{-qz}\right]e^{ikx+st} \qquad [2.2b]$$

and

$$p = p_0 + \delta\left\{-\frac{\rho s}{k}Ae^{-kz} + \left[\left(\frac{\mu q^3 - \rho sq}{k^2} - \mu q\right)Be^{-qz}\right]\right\}e^{ikx+st}. \qquad [1.2c]$$

Here k is the complex wavenumber ($k \equiv \frac{2\pi}{\lambda} + \beta i$), β is the spatial damping coefficient, s is the imaginary time coefficient ($s \equiv -i\omega$), ω is the wave frequency, and q is defined as $q^2 = k^2 + \frac{s\rho}{\mu}$. The subscript 0 refers to the base state in which the water pressure distribution is hydrostatic and the interface is planar and located at $z = 0$. To complete the above solution, the coefficients A and B are obtained after properly using the mass surface conservation equation and the kinematic condition together with the normal and tangential components of the surface stress balance cast in matrix form as

$$\begin{Bmatrix} 2k^3 s\mu - ks^2\rho - k^4\gamma_0 & q^3 s\mu - qs^2\rho + k^2 qs\mu - k^4\gamma_0 \\ k^2 s(1+\mu) + k^3\left[\varepsilon_0\Gamma_0 - s(\kappa_s + \mu_s)\right] & k^2 s\left[1 - q(\kappa_s + \mu_s)\right] + q^2 s\mu + k^2 q\varepsilon_0\Gamma_0 \end{Bmatrix} \begin{Bmatrix} A \\ B \end{Bmatrix} = 0. \quad [2.3]$$

Where γ_0, ε_0, and Γ_0 are respectively the surface tension, surface elasticity, and surface concentration of the base state, μ_s is the surface shear viscosity, and κ_s is the surface dilatational viscosity. Setting to zero the determinant of the characteristic matrix of Eq. 2.3 results in a non-trivial solution of the system known as the dispersion equation [30]. After independently measuring the wave parameters, surfactant monolayer properties, and bulk transport coefficients, the numerical solution of the dispersion equation yields the surface dilatational viscosity. The dispersion equation applies to transverse (capillary) as well as in plane (longitudinal) waves. At continuation, the capillary and longitudinal wave techniques are presented while mainly considering the surface wave generation mechanisms and the measurements of wave properties.

Surface transversal waves are generated without mechanically touching the air-water interface (1mm distant) by applying a sinusoidal and a DC offset voltage between a thin sharp metal blade and the air/water interface[31-33]. Because of the very sharp curvature of the razor tip an intense electric field is set up in a small volume near the edge. Since the dielectric constant of water is larger than that of air, water tends to rise up to the blade in the intense electric field and opposing this ascending motion is only surface tension because gravity is unimportant at capillary wavelengths. The frequency range is 50 to 1000 Hz. The waves are detected using a laser beam, a 50/50 beam-splitter, a position-sensing photo detector, a water incidence oval mirror, a focusing lens, a preamplifier, a lock-in amplifier, and a computer. To scan the water surface the incidence oval mirror and the focusing lens are mounted on a surface wave profiler capable of moving parallel to the Langmuir trough by a linear motor. The slope of the wave amplitude versus the scanned distance x provides the damping constant β measured with an accuracy of 1% and the wavelength λ is obtained from the plot of the phase angle as a function of x with an accuracy of 0.1. The initial amplitude of the transverse wave is determined from the distance between the blade and the water surface. However, a small variation in the measurement of the surface tension (0.5 mN/m) introduces a large change in the value of the surface dilatational viscosity.

Longitudinal waves are generated from oscillating in the plane of the surface a very thin wire (0.1mm in diameter) extending the entire trough width. Typically, the trough dimensions are selected such as to minimize reflection from the other walls of the trough.

Fig.2.1 illustrates three methods to monitor the oscillating surface tensions resulting from the longitudinal waves: the electrocapillary wave discussed in details in the above paragraph, motion of a tracer particle in the interface, and Langmuir surface balance with an oscillating barrier and a plate. As earlier noted, the electrocapillary technique is very convenient for measuring surface tension change since the transversal waves are generated without touching the fluid interface thus minimally perturbing the propagation of the also present longitudinal surface waves[16,26,27]. The surface tension change can be expressed as

$$\Delta\sigma = \sigma_0 e^{-\beta_l x} \cos\left(k_l x - \omega_l t\right). \qquad [2.4]$$

Here all the wave properties are measured from the electrocapillary wave analysis, σ_0 is the amplitude of the surface tension at $x = 0$, β_l is the damping coefficient of the longitudinal wave, k_l is the wave number, and ω_l is the wave frequency set to be 1 Hz.

In the tracer particle method, the motion of the interface is followed from the motion of a small Teflon particle having negligible inertia (smaller than 100 μm in diameter)[25]. The amplitude of the particle motion is measured using a calibrated microscope. The phase difference between the thin barrier and the particle motion is simply determined from triggering a relay when the barrier reaches its mean position using a timer knob. The relay starts an electrical timer and the experimenter looking in the microscope then stops the timer when the particle reaches a desired position. Again, the slope of the wave amplitude versus the scanned distance x provides the damping constant β_l and the wave number k_l is obtained from the plot of phase angle as a function

of x. In the Langmuir trough surface balance with and oscillating barrier method, the surface tension sinusoidal response is measured by introducing a plate in the surface connected to a digital balance[24]. Then, from the sinusoidal analysis of the surface tension the wave parameters are estimated. A problem with introducing a plate at the air-water interface is that it creates a stagnant surface even if a single fiber is used as the plate.

In the rubber band technique, a surfactant monolayer is spread inside the area enclosed by a squared rubber band resting on the surface of a trough. Then, the four corners of the rubber band are simultaneously moved diagonally by 1mm at a particular frequency resulting in an oscillatory area change of the spread surfactant monolayer. The resulting oscillatory surface tension is measured by introducing a Wilhelmy plate at the center of the rubber band connected to a digital balance. The area change is small and thus a linear viscoelastic analysis is applicable leading to the viscoelastic coefficients.

In the laminar vortex pair technique, an insoluble surfactant monolayer is spread at the air-water interface of a trough and then a vortex pair generator located in the water phase is used to produce a surface flow. The interface remains approximately flat during the vortex pair ascends vertically due to the velocity induced by each vortex core on the other vortex. Under these conditions, the tangential component of the surface stress balance reduces to

$$\mu\frac{\partial w}{\partial y}=\frac{\partial\gamma}{\partial\Gamma}\frac{\partial\Gamma}{\partial x}+\left(\kappa_s+\mu_s\right)\frac{\partial^2 w}{\partial x^2}. \qquad [2.5]$$

In Eq. [2.5], y points normal to the surface, x coincides with the surface, and w is the component of velocity in the x direction, γ is the compositional surface tension. The

velocity spatial derivatives are calculated using digital particle velocimetry and the compositional surface tension derivative is obtained using a Langmuir surface balance. The nonlinear optical technique of second harmonic generation is used to determine how the surfactant concentration changes with time and from the interaction of the vortex flow with the interface the temporal variations are converted to spatial variations. Before calculating the obtaining the surface dilatational viscosity the surface shear viscosity is separately measured using a surface shear viscometer. The technique in the published form is only applicable to surfactant systems with a strong nonlinear optical response but we think that perhaps by using neutron reflection to measure the surfactant surface concentration of the moving surface this limitation can be overcome[34].

2.3 Bubble and Drop Techniques for Measuring the Surface Dilatational Viscosity

In the maximum-bubble-pressure method, at the tip of a capillary tube a bubble is formed in a surfactant solution and then expanded fast such that the bubble surface expands as an insoluble surfactant monolayer[29]. The employed surface expansion rates were in the kilohertz range and did not generate bulk hydrodynamic stresses. The tangential component of the surface stress balance indicates that the compositional-dilatational surface tension is spatially uniform. Under such conditions, at the moment of maximum pressure the bubble is hemispherical and the normal component of the surface stress balance for a Boussinesq-Scriven surfactant monolayer reduces to

$$p_m - p_0 = \frac{2}{r_c}\left[\gamma + \kappa_s \frac{Q}{2\pi r_c^3}\right] \qquad [2.6]$$

Where p_m is the bubble maximum pressure, p_0 is the liquid static pressure, r_c is the capillary tube radius, and Q is the gas volumetric flow rate. Also, at the moment of maximum pressure the surface dilatational strain rate is given directly as a function of the gas volumetric flow rate. Eq. 2.6 is a simple relation for measuring the dilatational viscosity. Unfortunately, the authors of the technique reported that they inaccurately measured the gas volumetric flow rate at the moment of maximum pressure and suggested that at these high expansion rates the surfactant films did not obey a linear stress-strain constitutive equation. The surface dilatational viscosity was measured as the gradient of the maximum pressure with respect to gas volumetric flow rate.

In the oscillating bubble technique, the pressure and radius of a pulsating bubble are measured using respectively a pressure transducer and the known displacement of an actuator. The surface tension is then calculated from the interfacial pressure drop and radius using published tables generated by numerically solving the Young-Laplace equation. To form a bubble with an insoluble surfactant film at the air-water interface, a portion of a surfactant monolayer spread at the air-water interface of a Langmuir trough is transferred and then inflated at the end of a glass capillary tube. This approach has only been used a very small phase angle employing a frequency of 1/3 Hz, and area change of 1/4 resulting in an angular area strain rate of $\pi/6$ rad/s^{-1}. This area strain rate is relevant to the lung mechanics.

In the acoustical levitation technique, an acoustic radiation force is applied to a fluid particle to balance gravity and maintain the particle in a certain spatial

position[35,36]. To conduct the experiments, an optically transparent chamber is used as the resonant cavity of the levitation cell. A piezoelectric transducer is located at the bottom of the cell, and then the cell is filled with a host liquid. The top is either left open or contains a lid to reflect the acoustic wave. The transducer is connected to a voltage source with adjustable frequency and amplitude, and is used to excite the transducer creating an oscillatory vertical motion to the liquid adjoining the transducer at the bottom of the chamber. At a certain water level and frequency, the transducer-cell-water system longitudinally resonates, and standing waves are generated in the column of liquid. A fluid particle that does not mix with the hosting liquid is then levitated at a certain position and height where the acoustic radiation counterbalances gravity. Once suspended the fluid particle can be further triggered into free axisymmetric oscillations by giving another acoustic forcing via a frequency modulation near the resonant mode of the fluid particle. The levitated static drop shape is observed and recorded using a microscope and a camera. The oscillatory motion of the drop is detected by measuring its optical extinction cross section by impinging a parallel light beam on the levitated drop from the side and using a photodiode detector. Then, depending on the applied frequency and amplitude the surface viscoelastic coefficients are measured from the experimental drop or bubble shapes by employing a quadrupole shape analysis or boundary integral method.

2.4 Summary

In this chapter, we briefly described the trough, bubble and drop techniques used to obtain the surface dilatational viscosities of simple surfactant monolayers at the air-

water interface and examined the limitations of existing techniques. Most importantly, we generated Table 2.1 to help us to design our surfactant experiments and understand how the surface dilatational viscosity depends on the surfactant chemistry and architecture.

Table 2.1
Previous Surface Dilatational Viscosity Measurements of Simple Surfactant Monolayers at the Air-Water Interface at about 25 °C

Reference	Technique	Surfactant	Γ (molecule/Å^2)	C (mM)	κ_s (mNs/m)
Kao et al. 29	Bubble-1[a]	Octanoic acid	NF[l]	0.2-2	5-15 x10^{-6}
Hard et al. 37	Trough-1[b]	Octanoic acid	NF	0.2-1	< 1 x10^{-5}
Ting et al. 16	Trough-2[c]	Octanoic acid	NF	0.2-2	2-15 x10^{-2}
Snik et al. 38	Trough-3[d]	Decanoic acid	NF	NF	3
Hard et al. 37	Trough-1	Myristic acid	0.020-0.033	I[k]	< 1 x10^{-5}
Lemaire et al. 27	Trough-2	Myristic acid	0.016, 0.025	I	6, 5 x10^{-1}
Hall et al. 39	Bubble-2[e]	Palmitic acid	0.008	I	17
Hard et al. 37	Trough-1	Stearic acid	NF	I	< 6 x10^{-4}
Maru et al. 25	Trough-3	Stearic acid	0.023, 0.028	I	2, 25 x10^{-2}
Kao et al. 29	Bubble-1	SDS	NF	0.1-100	1-2 x10^{-5}
Tian et al. 35	Drop-1[f]	SDS	NF	0.5-8	4-9 x10^{-4}
Edwards et al. 5	Trough-3	SDS	NF	1.0-7.0	1-2
Hard et al. 37	Trough-1	Tetradecanol	NF	I	< 6 x10^{-4}
Tian et al. 35	Drop-1	OGP	NF	3-25	6-7 x10^{-4}
Tian et al. 35	Drop-1	DTAB	NF	1.5-14	2-23 x10^{-4}
Chen et al. 36	Drop-2[g]	Triton X-100	NF	0.14	2 x10^{-2}
Snik et al. 40	Trough-4[h]	DPPC	NF	I	< 2
Snik et al. 40	Trough-4	DPPC	NF	I	5 (37°C)
Hall et al. 39	Bubble-2	DPPC	0.004	I	32
Kragel et al. 17	Trough-5[i]	DPPC	0.011-0.018	I	150-400
Kragel et al. 17	Trough-5	DMPE	0.012-0.020	I	150-500
Hirsa et al. 41	Trough-6[j]	Hemicyanine	0.0118	I	<1.2

[a]Maximum Bubble Pressure Method.
[b]Thermal Capillary Wave Laser Light Scattering Technique.
[c]Longitudinal Electrocapillary Wave Technique.
[d]Longitudinal Wave Tracer Particle Technique.
[e]Pendant Oscillatory Bubble Pressure transducer Method.
[f]Levitated Oscillating Drop Quadrupole Shape Analysis.
[g]Levitated Oscillating Drop Boundary Integral Analysis.
[h]Squared Rubber Band Wilhelmy Plate Balance Technique.
[i]Longitudinal Wave Wilhelmy Plate Balance Technique.
[j]Laminar Vortex Pair and Digital Particle Image Velocimetry.
[k]Not found.
[l]Insoluble.

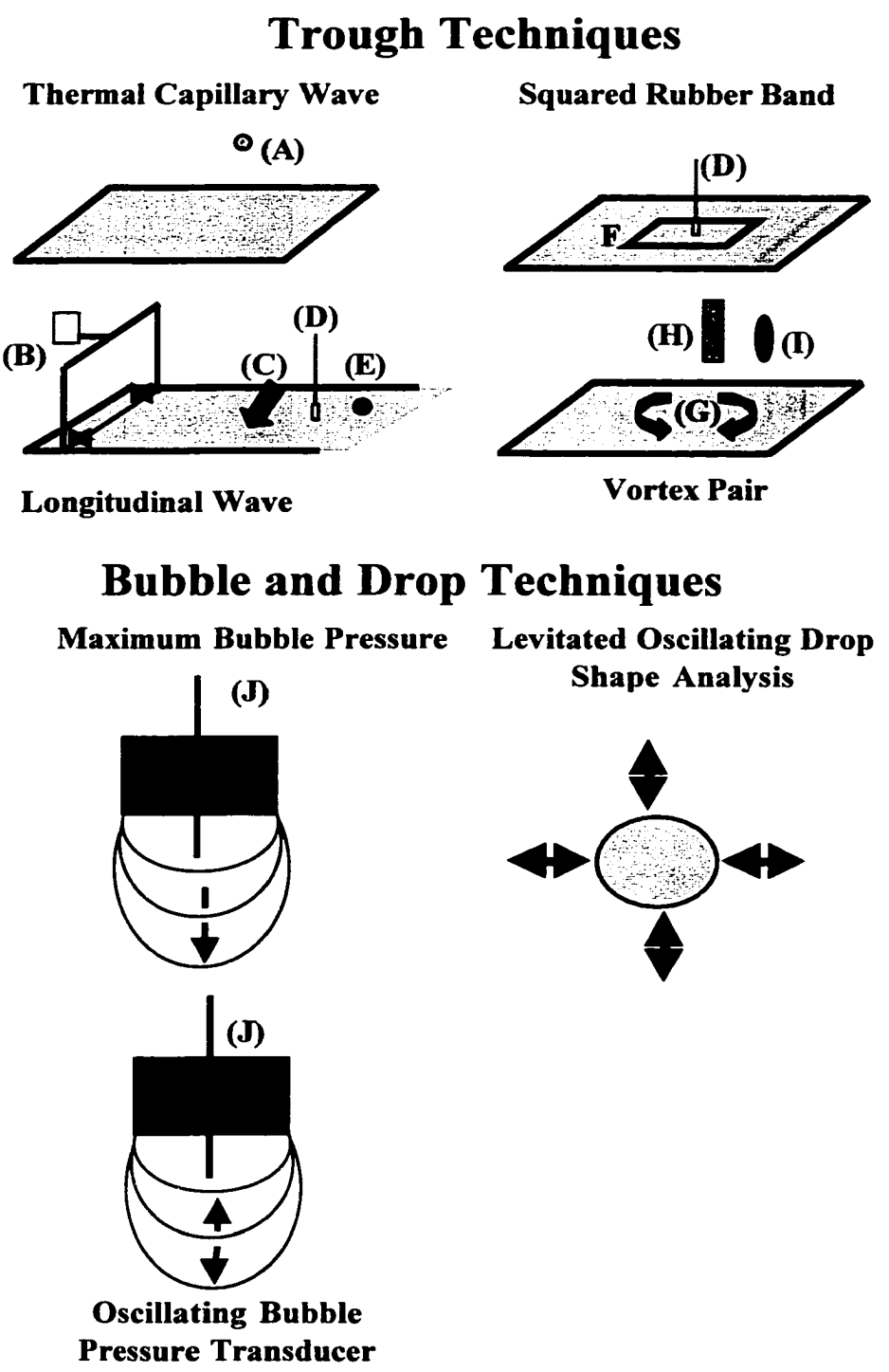

Fig. 2.1 Previous trough, bubble, and drop techniques for measuring the surface dilatational viscosity: (A) laser light scattering, (B) oscillating barrier, (C) electrocapillary wave, (D) Wilhelmy film balance, (E) tracer particle, (F) squared rubber band, (G) vortex pair, (H) particle velocimetry, (I) surfactant concentration optical meter, and (J) pressure transducer.

Chapter 3

Theory for Measuring the Surface Dilatational Viscosity of a Surfactant Monolayer by the Shape Analysis of a Deforming Pendant Drop

3.1 Introduction

In this chapter, we develop a surfactant hydrodynamic model to measure the surface dilatational viscosity of an insoluble surfactant monolayer at the air-water interface by the shape analysis of an axisymmetrically deforming pendant drop. A surfactant monolayer is insoluble if the number of surfactant molecules at the liquid interface does not change over the dilatational time defined as the time necessary to develop a considerable change in area. At continuation, we describe in Section 3.2 a well-posed system of equations for a surfactant free surface flow. Then, in Section 3.3 we establish a general equation from which the surface dilatational viscosity can be easily measured if bulk hydrodynamic effects are negligible as compare to capillarity and conclude with a summary in Section 3.4.

3.2 Surfactant Hydrodynamic Model

At rest at the tip of a capillary tube a pendant water drop with an insoluble surfactant monolayer at the air-water surface is in state of isotropic stress given by the

compositional surface tension as a function of the surfactant surface concentration, as shown in Fig 3.1 A. Then at time $t = 0$, the volume of the surfactant laden water drop is changed at a constant volumetric flow rate resulting in an axisymmetric incompressible water flow obeying the dimensionless continuity equation expressing conservation of mass

$$\nabla \bullet \mathbf{v} = 0 \qquad [3.1]$$

and the Navier-Stokes equation expressing conservation of momentum

$$We\left[\frac{\partial \mathbf{v}}{\partial t} + \mathbf{v} \bullet \nabla \mathbf{v}\right] = -\nabla p + Ca\nabla^2 \mathbf{v} + Bo\,\mathbf{i}_z . \qquad [3.2]$$

Where ∇ is the gradient operator, $\mathbf{v}$ is the flow velocity, p is the pressure, $\mathbf{i}_z$ is a unit vector pointing parallel to the acceleration of gravity, $We \equiv \frac{\rho a U^2}{\gamma_{cw}}$ is the Weber number, $Ca \equiv \frac{\mu U}{\gamma_{cw}}$ is the capillary number, and $Bo \equiv \frac{\rho a^2 g}{\gamma_{cw}}$ is the Bond number for separately measuring the importance of inertial, bulk shear viscous, and gravity forces to capillary forces. The characteristic length is the capillary tube inner radius a, the characteristic velocity is U, the ratio of the constant volumetric flow rate and inner cross sectional area of the capillary tube, g is the magnitude of the acceleration due to gravity, and ρ, μ, γ_{cw} are respectively the clean water density, viscosity, and surface tension. The density and viscosity of air are a thousand times less than the density and viscosity of water and therefore allow substituting the air bulk phase by a constant pressure that without the loss of generality is considered here to be zero.

At continuation, the boundary conditions for numerically integrating Eqs. 3.1 and 3.2 in the time-dependent computational domain shown in Fig. 3.1 B will be presented. The independent spatial variables are the cylindrical coordinates r and z. The flow is symmetric with respect to the z coordinate and at the drop axis of symmetry the flow is bounded

$$v_r(r=0,z;t)=\frac{\partial}{\partial r}v_z(r=0,z;t)=0. \qquad [3.3]$$

Along the tube wall the velocity is zero at all time

$$\mathbf{v}(r=1,z<0;t)=0\ . \qquad [3.4]$$

And far upstream of the tube outlet at z^*, the flow velocity is fully developed

$$v_r(r,z=z^*;t)=0\ ;v_z(r,z=z^*;t)=2(1-r^2). \qquad [3.5]$$

A recent numerical computation [42] reports that z^* is twice the tube radius. It has been experimentally observed and numerically implemented that the contact line where tube, air, and water meet remains pinned during the imposed flow to the outer edge of the tube therefore is not required to specified the contact angle.

The shape and position of the air-water interface are unknown a priori and the boundary conditions at the air-water interface are also less straightforward due to the presence of surfactant molecules. To satisfy insolubility the surfactant diffusive and kinetic adsorption and desorption times must be substantially larger than the dilatational time so that the surfactant does not get an opportunity to exchange between the interface and the bulk phases. Recently, Pan et al. [43] showed using a pendant drop apparatus that

some polyethoxylated surfactant monolayers adsorbed at the air-water surface are insoluble. The investigated adsorbed surfactant monolayers were rapidly expanded and compressed or vice versa over a time period of only a few seconds and resulted in the same relationship between the surface tension and relative surfactant surface concentration. This result indicated that the amount of surfactant molecules were conserved at the interface over the area change thus the diffusive and kinetic times were substantially larger than the dilatational times. The pendant drop dilatational times were short because the relative dilatational strain rates were large due to the small radii of the drops. The used bulk concentrations were low enough so that diffusive times were larger than the short dilatational times. Also, the result indicated that the surface tensions were a unique function of the surfactant surface concentrations and consequently the dilatational surface tensions, the product of the surface dilatational viscosity and dilatational strain rate, were negligible at the low imposed dilatational strain rates. The surface dilatational viscosities of soluble surfactant monolayers as reported in Table 2.1 are much less than 1 mNs/m and the drop area strain rates were less than 1 s^{-1} thus resulting in a dilatational surface tension of much less than 1mNs/m.

Moreover for an insoluble surfactant monolayer adsorbed or spread, the dimensionless surface mass balance is

$$\frac{\partial \Gamma}{\partial t} + \Gamma \nabla_s \bullet \mathbf{v}_s + \mathbf{u} \bullet \nabla_s \Gamma = 0. \qquad [3.6]$$

The initial surfactant concentration Γ_i has been used to make the surfactant concentration dimensionless and ∇_s is the surface gradient operator, $\nabla_s \bullet \mathbf{v}_s$, the surface divergence of

the surface velocity is the dilatational strain rate, and **u** is the intrinsic velocity of a surface fluid particle. A surface diffusion term does not appear in Eq. 3.6 since for an insoluble surfactant monolayer typically the ratio of surface convection to surface diffusion known as the surface Peclet number is substantially larger than one, $Pe_s = \frac{aU}{D_s}$ and D_s is the surface diffusion coefficient. For instance, for a characteristic surface diffusion coefficient of 10^{-4} mm^2/s, a tube inner radius of 1mm and a velocity as small as 1mm/s the surface Peclect number is as high as 10^4 [44]. The surfactant mass balance equation has been solved numerically under the conditions that the intrinsic velocity is zero at the drop apex and at the tube rim while requiring having finite surface concentration gradients at both locations.

Before presenting the surface stress balance corresponding to the air-water interface, it is appropriate to discuss the commonly used Boussinesq-Scriven constitutive equation for linearly relating the interfacial stress and strain rate[1]. In which, the interfacial stress consists of an isotropic term, the sum of the surface compositional tension and the product of the surface dilatational viscosity and dilatational strain rate, and a shear term, the product of the surface shear viscosity and shear strain rate. Surface shear viscous contribution will not appear on the surface stress balance since generally surface rheological measurements indicate that the surface shear viscosity is at least two orders of magnitude less than that the surface dilatational viscosity [3,5,10,16,17]. Therefore, only the dilatational viscous term is considered here

$$\overline{\sigma} = \gamma + Ca_s \nabla_s \bullet \mathbf{v}_s \qquad [3.7]$$

It is convenient to refer to $\bar{\sigma}$ as the compositional-dilatational surface tension, to γ as the compositional surface tension, and to $Ca_s \nabla_s \bullet \mathbf{v}_s$ as the dilatational surface tension. Here, $Ca_s \equiv \frac{\kappa_s U}{a\gamma_{cw}}$ is the surface dilatational capillary number, the ratio of surface dilatational viscous forces to static capillary forces and κ_s is the surface dilatational viscosity. Then on the drop free surface, the tangential and normal components of the surface stress balance are

$$Ca\left[\mathbf{n} \bullet \left(\nabla \mathbf{v} + \nabla \mathbf{v}^t\right) \bullet \mathbf{t}\right] = \nabla_s \bar{\sigma} \qquad [3.8]$$

and

$$Ca\left[\mathbf{n} \bullet \left(\nabla \mathbf{v} + \nabla \mathbf{v}^t\right) \bullet \mathbf{n}\right] = p + \bar{\sigma} \nabla_s \bullet \mathbf{n} \qquad [3.9]$$

Where $\mathbf{n}$ and $\mathbf{t}$ are unit vectors normal and tangent to the surface as illustrated using cylindrical coordinates in Fig. 3.1 B.

In addition, the constant volumetric flow rate condition requires that

$$2\int_{s_0}^{s_f} v_n \, r \, ds = \pm 1 \qquad [3.10]$$

where $v_n = \mathbf{v} \bullet \mathbf{n}$ is the magnitude of the surface normal velocity, s is the arc length, and the positive and negative sign corresponds to drop expansion and compression respectively.

The initial conditions for the velocity and for the surfactant surface concentration are respectively

$$\mathbf{v}\left(r, z; t = 0\right) = 0 \qquad [3.11]$$

and

$$\Gamma(r,z;t=0)=1. \qquad [3.12]$$

Since the shape and position of the air-water interface are unknown a priori, the above model describes a surfactant dilatational viscous Newtonian incompressible axisymmetric unsteady two-dimensional free surface flow. Several studies including inertia and bulk shear viscous effects have dealt successfully with the free surface flow of water exiting a tube into another fluid without surfactants by implementing RIPPLE, a numerical scheme for obtaining finite difference solutions of free surface flows having significant surface tension forces [42,45-47]. RIPPLE is written in primitive variables. Key features of RIPPLE are representing the surface tension as a localized volume force, a volume of fluid VOF [48] free surface treatment. An Euler VOF approach is used because the concept of fractional volume of fluid is somewhat practical tracking free fluid surfaces. A detailed user manual and the computer source code of RIPPLE are available to the general public from the Energy Science and Technology Software Center in TN and we obtained both. We wanted to modify RIPPLE to compute the surface dilatational viscosity by comparing numerical and experimental drop shapes with a spread surfactant monolayer at the air water interface but we found that RIPPLE is inadequate to resolve smoothly the interface. Then, we opted for a boundary fitted grid instead of a stationary grid to resolve the interface with the highest possible accuracy. But after reviewing the Journal of Computational Physics from 1990 to present, and the Handbook of Grid Generation and consulting with several[49] authorities on modeling free surface flows, we

decided to put our efforts on oscillatory experiments (Chapter 5) instead of numerically solving the full surfactant hydrodynamic model.

3.3 Solution of the Hydrodynamic Surfactant Model

If bulk hydrodynamic effects are substantially less than capillarity then for a deforming pendant water drop with a viscous surfactant monolayer at the air-water interface the equation of motion and the tangential and normal components of the surface stress balance simplify to

$$-\nabla p + \mathrm{Bo}\,\mathbf{i}_z = 0, \qquad [3.13]$$

$$\nabla_s \overline{\sigma} = \nabla_s\left(\gamma + \mathrm{Ca}_s \nabla_s \bullet \mathbf{v}_s\right) = 0, \qquad [3.14]$$

and

$$p + \overline{\sigma}\nabla_s \bullet \mathbf{n} = 0. \qquad [3.15]$$

The tangential component of the surface stress balance (Eq. 3.14) indicates that the compositional-dilatational surface tension is spatially uniform. For small changes in the surfactant surface concentration, we adopt a constant property formulation in which case the surface dilatational viscosity is constant and a linear equation of state can well relate the compositional surface tension and surfactant surface concentration. Under these conditions, we establish that the compositional-dilatational surface tension Eq. 3.7 can be integrated analytically over the drop surface applying surface tensor analysis[5,50] to obtain an equation for measuring the surface dilatational viscosity

$$\sigma = \left(bm + \kappa_s \frac{dA}{dt} \right) A^{-1} + c \qquad [3.16]$$

Where b and c are the slope and intercept of the linear equation of state relating the surface compositional tension and surfactant concentration, m is the constant number of surfactant molecules on the drop surface, A is the drop surface area, and $\frac{dA}{dt}$ is the area rate of change. Equation [3.16] is general since it can be used for arbitrary types of changes in area for example if the area change is oscillatory it reduces to an existing relationship for measuring the surface dilatational viscosity [51, 18]

$$\kappa_s = \frac{A_0 \sigma_a \sin\delta}{A_a \omega}. \qquad [3.17]$$

Here A_0 is the base state area, σ_a is the tension amplitude, δ is the phase angle, A_a is the area amplitude, and ω is the forcing angular frequency.

In Chapters 4 and 5, we illustrate how to measure the surface dilatational viscosity employing the above model and in what follows we concisely describe how to compute each quantity entering in these equations for measuring the surface dilatational viscosity. For a compressing drop the rate of area change is constant and the surface dilatational viscosity is obtained directly from Eq. 3.16 from the slope of the straight line relating the compositional-dilatational surface tension and inverse area. For an oscillating drop Eq. 3.17 allows measuring the surface dilatational viscosity after properly fitting the oscillating area and compositional-dilatational surface tension to sine functions with a phase angle. The properties of the surfactant monolayer b, c, and m are determined by considering a particular phase of an experimentally measured Langmuir isotherm.

The normal component of the surface stress balance (Eq. 3.15) governs the drop shape and relates the hydrostatic pressure difference, the local mean curvature of the surface, and the compositional-dilatational surface tension. If only compositional effects are important Eq. 3.15 reduces to the static Young-Laplace equation. At each instant, we measure the compositional-dilatational surface tension from digitized shapes of a deforming drop with a surfactant monolayer on its surface by expressing the new version of the Young-Laplace equation as a set of three ordinary differential equations for the dimensionless spatial coordinates r, z, and the turning angle ϕ as a function of the dimensionless arc-length s calculated from the drop apex as shown in Fig. 3.2

$$\frac{\partial z}{\partial s} = \sin\phi, \qquad [3.18a]$$

$$\frac{\partial r}{\partial s} = \cos\phi, \qquad [3.18b]$$

and

$$\frac{\partial \phi}{\partial s} = 2 - Bz - \frac{\sin\phi}{r} \qquad [3.18c]$$

where B is defined as $\frac{\Delta\rho g R_0^2}{\sigma}$. These equations are subject to the boundary condition

$$r(s=0) = z(s=0) = \phi(s=0) = 0 \qquad [3.19]$$

and integrated by using a fourth-order Runge-Kutta scheme initialized with the approximations valid near the drop apex where $\phi << 1$

$$\begin{bmatrix} r \\ z \\ \phi \end{bmatrix} = \begin{bmatrix} 1 & 0 & -1/6 \\ 0 & 1/2 & 0 \\ 1 & 0 & B/8 \end{bmatrix} \begin{bmatrix} s \\ s^2 \\ s^3 \end{bmatrix} \qquad [3.20]$$

To calculate the surface tension an objective function[52] E is constructed as the sum of the normal distance between the experimental points and the theoretically points from the integration of Eq. 3.18

$$E(B,R_0) = \frac{1}{2}\sum_{1}^{N}\left[(r_t - r_e)^2 + (z_t - z_e)^2\right]. \qquad [3.21]$$

To obtain the optimal congruence among the experimental and theoretical total number of points N, E is minimized with respect to B and R_0, and the minimization equations are solved with a Newton-Raphson method. The optimum values of the two parameters yield the dynamic surface tension.

We obtain the initial guess vector required by the Newton-Raphson algorithm in a few tenths of a second by implementing a recent method[53] that also uses the experimental drop shape. However, the accuracy of the recent method is less than the accuracy of the Newton-Raphson procedure. In this method, the coordinates of the theoretical Young-Laplace shape are the distance r_i from the axis of symmetric and z_i the vertical distance from the apex as shown in Fig. 3.3. Then, integrating analytically the Young-Laplace Equation yields an expression for the volume V_i enclosed within the drop apex and a plane at a distance z_i

$$F\left(V_i - z_i r_i^2\right) + \frac{r_i^2}{R_0} - r_i \sin\theta_i = 0 \qquad [3.22]$$

where F is defined as $\frac{\Delta\rho g}{2\sigma}$ and the angle formed by the tangent to the ith point and the horizontal axis is θ_i. For a given experimental set of coordinates corresponding to a digitized drop image, the apex is located as the centroid of the distribution of horizontal coordinates and the intercept with the axis of symmetry. The apex is taken as the origin and the experimental coordinates are referenced with respect to it to form a set $r_{i,exp}$ and $z_{i,exp}$. The volume enclosed within the bubble from the apex to the horizontal plane with coordinate $z_{i,exp}$ can also be computed numerically $V_{i,exp}$. For determining $\theta_{i,exp}$, a curve is fitted to the experimental points in the vicinity of the ith point and then the tangent angle is derived from the curve. Since the set ($V_{i,exp}$, $\theta_{i,exp}$, $z_{i,exp}$, $r_{i,exp}$) satisfied Eq. 3.22, an error criterion is defined over all points of the profile

$$E_{igm}\left(F, R_0\right) = \sum_{i}^{N-1}\left[F\left(V_{i,exp} - z_{i,exp}\, r_{i,exp}^2\right) + \frac{r_{i,exp}^2}{R_0} - r_{i,exp} \sin\theta_{i,exp}\right]^2 \qquad [3.23]$$

Thus, a minimization of E_{igm} with respect to F and R_0 provides two equations for measuring the apex radius of curvature and the surface tension.

3.4 Summary

In this chapter, we developed a model for measuring the surface dilatational viscosity from the experimental shape of an axisymmetrically deforming pendant water drop with an insoluble surfactant monolayer at the air-water interface. The main result

from this chapter is that now we have an equation for measuring the surface dilatational viscosity for arbitrary area strain rates as for example a constant strain rate resulting from a drop or bubble compression or expansion. The newly derived equation properly yields the published oscillatory equation of Lucassen, Hansen, and collaborators [51, 18].

.

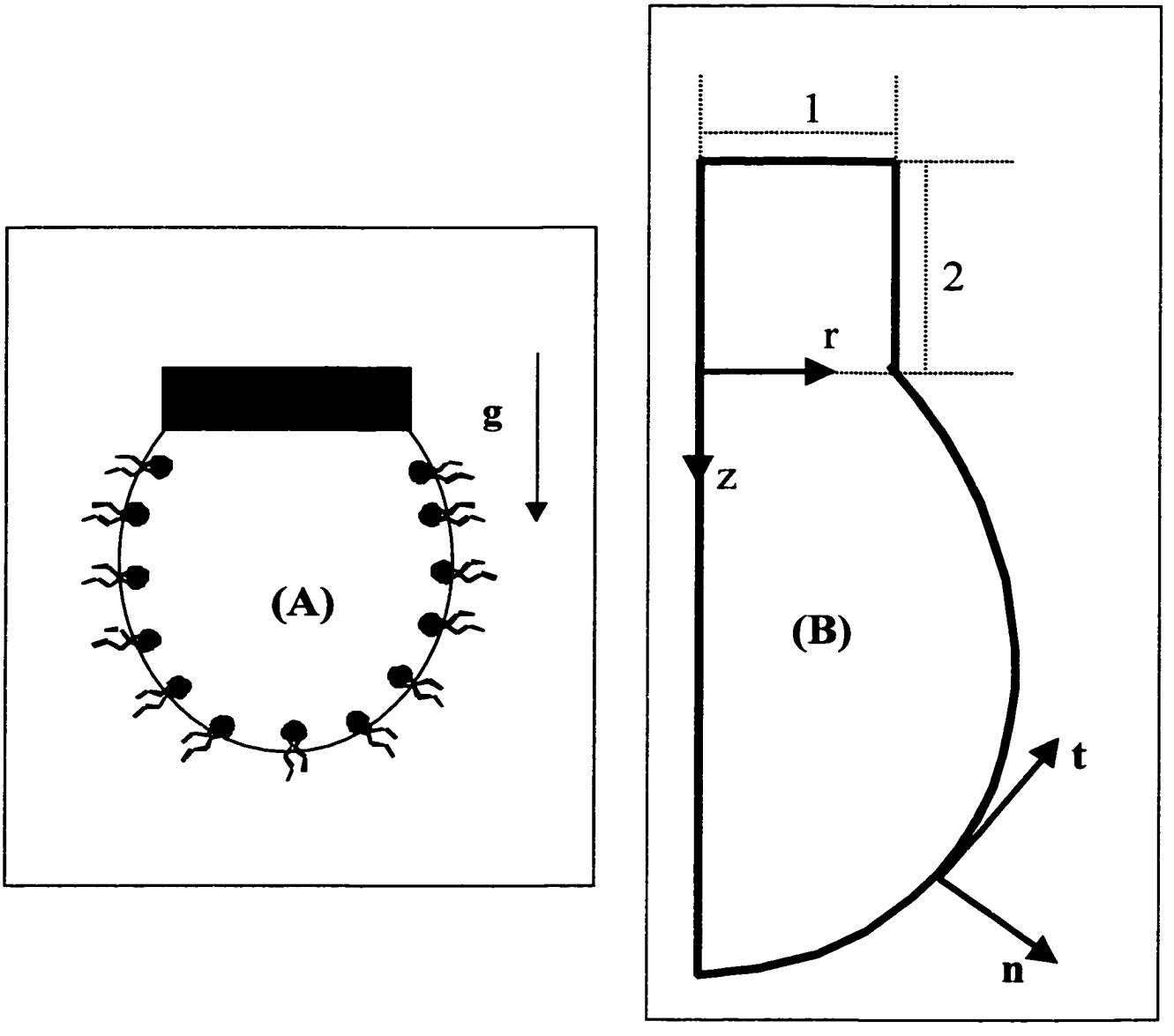

Fig. 3.1 (A) Pendant drop at rest with an insoluble surfactant monolayer at the air-water interface and (B) pendant drop geometry for the boundary conditions of a deforming pendant drop.

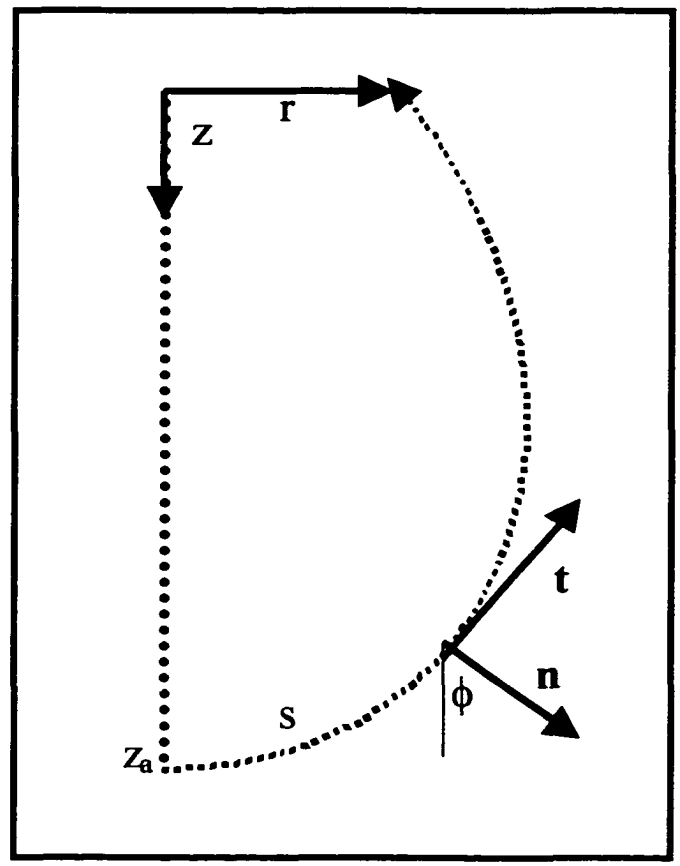

Fig. 3.2 Pendant drop geometry for numerically integrating the Young-Laplace equation for measuring the surface tension.

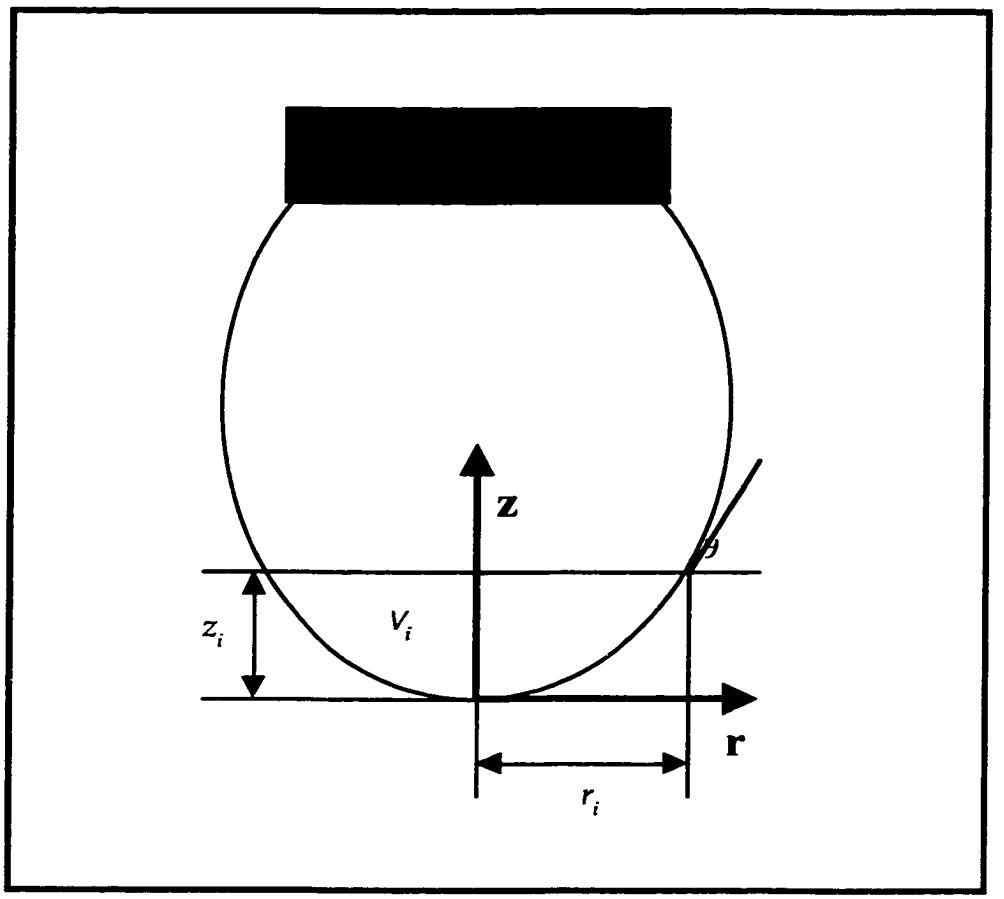

Fig. 3.3 Pendant drop geometry for the initial guess method for measuring the surface tension.

Chapter 4

Measuring the Surface Dilatational Viscosity of a Surfactant Monolayer at the Air-Water Interface by the Shape Analysis of a Compressing Pendant Drop

4.1 Introduction

In this chapter, we introduce a new technique for measuring the surface dilatational viscosity based on a constant rate of area change instead of an oscillatory rate of area change. This can be done because of the new equation that we introduced in Chapter 3. The results from the constant rate of area change will be compared with those given in Table 2.1 and with the results that we will obtain in Chapter 5 from oscillatory experiments. Generally, it is less expensive to generate a rapid compression or expansion than to generate an oscillatory flow. We measure the surface dilatational viscosity by changing the volume of a pendant water drop with a Langmuir surfactant monolayer at the air-water interface. The imposed constant volumetric flow rates generate negligible bulk hydrodynamic effects thus the tangential component of the surface stress balance indicates that the dilatational viscoelastic surface tension is constant. Under these conditions, the Young-Laplace equation governs the drop shape with the compositional surface tension replaced by the compositional-dilatational surface tension. Also, we establish that the compositional-dilatational surface tension can be analytically integrated yielding an equation that is valid for arbitrary types of changes in area for directly

measuring the surface dilatational viscosity. We experimentally verify the theory using a pendant drop apparatus improved with a fast motion analyzer and measure that the surface dilatational viscosity of the liquid expanded phase of the phospholipid DPPC is approximately 1.3 mNs/m. The results obtained using this new technique agree reasonably well with earlier reported results corresponding to DPPC, as listed in Table 2.1.

Besides the theory that we describe in Section 3.1, there is another drop-deformation theory based on the spinning drop apparatus due to John Slattery et al. [54] and briefly discussed elsewhere[5]. The spinning drop apparatus is a standard instrument for measuring ultra low tensions. A round tube filled with a host liquid and a suspended fluid particle is rotated with constant angular velocity about the axis of the tube. Due to the centrifugal force the suspended drop elongates. The host fluid and drop are assumed to rotate as rigid bodies and by measuring appropriate geometrical parameters the interfacial tension is determined. The proposed method for measuring the surface viscosities suggests applying small oscillations in the angular velocity and measuring the amplitude of the drop radius in the region where the drop is reasonably approximated as being cylindrical as well as the phase angle. A major limitation with this technique is that the amplitude of the oscillating drop radius is apparently too small for practical measurements when liquid-liquid systems are used thus the approach will only be applicable to gas-liquid systems. The pendant drop technique can compete with the

spinning drop technique in the determination of ultra low interfacial tension of the order of μN/m as demonstrated by the work of D. Kwok et al. [55].

4.2 Experimental Section

To conduct the experiments, we built a pendant drop apparatus enhanced with a fast motion analyzer Kodak Ektapro, capable of recording up to 12,000 f/s. The pendant drop apparatus was introduced in 1994 as an accurate, versatile, and non-invasive surfactant film balance and since then it has been used extensively [56-60]. Fig. 4.1 shows our pendant drop apparatus. A surfactant monolayer is spread at the air-water interface of a pendant drop formed at the tip of a Peek needle and enclosed in a quartz cuvette. The Peek needle is used instead of a stainless needle to prevent water from climbing the otherwise steel needle and the quartz cuvette protects the drop from airborne contaminants and air currents. For coating the drop with an aqueous insoluble surfactant monolayer, a solution is prepared by dissolving the surfactant in a more polar volatile solvent and transferred to the drop surface using a micro-syringe. Here, the initial amount of surfactant spread at the drop surface is calculated from the surface tension versus absolute surface concentration curve obtained using a Langmuir trough surface balance simply because the amount spread at the trough surface is higher than at the drop surface. Therefore, to know the initial amount of surfactant spread at the drop surface a pendant drop experiment can not start inside a first order phase transition because the same surface tension value corresponds to several surfactant surface concentrations. Then after

full evaporation of the solvent from the drop surface typically less than 50 seconds but we allow 3 minutes, the drop is compressed at a constant volumetric flow rate controlled by adjusting the speed of the linear motor. This non-invasively reduces the drop surface area and therefore leads to the compression of the monolayer. Then, an edge detection procedure with sub-pixel resolution is used to obtain the drop shapes from the recorded drop images.

A Langmuir trough surface balance is a miniature swimming pool, with a temperature controller, a wettable plate connected to an electronic balance located at the trough center for measuring the surface tension, and an automated pair of symmetrically moving barriers for changing the surface concentration, see Fig. 4.2. Here we employ a mini trough (M601) from NIMA Technology in UK. Surfactants are spread on the trough surface at some known surface concentration then the surface concentration is changed by moving the trough barriers with an area measurement accuracy of 0.5%. For soluble surfactants the compression has to be done fast enough to avoid surfactant exchange but slow enough so that surface viscous effects do not affect the surface tension measurement. In connection with the thermodynamic phase rule, the Langmuir balance data permits establishing the surfactant phases whose morphologies can be directly observed using optical techniques. The force on the plate is obtained from balance with an accuracy of ± 0.1 dynes. The highest compression rate that the mini trough is operated is 5 m/s to avoid bulk hydrodynamic effects. A force balance on the wettable plate accounting for gravity, bouyancy, and surface tension yields

$$f_p = (\rho_p lwt)g - (\rho_l hwt)g + 2\sigma(w+t)\cos\theta \qquad (4.1)$$

where ρ_p is the plate density, ρ_l is the liquid density, g is gravity, l is the total plate length, w is the plate width, t is the plate thickness, h is the liquid immersed plate length, σ is the surface tension, and θ is the contact angle between the liquid and plate. By using a Wilhelmy paper plate that has a zero contact angle, leveling the paper plate edge with the liquid surface to eliminate bouyancy, and zeroing before making a measurement the paper plate weight, Eq. 4.1 considerably reduces leading to

$$\sigma = \frac{f_p}{2(w+t)} \qquad (4.2)$$

The surfactants that we selected are water insoluble, octadecanol (OD) and the phospholipid 1,2-Dipalmitoyl-sn-Glycero-3-Phosphocholine (DPPC) respectively purchased from Fluka and Avanti Polar Lipids with purity greater than 99%. The solvent used to dissolved OD and DPPC is Chloroform from SIGMA with purity greater than 99.9% (HPLC grade). Chemicals are used as received without further purification. Water used in all experiments is deionized and filter with a system fitted with a column to remove trace contaminants from Millipore. The resistivity of the purified water is 18 $M\Omega$ cm. All glass, Teflon, and steel pieces are thoroughly cleaned before each experiment.

4.3 Results and Discussion

To use the new equation that we developed in Section 3.3 to measure the surface dilatational viscosity requires having negligible bulk hydrodynamic effects and an equation of state relating the compositional surface tension and surfactant surface concentration, the Langmuir isotherm of the surfactant monolayer. We first observe when bulk hydrodynamic effects become important by changing the volumetric flow rate of a clean pendant water drop since bulk hydrodynamic effects are proportional to the magnitude of the volumetric flow rate and then measure the Langmuir isotherms of the surfactant monolayers. The static Young-Laplace numerical formulation for measuring the surface tension of water (72 mN/m at 25 °C) does not include bulk hydrodynamic effects therefore it must fail to report the true value of the surface tension when bulk hydrodynamic effects are significant. During a drop compression or expansion the volumetric flow rate is constant and leads to and also constant area rate of change a typical run is shown in Fig. 4.3. Both rates are then set by adjusting the speed of a linear motor and have been first reported elsewhere [56, 61] to be constant. The water volumetric flow rate is expected to be constant since the syringe plunger velocity is constant and the cross sectional area of the syringe does not change. We think that the area rate of change is constant because the drop changes its volume as a right cylinder with constant local radius. Figs. 4.4 A and 4.5 show respectively pure water compressions and expansions and dictate how large are the volumetric flow rates that the Young-Laplace formulation can accommodate for our system. Failure of the Young-Laplace formulation due to bulk hydrodynamic effects is at once established observing an accuracy constraint of ±1 mN/m

on the measurement of the surface tension. Then, it is clear that we can compress and expand respectively at volumetric flow rates equal or smaller than 34.5 mm^3/s and 20.74 mm^3/s with minimal bulk hydrodynamic effects. The Weber and Capillary numbers for 34.5 mm^3/s are respectively $3.6x10^{-3}$ and $2.6x10^{-4}$. Why does bulk hydrodynamic effects become important for expansion at a smaller volumetric flow rate than for compression? A possible explanation based on a recent experimental and numerical study [42] is that during a drop formation depending on the volumetric flow rate flow recirculation occurs. The liquid elements entering the drop from the tube tend to flow toward the apex of the drop along its axis of symmetry until impinging on the drop apex then flow tangentially up into an annular space along the drop surface resulting in recirculation within the drop. Eventually, recirculation stops at some critical drop size and the fluid motion is basically in the downward direction as the drops fall, and our premise is that during drop compression recirculation does not occur.

We tried to correct the Young-Laplace surface tensions of the clean water compression experiments by accounting for the acceleration of the location of the apex or the location of the centroid as respectively shown in Figs. 4.4 B and 4.4 C. Because, we noted that as a drop reduces its volume it also oscillates as clearly displayed in Figs. 4.4 D and 4.4 E. We numerically obtained the drop acceleration as a function of time from the second derivatives of a cubic spline fitted to the experimental location of the apex or the location of the centroid versus time. We wrote the cubic spline computer program in FORTRAN 77[62-64]. The location of the centroid follows the location of the apex the

only difference is that the change in the magnitude of the centroid is smaller than for the apex, the same is true for the accelerations. We could not analytically obtained the accelerations because as the drop changes its volume it also changes its frequency. At the end, we can conclude by saying that our correction did not work for the clean water compression experiments because the flows had two components, an oscillatory flow and a dominant constant flow. But as we will demonstrate in Section 5.3 our correction works nicely for clean water drop oscillation experiments at considerably high forcing frequencies possibly because the flow is only oscillatory with a single frequency.

In what follows, we report measurements corresponding to the Langmuir monolayers of OD and DPPC. We selected OD because it is a simple saturated alcohol, a stearic chain with an OH group, and DPPC because it has the highest surface dilatational viscosity listed in Table 2.1 probably due to the entanglement generated by its two palmitic chains. When OD molecules are spread at the air-water interface to form an insoluble surfactant monolayer with the aid of a volatile solvent Langmuir trough compression measurements in connection with the thermodynamic phase rule indicate that octadecanol form the so called gaseous (G), liquid condensed (LC), and liquid solid (LS) phases. Fig. 4.6 reports our Langmuir trough isotherm of OD at 25 °C and pH 5.5. Recently, the Langmuir isotherm of OD was measured using the pendant drop apparatus as a Langmuir surface balance and the phase behavior was the same as on the flat interface of a Langmuir trough[56,60]. They also found that the collapse pressure of OD depends on the pendant drop molecular compression rate (PDMCR), the ratio of the area rate of change to the constant number of molecules spread at the interface. They explained their

findings based on Brewster angle microscopy done at a flat Langmuir trough interface. The PDMCR that they employed were as low as 0.081 $Å^2$/s-molecule and as high as 0.86 $Å^2$/s-molecule. We decided to extent their PDMCR range to see what happen above 0.86 $Å^2$/s-molecule. In Fig. 4.7 we show that the isotherms of OD obtained using the pendant drop apparatus at permitted expansion rates, as high as 9.26 $Å^2$/s-molecule, agree with the compression Langmuir isotherm of OD done at 0.17 $Å^2$/s-molecule. In Fig. 4.8 we show that the isotherms of octadecanol obtained using the pendant drop apparatus at permitted compression rates agree with the compression Langmuir isotherm of OD. For compressions, the agreement is true except when the PDMCR is increased by less than an order of magnitude in which case the OD monolayer locally collapses in the drop regions of higher area strain rates. A reasonable explanation is that the LC phase of OD is like a solid and can not withstand meaningful changes in area at considerably area rate of change. Clearly the experiments are measuring what they were designed to measure is just that OD is like a solid it prefers to collapse rather than to deform viscously like a liquid. It is also important to note that the area of the pendant drop is as good as the area of the Langmuir trough demonstrating that the computer program that we wrote to measure the area from the drop shape is highly accurate and precise.

At continuation, we measure the relationship between the compositional surface tension and the surfactant concentration of DPPC, a neutrally charged molecule with two lipophilic palmitic chains connected to a hydrophilic choline head. When DPPC molecules are spread at the air-water interface to form an insoluble surfactant monolayer with the aid of a volatile solvent Langmuir trough compression measurements in

connection with the thermodynamic phase rule indicate that DPPC form the so called gaseous (G), liquid expanded (LE), and liquid condensed (LC) phases [59,65-67]. In Fig. 4.9 we report the Langmuir trough isotherm of DPPC at 25 °C and pH 5.5. At flat Langmuir trough interfaces, the domains of these phases have been observed under the microscope using Brewster Angle and Fluorescence techniques. DPPC molecules are very far apart in the G, in an amorphous state characterized by random orientations of the hydrophobic chains with only the polar functional groups on the polar subphase in the LE, and with the hydrophobic chains tilted slightly with respect to the surface normal in the LC. DPPC does not form the liquid solid phase (LS) due to its large polar head. As mentioned in the introduction, ADSA can also be used as a Langmuir balance and in the past the results obtained with the traditional Langmuir balance have been compare with those obtained using the pendant drop apparatus. The conclusions of the systematic study of Miller and coworkers [60] are ADSA isotherms are consistent and Langmuir trough isotherms are also consistent for all the permissible compression rates but the shapes of the ADSA isotherms and the Langmuir trough isotherms are not identical. The Langmuir trough isotherms show a distinct plateau indicative of the LE-LC phase transition that is less observable in ADSA isotherms. We have also conducted the same Langmuir trough and ADSA study for DPPC and our results and conclusions are the same as those reached by Miller and coworkers. It was recently suggested [68] that the pendant drop curvature varies the domain shape and size during domain formation and growth and consequently does not allow the formation of the LE-LC phase transition of DPPC, if the

transforming units have a small size they increase the slope of the isotherm. The verification of this prevailing hypothesis is part of what we will suggest as future work. There are many applications of surfactant involving curve interfaces and thus it is important to further quantify how curvature affects the domain morphology and hence the compositional surface tension. Figure 4.10 reports the Langmuir trough and ADSA isotherms of DPPC at 0.28 $Å^2$/s-molecule and 0.2$Å^2$/s-molecule respectively.

The Langmuir trough and pendant drop isotherms agree within the LE phase of DPPC and allow determining the number of DPPC molecules spread at the air-water interface of a pendant drop. For the LE phase both techniques yield the same curves upon compressions and expansions and the collapse pressure of the phospholipid is 58 mN/m. Figure 4.11 shows that for the LE phase of DPPC a linear equation of state properly relates the surface tension and surface concentration. The slope of the linear equation of state also known as the compositional elasticity is -2699.9 (mN/m)/(molecule/$Å^2$) and the intercept is 99.47 mN/m. The number of surfactant molecules spread on a Langmuir trough is larger and therefore more accurately measured than the number of molecules spread at the drop surface. The number of molecules spread at the drop surface has also been measured directly from the surfactant solution concentration and spreading volume with a large error bar[59]. The LE compositional surface tension of DPPC for both Langmuir trough and ADSA is only a function of the surfactant concentration and for the same surface tension the number of molecules spread at the drop surface is just the product of the corresponding Langmuir trough surfactant concentration and drop area.

Now we are ready to measure the surface dilatational viscosity after showing how the conditions of negligible bulk hydrodynamic effects and linearity of the equation of state within a surfactant phase can be satisfied. A recent study[60] conducted at the air/water interface at 23 ^{0}C using the Pendant Drop Apparatus to quantify the effect of the molecular compression rate on the phase behavior of DPPC found that the area strain rate does not change the shape of the isotherm of DPPC. Their finding is correct but it does not extent to higher area strain rates, as it will be shown shortly. To increase the area strain rate to study DPPC we added to the Pendant Drop Apparatus a fast motion analyzer capable of recording 1000 full frames per second and found that the LE phase has a measurable surface dilatational viscosity as indicated by Fig. 4.12. A possible explanation for this behavior is that the energy required for making the hydrophobic tails of DPPC move vertically is inefficiently spent in the LE phase because of its intrinsic randomness[60]. The surface dilatational viscosity can be measured from Fig. 4.13 (compositional-dilatational surface tension versus inverse area) a linear regression is appropriate and yields a slope from which the surface dilatational viscosity can be calculated using Eq. 3.16. When doing the fit we use the intercept of the equation of states of the LE phase of DPPC, 99.47 mN/m, as theoretically required and experimentally measured using both the pendant drop apparatus and the Langmuir trough surface balance. Table 4.1 covers our fast compression runs and indicates that the surface dilatational viscosity of the LE phase of DPPC is approximately 1.3 mNs/m. At point, it is important to compare our results with the values listed in Table 2.1. The upper limit

reported by Snik and collaborators is the closest to our results. The surface dilatational viscosities obtained using the Longitudinal Wave Technique are two orders of magnitude larger than our numbers partly due to the invasive role of the Wilhelmy plate. We will not compare our numbers with those of Palmer and collaborators since they were obtained at extremely low surfactant concentrations. The fast compression data indicate that the LC phase of DPPC is inviscid since rapid compression of this phase yield the same Langmuir trough results, as shown in Fig. 4.12 at 22.5 $Å^2$/s-molecule

3.4 Summary

In this chapter, we established a new technique for measuring the surface dilatational viscosity based on a constant rate of area change instead of an oscillatory rate of area change. It is less expensive to produce a constant rate of area change than to produce an oscillatory rate of area change. We also validated experimentally the theory developed in Chapter 3. The results of our compression experiments show that the surface dilatational viscosity of the expanded phase of DPPC is approximately 1.3 mNs/m. This value agrees with the upper limit reported by Snik and collaborators and also with the values that we will report in the next chapter from oscillatory experiments. We conducted the experiments after enhancing the pendant drop apparatus with a fast motion analyzer.

Table 4.1
Pendant Drop Surface Dilatational Viscosity Measurements from Fast Compressions within the Liquid Expanded Phase of DPPC at 25 ^{0}C

A_0 (mm^2)	dA/dt (mm^2/s)	σ_0 mN/m	Γ_0 (molecule/Å^2)	PDMCR Å^2/s-molecule	κ_s (mNs/m)
32.50	14.88	67.0	0.0120	36.4	1.3 ± 0.2

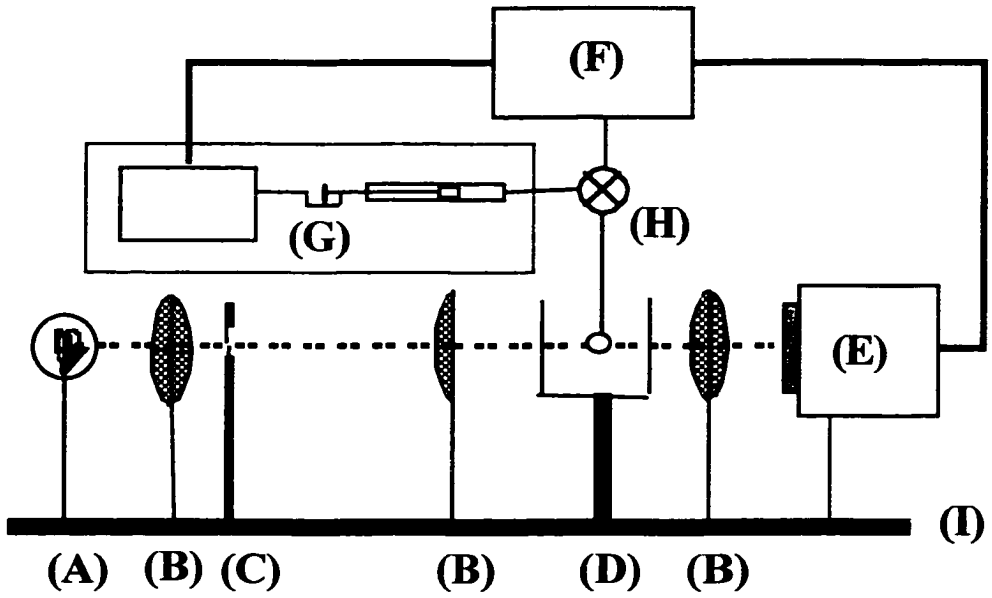

Fig. 4.1 Pendant drop apparatus for measuring the surface dilatational viscosity from compression experiments: (A) light source, (B) lens, (C) pin hole, (D) quartz cuvette and surfactant laden water drop, (E) fast motion analyzer, (F) computer, (G) linear syringe pump, (H) valve, and (I) isolation vibration table.

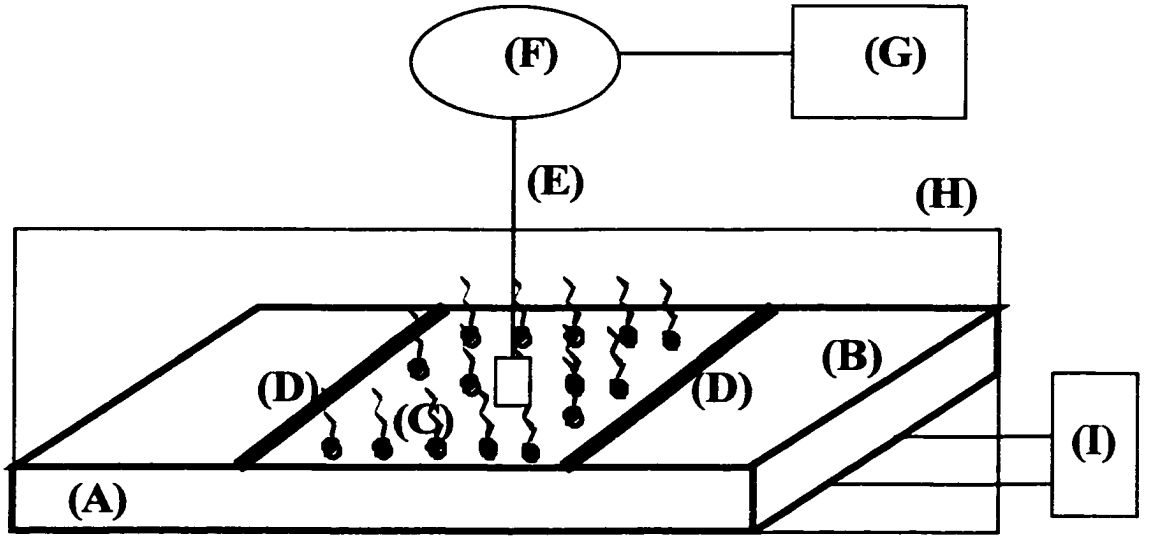

Fig. 4.2 Langmuir trough surface balance for measuring surface tension versus surfactant surface concentration: (A) trough, (B) water, (C) insoluble surfactant monolayer, (D) moving barrier, (E) paper plate, (F) balance arm, (G) computer, (H) protection rectangle, and (I) temperature controller.

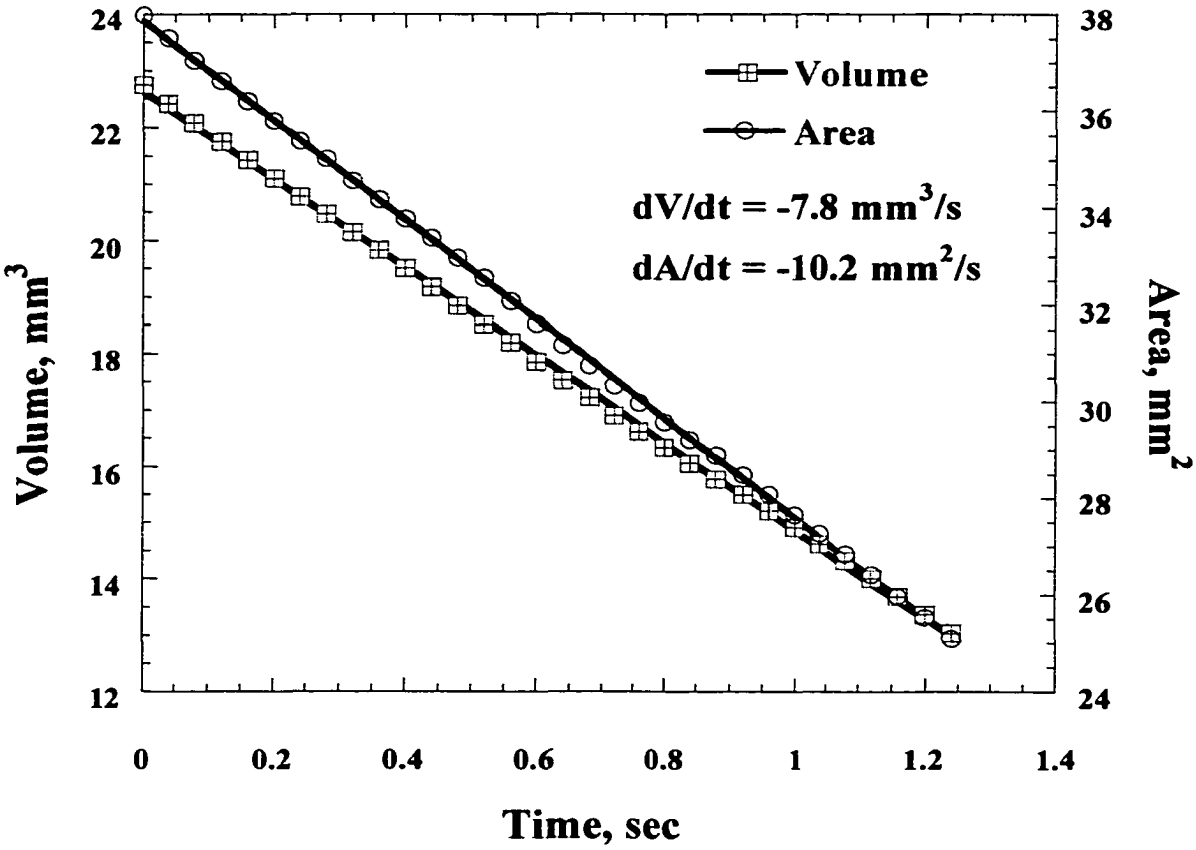

Fig. 4.3 Area and volume versus time of a compressing pendant drop.

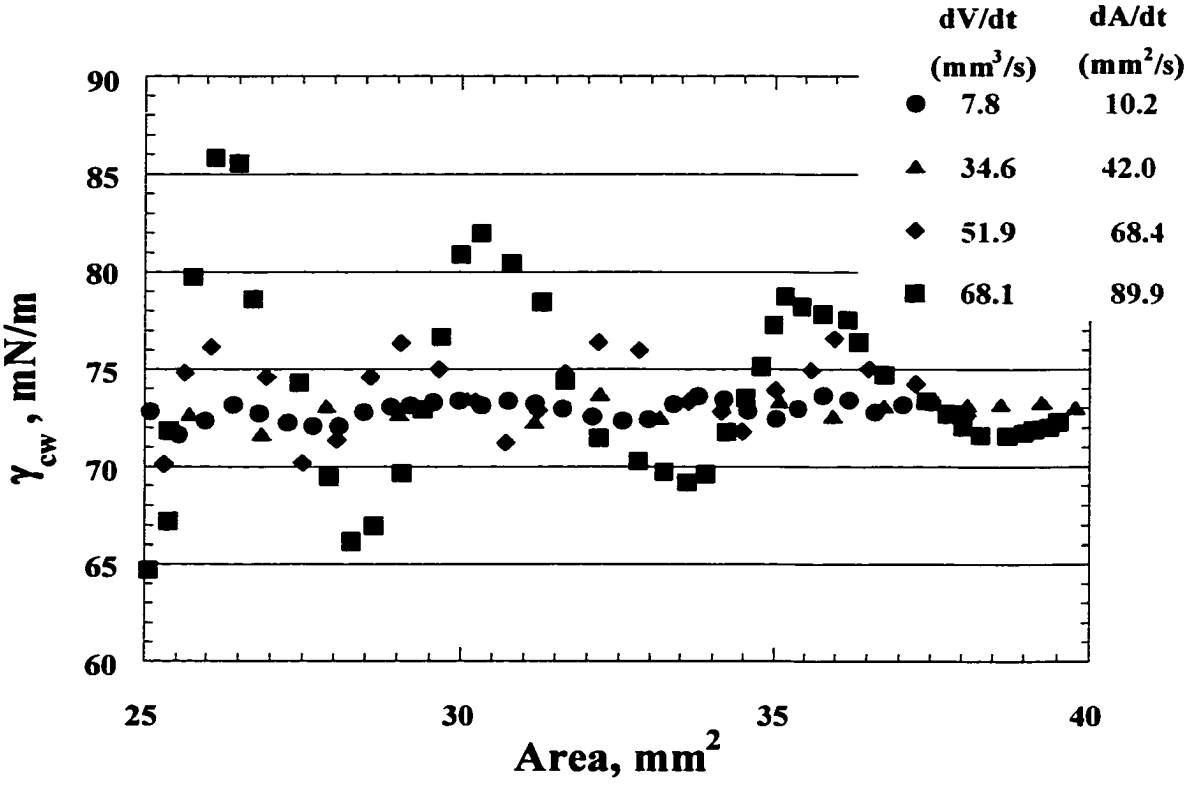

Fig. 4.4 A Compressions of clean water pendant drops at different volumetric flow rates: Young-Laplace surface tension versus area.

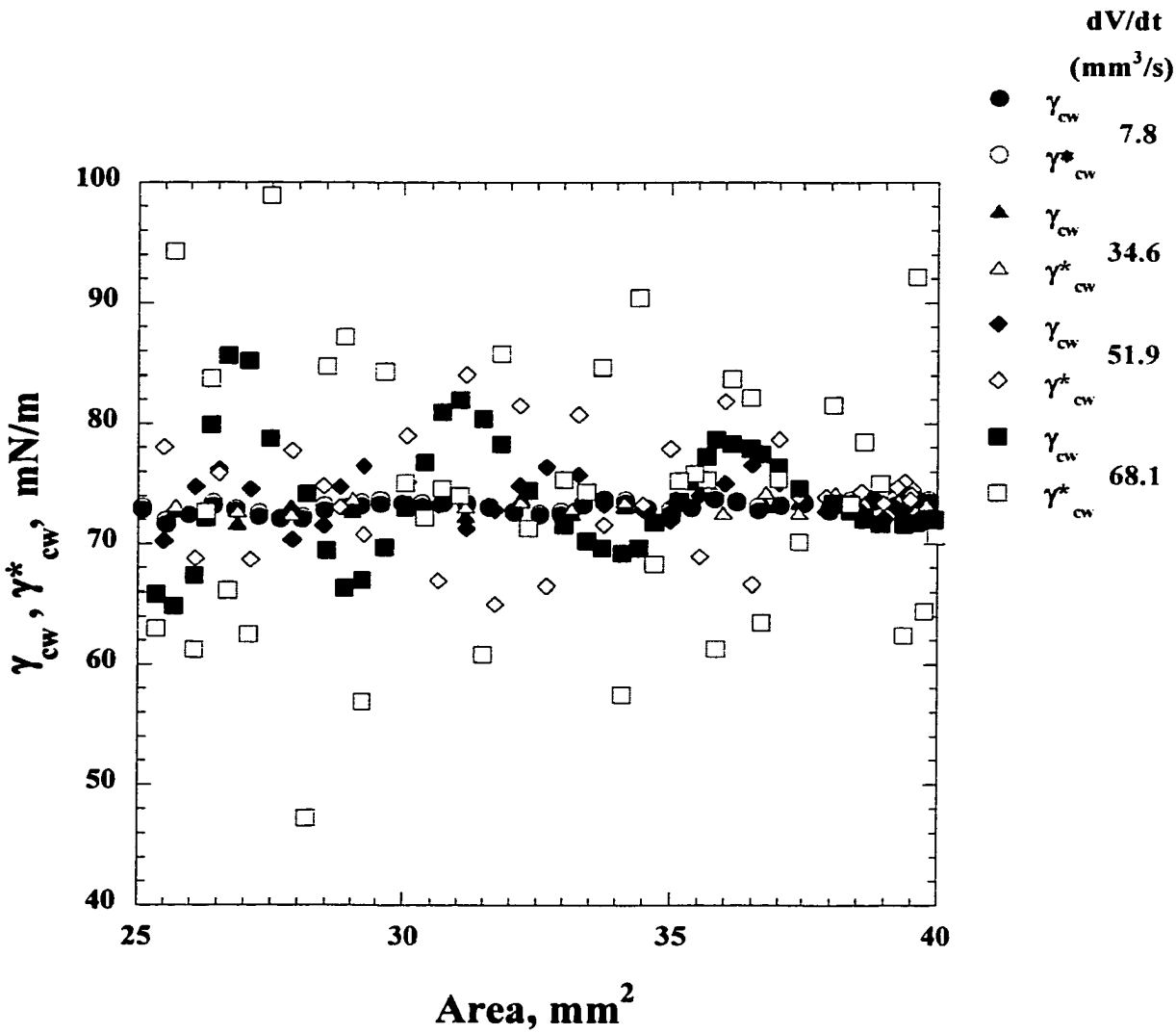

Fig. 4.4 B Compressions of clean water pendant drops at different volumetric flow rates: Young-Laplace surface tension and corrected surface tension using the acceleration of the vertical location of the apex versus area.

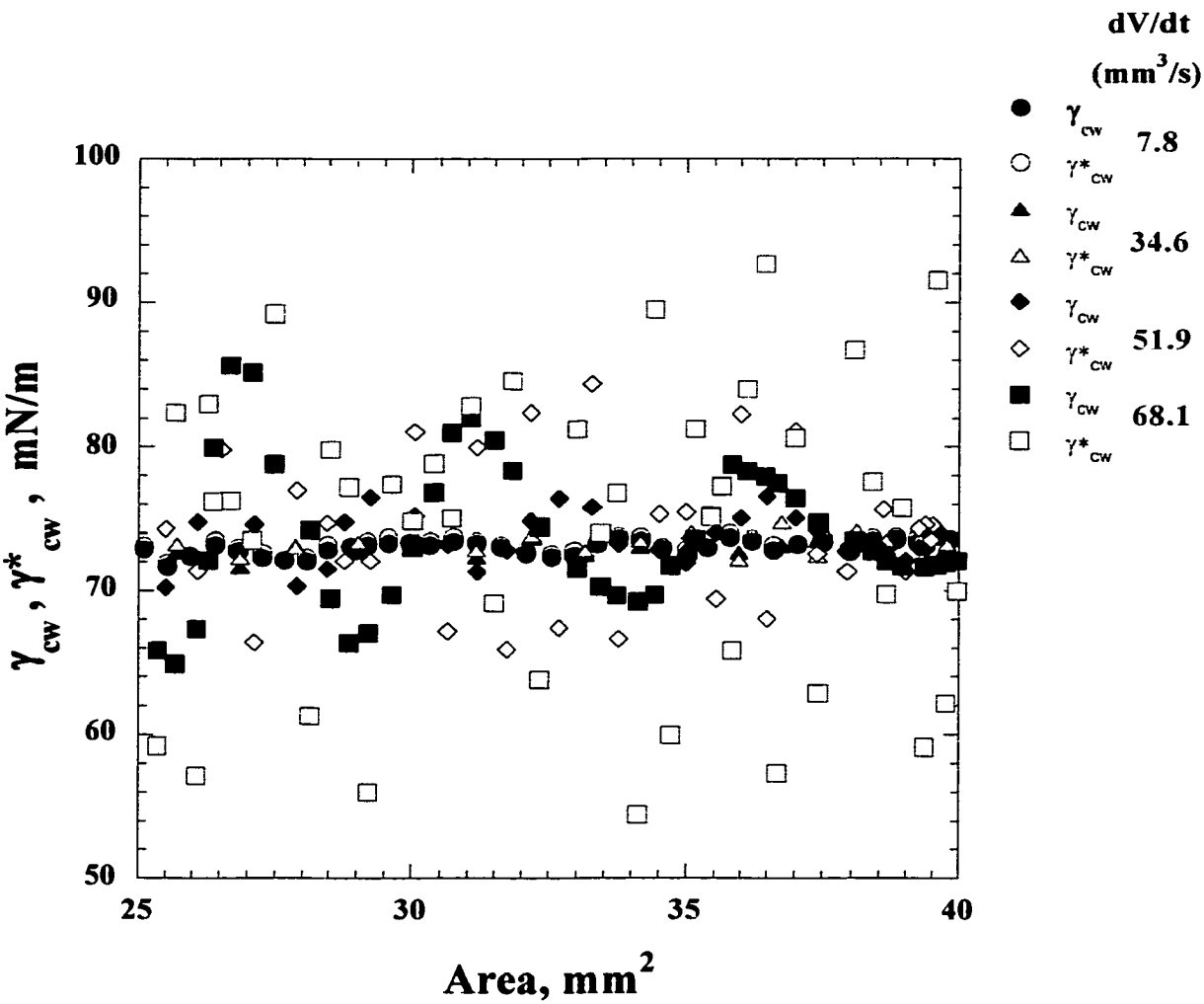

Fig. 4.4 C Compressions of clean water pendant drops at different volumetric flow rates: Young-Laplace surface tension and corrected surface tension using the acceleration of the vertical location of the centroid versus area.

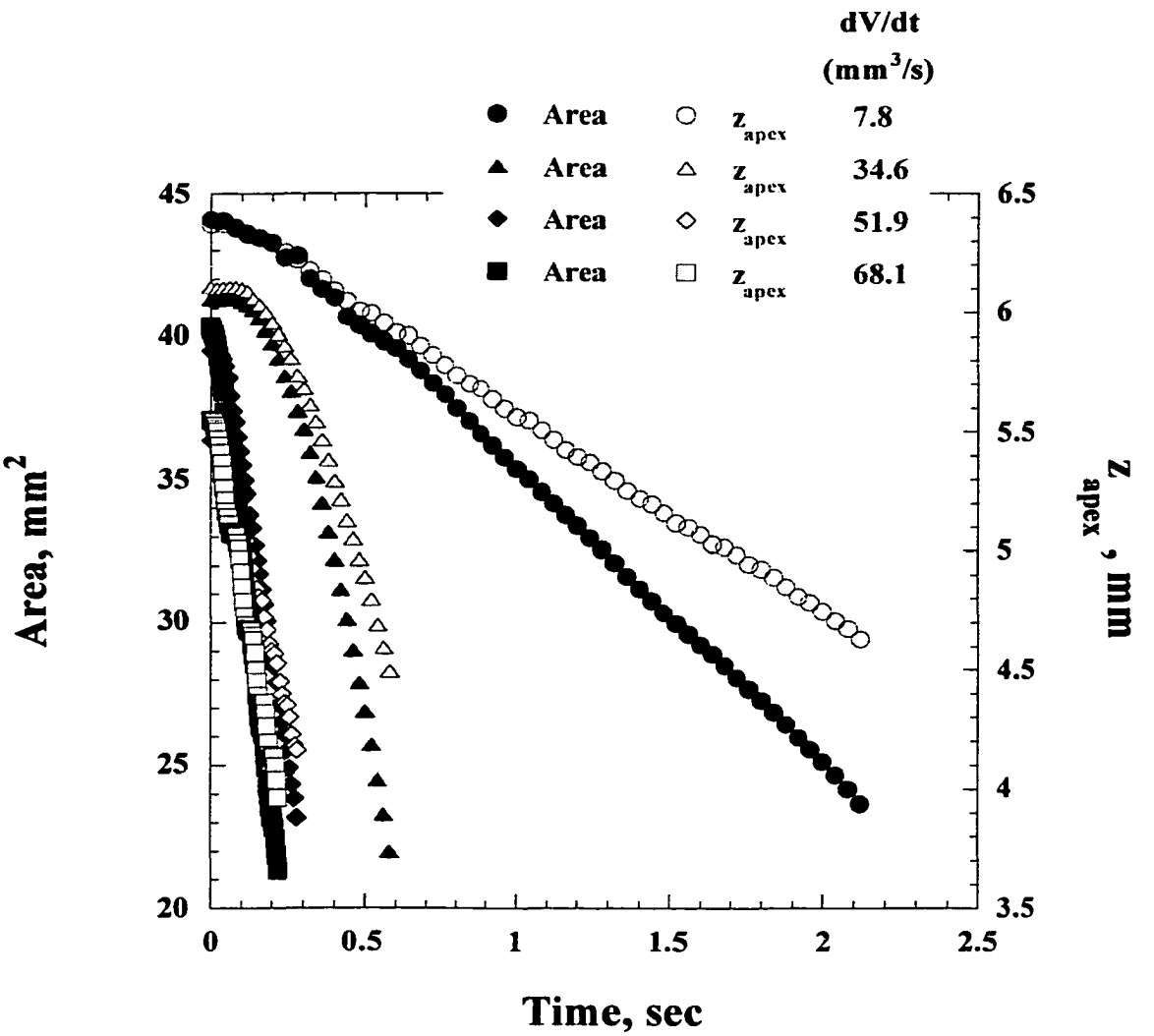

Fig. 4.4 D Compressions of clean water pendant drops at different volumetric flow rates: area and vertical location of the apex versus time.

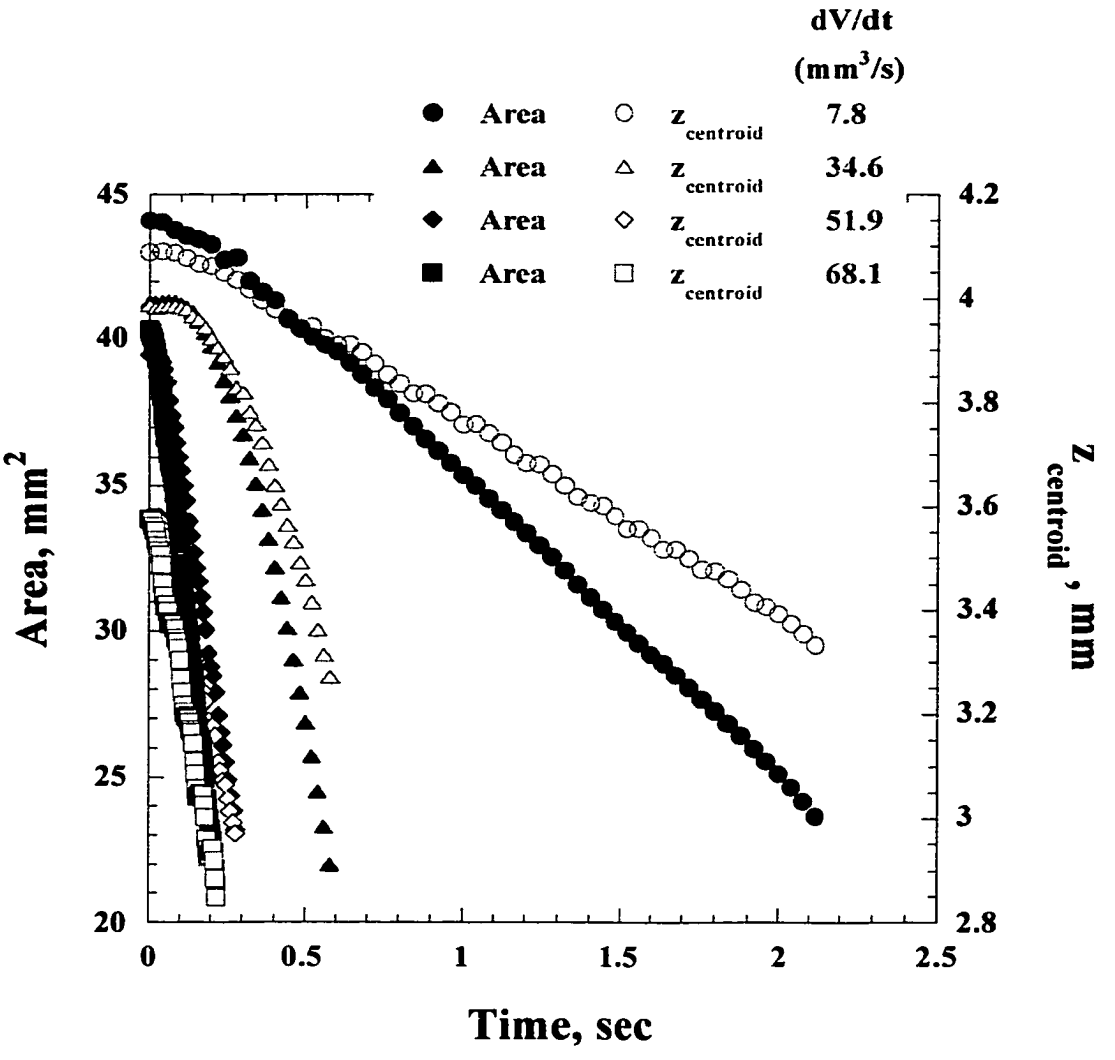

Fig. 4.4 E Compressions of clean water pendant drops at different volumetric flow rates: area and vertical location of the centroid versus time.

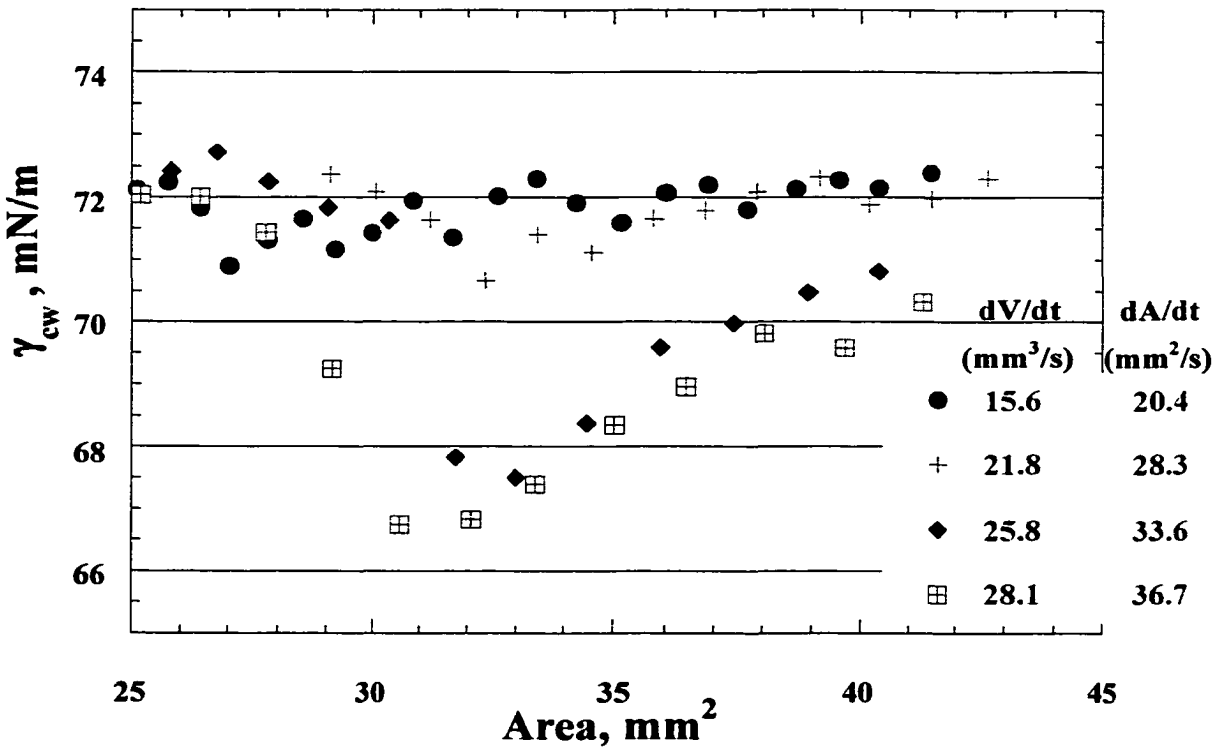

Fig. 4.5 Expansions of clean water pendant drops: Young-Laplace surface tension versus area as a function of volumetric flow rate.

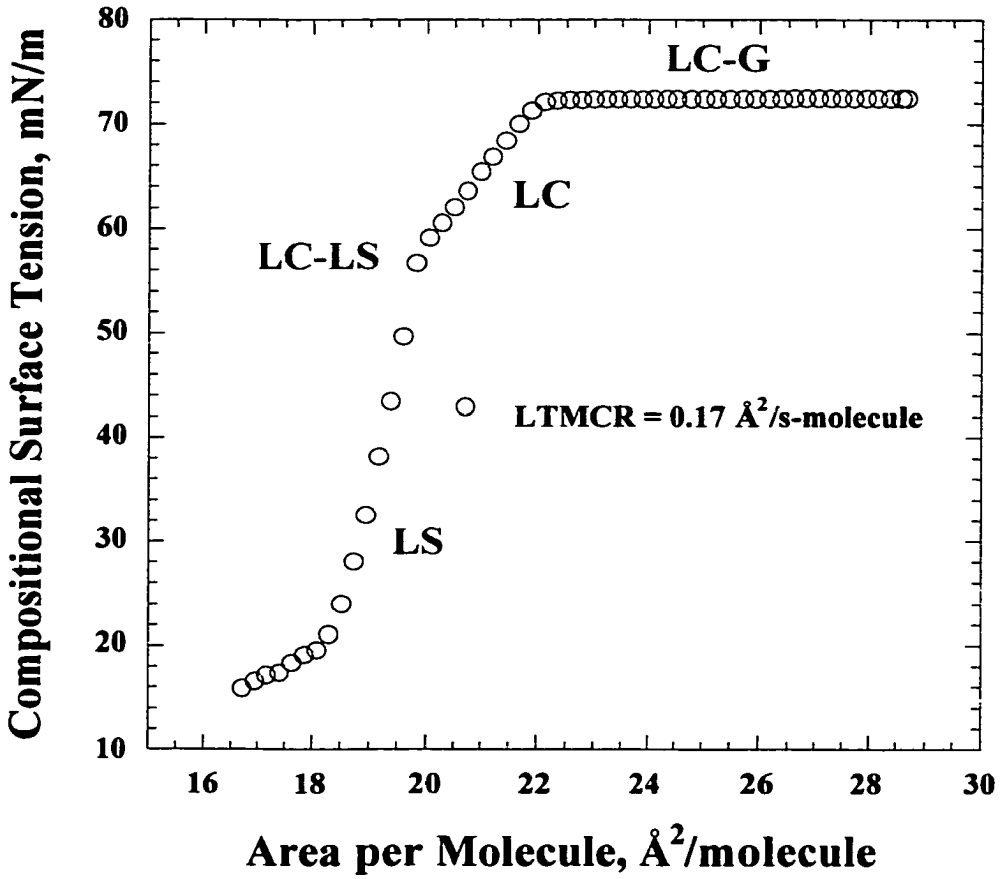

Fig. 4.6 Langmuir trough isotherm of octadecanol obtained at 25 ^{0}C and pH 5.5: compositional surface tension versus area per molecule.

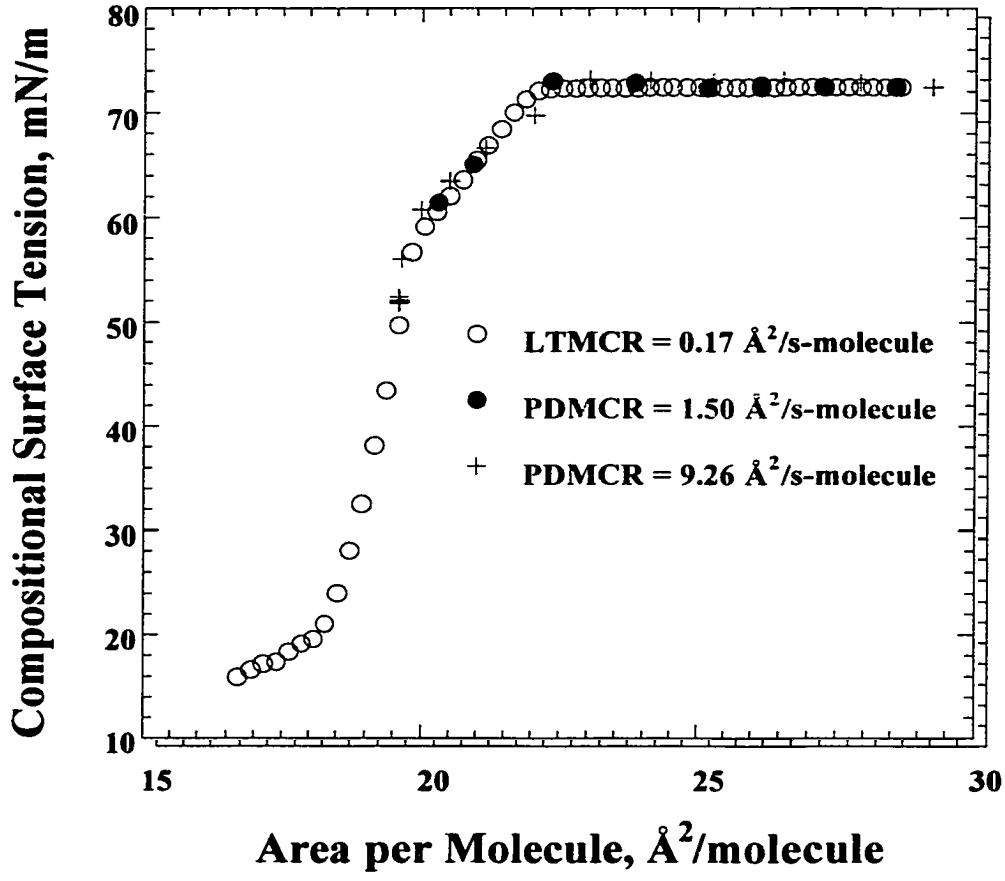

Fig. 4.7 Comparison of the isotherms of octadecanol obtained using the Langmuir trough and the pendant drop apparatus at different expansion strain rates: compositional surface tension versus area per molecule.

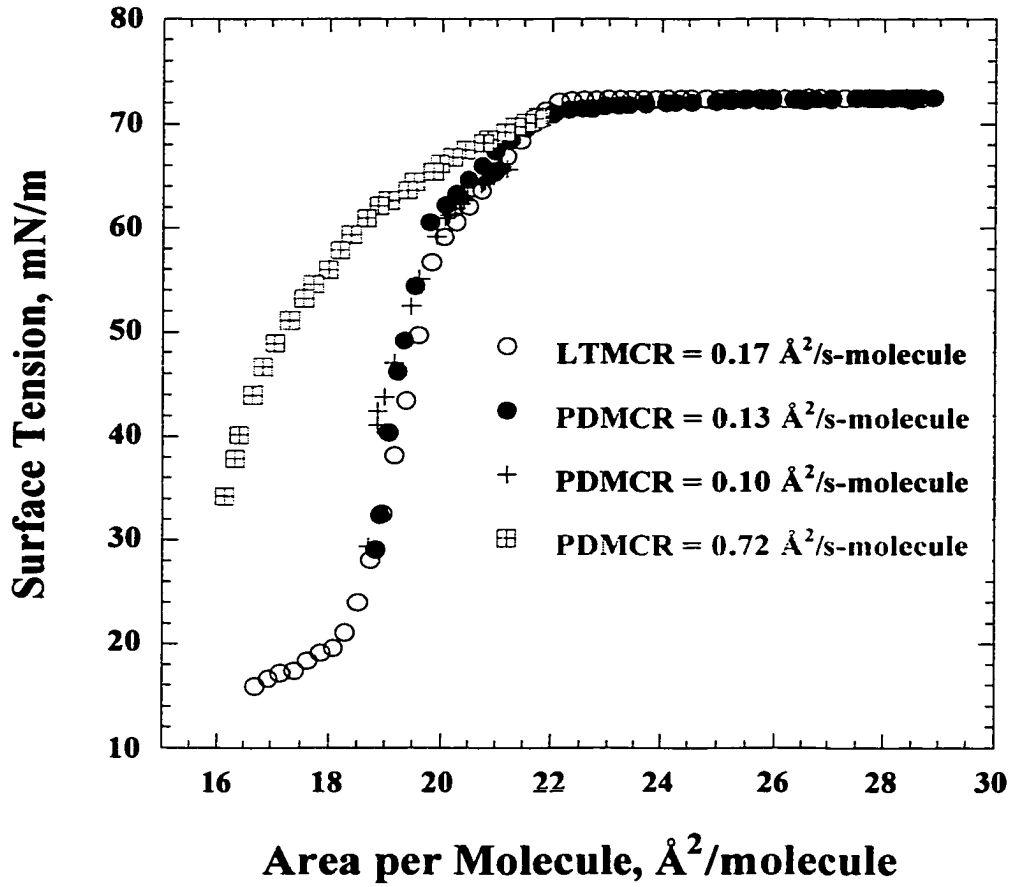

Fig. 4.8 Comparison of the isotherms of octadecanol obtained using the Langmuir trough and the pendant drop apparatus at different compression strain rates: surface tension versus area per molecule.

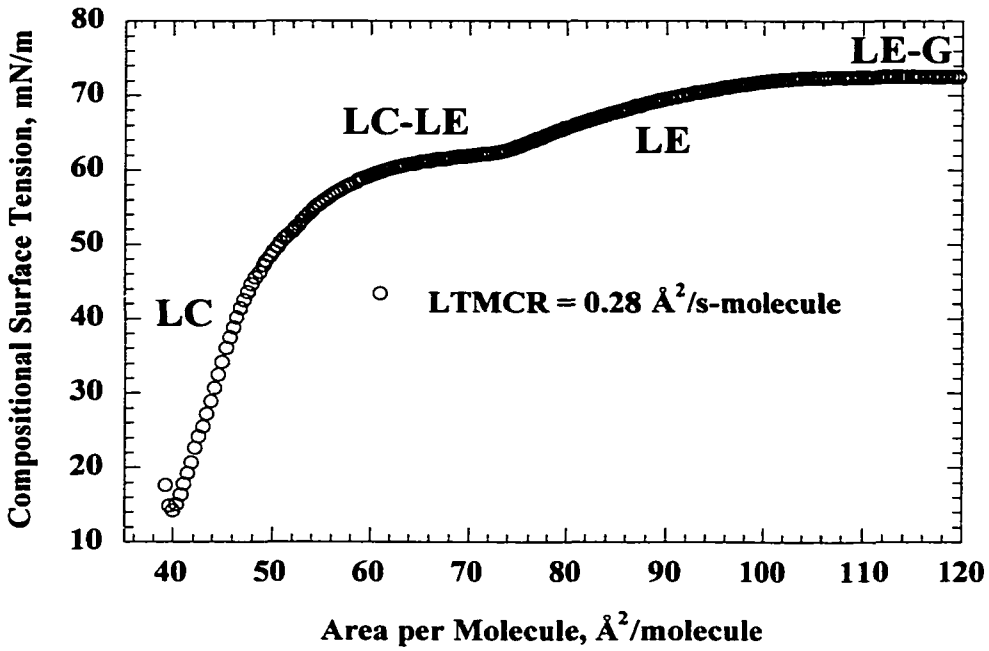

Fig. 4.9 Langmuir trough isotherm of DPPC measured at 25 ^{0}C and pH 5.5: compositional surface tension versus area per molecule.

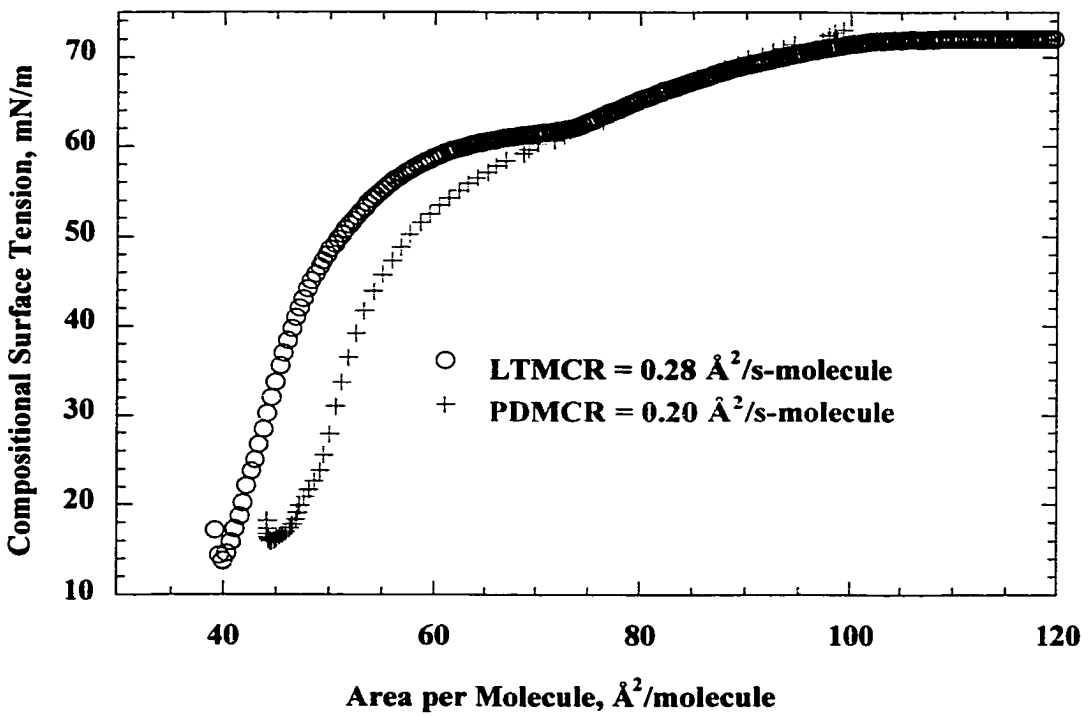

Fig. 4.10 Comparison of the isotherms of DPPC obtained using the Langmuir trough and the pendant drop apparatus: compositional surface tension versus area per molecule.

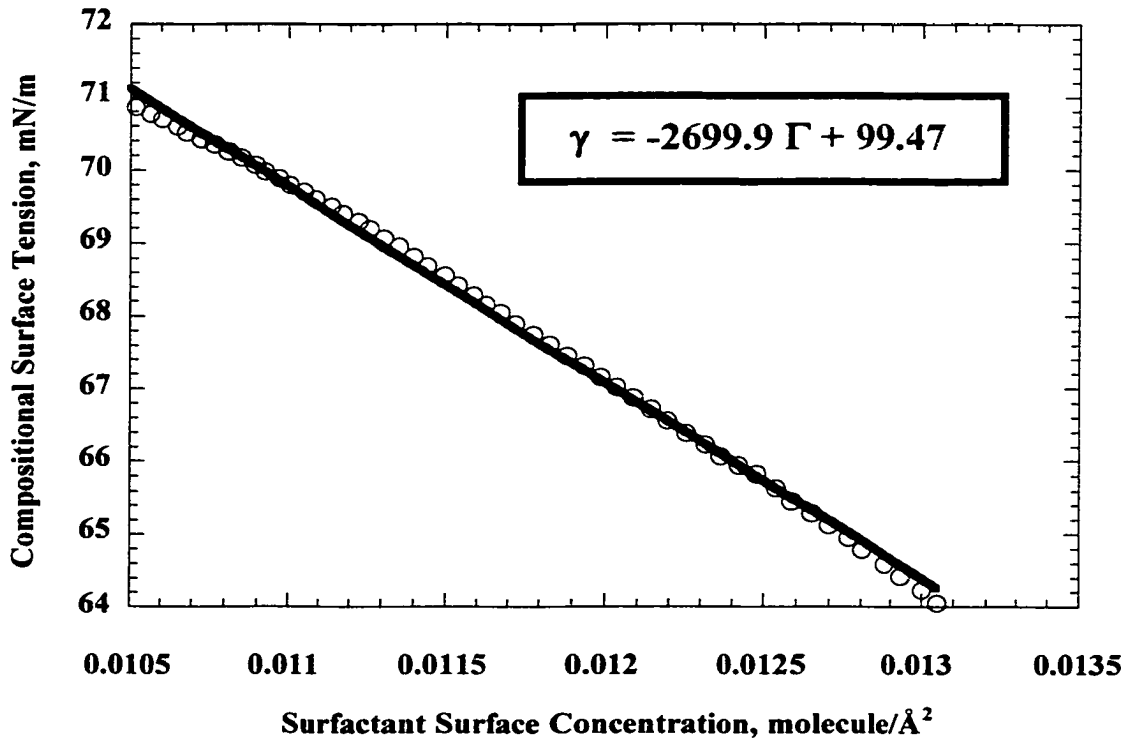

Fig. 4.11 Equation of state of the liquid expanded phase of DPPC: compositional surface tension versus surfactant surface concentration.

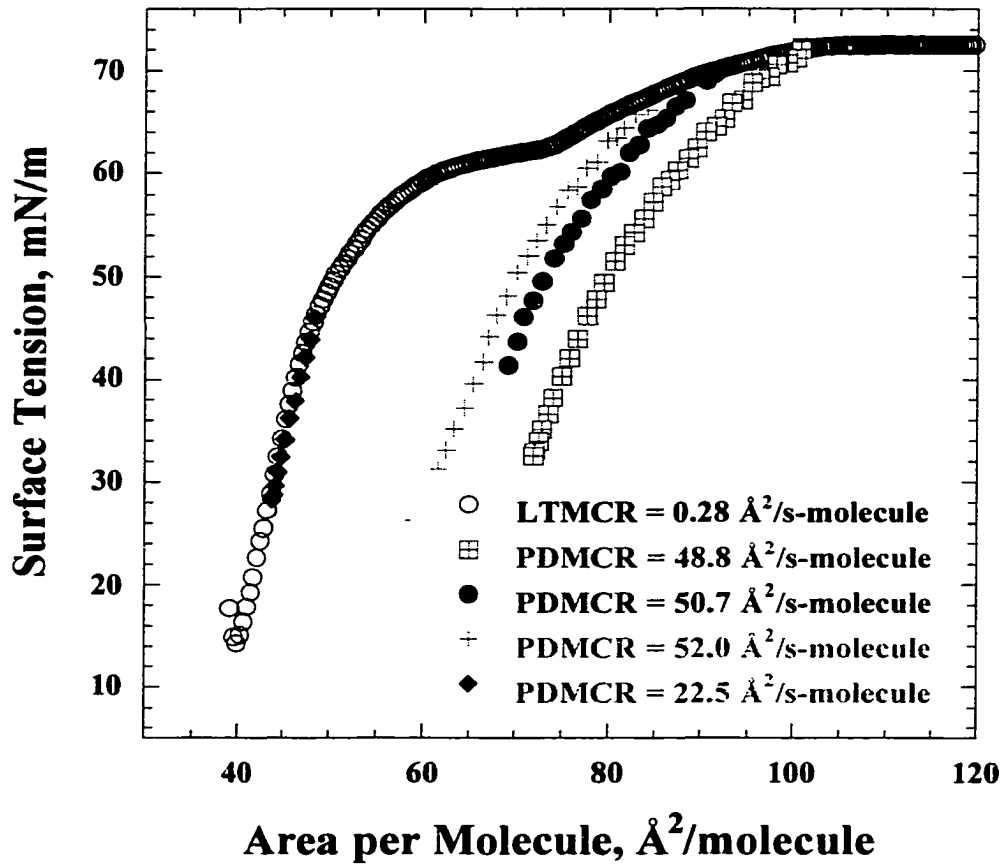

Fig. 4.12 Langmuir trough isotherm and fast pendant drop compressions of DPPC: surface tension versus area per molecule.

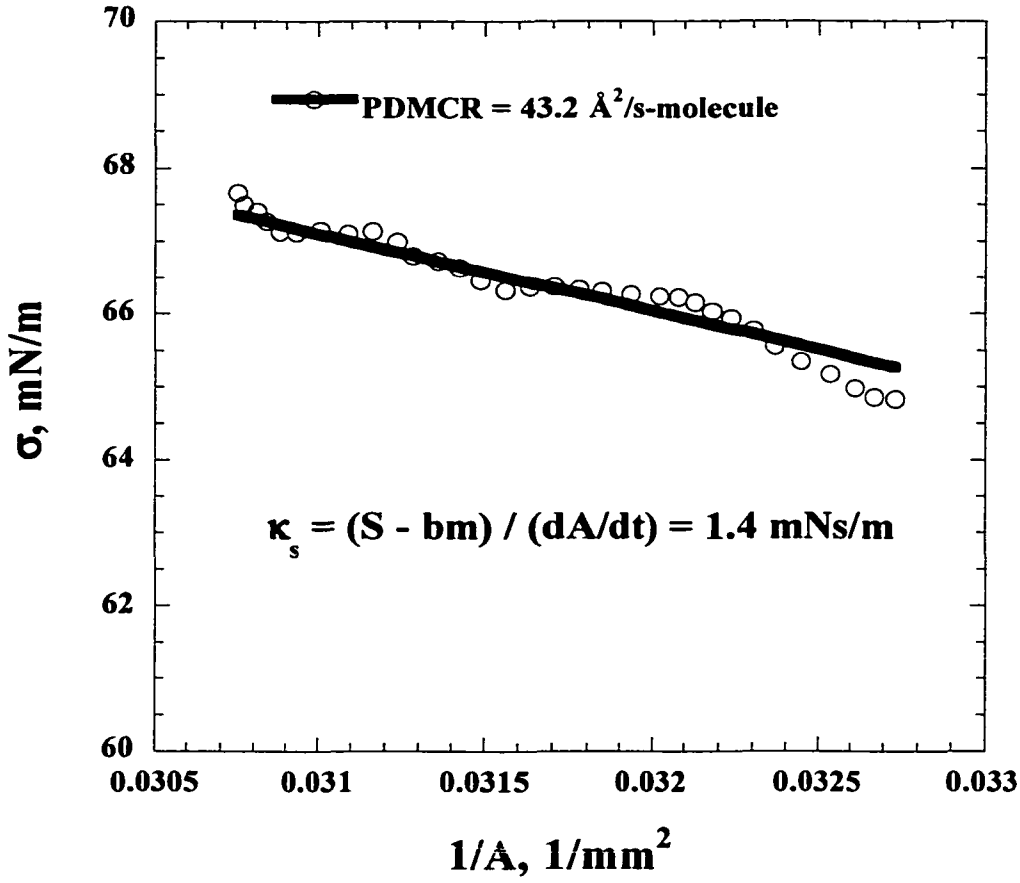

Fig. 4.13 Compositional-dilatational surface tension versus inverse area within the liquid expanded phase of DPPC corresponding to a fast-pendant-drop compression.

Chapter 5

Measuring the Surface Dilatational Viscosities of Surfactant Monolayers at the Air-Water Interface by the Shape Analysis of Oscillating Pendant Drops

5.1 Introduction

The oscillatory axisymmetric drop shape analysis (OADSA) for non-invasively measuring the viscoelasticities of surfactant monolayers at soft interfaces was introduced in 1996 by J. Benjamins, A. Cagna, and E. Lucassen-Reynders[51] and independently reintroduced in 1998 by Rolf Myrvold and Finn Hansen[18]. OADSA is based on the axisymmetric drop shape analysis (ADSA) of quasistatic pendant drops and bubbles rather than spherical bubbles and drops. ADSA provides accurate surface tension measurements if bulk hydrodynamic effects are substantially less than capillarity. In this method the silhouette of the bubble (drop) is image onto a video camera and the drop shape or interface is obtained by edge detection of the video image. Then, an experimental shape is compared with theoretical shapes corresponding to solutions of the Young-Laplace equation generated for different values of the surface tension until computing a theoretical shape that optimally matches the experimental shape. The tension so obtained is more accurate than other methods relying on a single measurement such as the force on a Wilhelmy plate or the pressure in a bubble. Due to the improved accuracy on the surface tension measurement, the shape analysis technique has been used

as an accurate surface film balance for measuring Langmuir isotherms. In this application, a drop is formed at the tip of a needle and an insoluble surfactant monolayer is spread at the drop air-water interface. The drop area is then reduced by slowly decreasing the drop volume, and the tension is measured from the drop shape as before.

OADSA has only been used for polymeric surfactant systems yielding a very small phase angle employing frequencies as low as 0.2 Hz and as high as to 2 Hz, area changes as low as 2 % and as high as 5 %, and resulting area strain rate as high as 0.45 s^{-1}. The first results from OADSA correspond to three different adsorbed proteins at the air-water surface and oil-water interface. The second results from this oscillatory pendant drop technique are due to Hansen and coworkers and correspond to measurements of the viscoelasticities of three adsorbed polymeric surfactant monolayer at the air-water interface of a bubble.

In this chapter, our first objective is to use OADSA to accurately measure the surface dilatational viscosities of non-polymeric surfactant monolayers at the air-water interface and our second objective is to increase the forcing frequency at which the technique can be used. The second objective addresses a suggestion given as future work by the originators of OADSA to oscillate at frequencies found in practical applications. If the frequency increases, the dilatational strain rate increases and thus the surface dilatational viscous contribution is larger. We consider at the air-water interface the simple surfactant monolayers of DPPC and TP together with mixed DPPC/OD monolayers in mole ratios 1:1 and 3:1. The reason to consider only monolayers of water insoluble surfactants is to easy the measurement since mass transfer between the bulk and

the interface does not occur. We selected DPPC because it will allow us to compare with the results listed in Table 2.1 and the values that we obtained in Chapter 4. We selected TP because it has three chains and thus we expect considerable entanglement. The mixed monolayers are considered just because Djabbarah et al. [69] using the surface longitudinal wave tracer particle technique found that the net surface dilatational viscosity of a Gibbs monolayer of SDS increases by adding dodecanol by one order of magnitude from 3.5 to 24 μNs/m. The net surface viscosity is the sum of the compositional, shear, and dilatational viscosities. Another reason to study mixed monolayers is because many relevant systems are mixed. We will only be able to compare our results with those published in the literature for DPPC because the viscoelasticities of TP and the binary mixtures that we opted for are not reported in the literature to the best of our knowledge.

4.2 Experimental Section

To conduct the oscillatory experiments we designed and built an oscillatory piezoelectric syringe pump and then added the pump to the pendant drop apparatus early described in Section 4.2. The oscillatory syringe pump consists of a 25 ml Hamilton gas tight syringe, a piezoelectric pusher (PZL-060-11, Burleigh Instruments, Inc.), a voltage amplifier (PZ-150-1, Burleigh Instruments, Inc.), and an arbitrary waveform generator (HP-33120A, Hewlett Packard). The total cost of the new oscillatory piezoelectric syringe pump was only approximately 6,000 dollars. The first experimental step is to spread a Langmuir monolayer at the air-water interface of a

pendant water drop a few mm in diameter at the tip of a needle as we do in the beginning of a drop compression experiment, please refer to section 4.2 for the details. Then instead of rapidly compressing the drop, we use the oscillatory syringe pump to oscillate the drop volume and consequently the drop area, surfactant surface concentration, and surface tension. We can easily set the amplitude and frequency of the drop volume with the oscillatory pump wave generator. The interfacial tension and dilatational strain rate are measured simultaneously as a function of time from the oscillating drop shape obtained using the pendant drop apparatus. From the phase angle between the surface area and tension the surface dilatational viscosity is obtained.

5.3 Results and Discussion

The theory presented in Chapter 3 for measuring the viscoelasticities of surfactant monolayers using a pendant drop apparatus requires having negligible bulk hydrodynamic effects. The static Young-Laplace equation used for measuring the surface tension is valid only if bulk hydrodynamic effects are negligible and thus fails to report the true value of the surface tension when bulk hydrodynamic effects are important. For this reason in the past, oscillatory surfactant experiments were conducted at low frequencies from 0.2 Hz to 2 Hz and reasonable changes in area to avoid bulk hydrodynamic effects. We found that to completely capture an oscillation at 20 Hz requires a recording rate of 500 f/s. At continuation, we describe what happens when a clean water drop is oscillated at 0.2, 1, 2, 10, and 20 Hz to determine the most convenient changes in area at which some of these frequencies can be used to conduct the surfactant experiments with minimal bulk

hydrodynamic effects. Figs. 5.2 and 5.3 show respectively experimental area and surface tension versus time for 0.2 Hz and 1 Hz. The experimental areas follow closely a sine curves with forcing frequencies almost identical to the set electronic frequencies and the surface tension is 72 ± 0.3 mN/m measured using the static Young-Laplace equation for the small changes in area. Fig. 5.4 A shows area, surface tension again measured using the static Young-Laplace equation, and corrected surface tension measured using our dynamic version of the Young-Laplace equation. The area still follows closely a sine curve with a forcing frequency equal to the set electronic frequency and the corrected surface tension is substantially closer to the true value of the surface tension than the surface tension obtained from the static Young-Laplace equation. To conduct the correction only requires calculating the axial inertia acceleration from the location of the apex or the centroid as a function of time from data similar to Figs 5.4 B and C. To complete the correction just requires adding to the static Young-Laplace equation the drop axial inertia acceleration to account for bulk hydrodynamic effects. The reason that the uncorrected surface tension is 180 degrees out of phase with the area is that the area is totally in phase with the location of the apex and the centroid. Table 5.1 summarizes our clean water drop results for the five considered frequencies and amplitudes and suggests using our correction only for the high frequencies, 10 and 20 Hz. The reason that the correction is not needed at low frequencies is because the acceleration is very small, of the order of the frequency squared.

Now guided by the numbers reported in Tables 2.1 and 5.1 we designed the surfactant experiments so that the change in the compositional-dilatational surface tension

is larger than the undesired bulk hydrodynamic effect. The expanded phase of DPPC has a measurable surface dilatational viscosity and is a good starting point to begin our surfactant oscillatory experiments. The surface dilatational viscosity is calculated from a figure called the oscillatory viscoelastic figure showing the experimental and fitted areas and compositional-dilatational surface tensions versus time. From the experimental and fitted areas versus time we obtain the area amplitude, area reference, and area frequency and from the compositional-dilatational surface tensions versus time we obtain the surface tension amplitude, surface tension reference, and surface tension phase angle. The area frequency is used as the forcing frequency of the surface tension. The experimental data are fit numerically using sine curves by a non-linear Levenberg-Marquardt procedure capable of obtaining the optimal parameters even if the data is noisy[18]. The initial guesses required by the non-linear fit are obtained by pre-processing the data, for instance, the reference and amplitude values can be estimated from the arithmetic mean. Also, in our experiments it turns out that the forcing frequencies are almost identical to the electronic frequencies. Using the above numerical procedure usually yields an excellent fit of sine functions to the experimental data. According to Hansen and collaborators[18] a Fourier transform is not used because "the transformed time function should only contained ideally the main harmonic components, however, minimal noise in the experimental data usually give rise to higher harmonics content, which may complicate the analysis."

At this point, we discuss our results corresponding to the Langmuir monolayers of DPPC and TP. The reason that we became interested in TP was because it has three palmitic chains instead of two palmitic chains as is the case with DPPC and we think that the number of chains is proportional to entanglement and entanglement is proportional to the surface dilatational viscosity. Also, TP together with DPPC is an active ingredient in a formulation use to treat a lung deficiency. Table 5.2 summarizes the analysis of Figs. 5.5, 5.6 and 5.8 are the oscillatory viscoelastic figures of DPPC and TP at 0.2 and 1 Hz. Fig. 5.7 is the Langmuir isotherm of TP obtained at 25 °C and pH 5.5. The isotherm of TP has been measured in the past and our results agree with those published in the literature. It is important to mention that we have compared the elasticities measured using OADSA with those measured using the Langmuir trough and compare our results with the values listed in Tables 2.1 and 4.1 for DPPC, the upper limit reported by Snik and collaborators is the closest to our results. The surface dilatational viscosities measured using the longitudinal wave technique are two orders of magnitude larger than our numbers but perhaps this is partly due to the invasive role of the Wilhelmy plate. We will not consider the values reported by Palmer and collaborators since they were obtained at extremely low surfactant surface concentrations.

In what follows, we measure using OADSA the viscoelasticities of the mixed binary monolayers of DPPC and OD in mole ratios 1:1 and 3:1. The model that we derived in Chapter 3 is also applicable to measuring the viscoelasticities of a mixed surfactant monolayer but instead of obtaining the viscoelasticities of the individual component we will obtain those of the mixture. Our results for the mixed systems are

shown in Table 5.3. The measurements indicate that the surface viscoelasticities of DPPC twice by the addition of OD.

5.4 Summary

In this study, we extended the frequency range of OADSA from 0.2-2 Hz to 0.2-20 Hz. This increment was possible due to the first order correction of the static Young-Laplace equation that we proposed and experimentally validated. To force the pendant drop to oscillate smoothly at high frequencies, we designed a piezoelectric syringe pump and added it to the pendant drop apparatus capable of capturing 1000 full frames per second. Then, we found experimental conditions under which the phase angle could be directly observed and measured for the first time owing only to surface dilatational viscous effects. We measured the surface dilatational viscosities of the LE phase of DPPC and the LC phase of TP. As permitted, we compared our results with those reported in the literature and found a reasonable agreement. Our results on the mixed monolayers indicate that the surface viscoelasticities of DPPC twice by the addition of octadecanol as shown in Table 5.3. Therefore, we learned how to control the surface dilatational viscosity by using a co-surfactant.

Table 5.1
Surface Tension Measurements of Oscillating Clean Water Pendant Drops Using the Static Young-Laplace Equation and Our Correction

f (Hz)	A_a/A_0 (%)	$(\gamma_{cw,\,max} - \gamma_{cw,\,min})/2$ (mN/m)	$(\gamma^*_{cw,\,max} - \gamma^*_{cw,\,min})/2$ (mN/m)
0.2	1.6	0.3	0.3
	4.6	0.5	0.5
	11.7	0.8	0.8
1	2.8	0.2	0.2
	4.7	0.5	0.5
	5.7	0.4	0.4
2	2.4	0.7	0.7
10	1.2	1.6	0.7
	3.5	3.4	1.3
	4.2	6.1	3.4
20	1.3	6.0	1.1
	2.2	7.1	1.5
	2.9	14.0	5.2

Table 5.2
Pendant Drop Viscoelastic Measurements from Oscillating the LE Phase of DPPC and the LC Phase of TP at the Air-Water Interface at 25 °C

Surfactant	f (Hz)	A_a/A_0 (%)	σ_0 (mN/m)	σ_a (mN/m)	δ (deg)	κ_s (mNs/m)	E_0	Γ_0 (molecule/Å^2)
DPPC	0.2	1.5	65.5	0.9	3.8	2.3	0.8 (0.5)	0.0126
	1	2.7	66.2	1.3	6.5	0.8	0.7 (0.5)	0.0122
TP	1	1.5	68.0	1.2	4.9	1.0	1.1 (1.0)	0.0146

The dimensionless reference elasticities given in parentheses and the surfactant surface concentrations were obtained from the Langmuir trough isotherms.

Table 5.3
Pendant Drop Surface Viscoelastic Measurements from Oscillating Mixed DPPC/OD Monolayers at 1 Hz at the Air-Water Interface at 25 °C

Mole Ratio	A_a/A_0 (%)	σ_0 (mN/m)	σ_a (mN/m)	δ (deg)	κ_s (mNs/m)	E_0
1:1	2.5	67.0	3.5	4.1	1.6	2.1 (0.5; 2.1)
3:1	1.8	66.5	3.1	[a]	[a]	2.7 (0.5; 2.1)

The dimensionless reference elasticities given in parentheses were obtained from the Langmuir trough isotherms of the single components at the reference surface tensions. In the parentheses, the numbers on the left are for DPPC and the numbers on the right are for OD. [a]The phase angle and surface dilatational viscosity of the 3:1 mixed DPPC/OD system are zero within experimental errors.

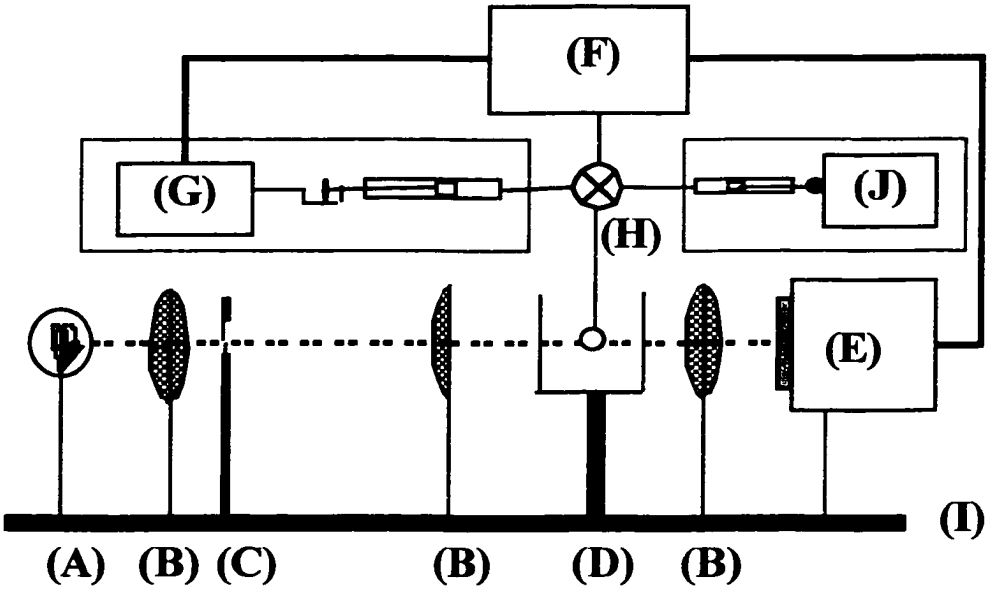

Fig. 5.1 Pendant drop apparatus for measuring the surface dilatational viscosity from oscillatory experiments: (A) light source, (B) lens, (C) pin hole, (D) quartz cuvette and surfactant laden water drop, (E) fast motion analyzer, (F) computer, (G) linear syringe pump, (H) valve, (I) isolation vibration table, and (J) oscillatory piezoelectric syringe pump.

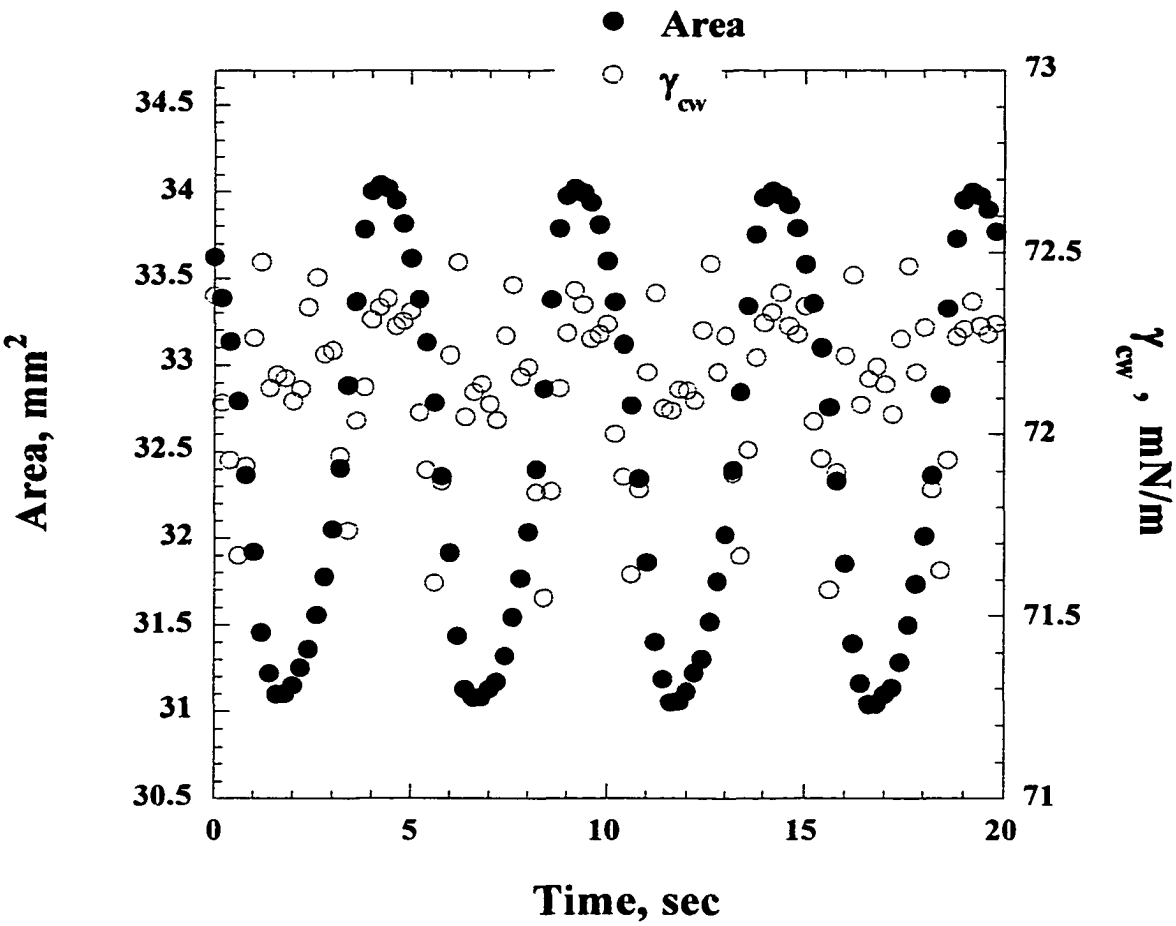

Fig. 5.2 Area and surface tension versus time of an oscillating clean water pendant drop at 0.2 Hz and 4.6 % change in area.

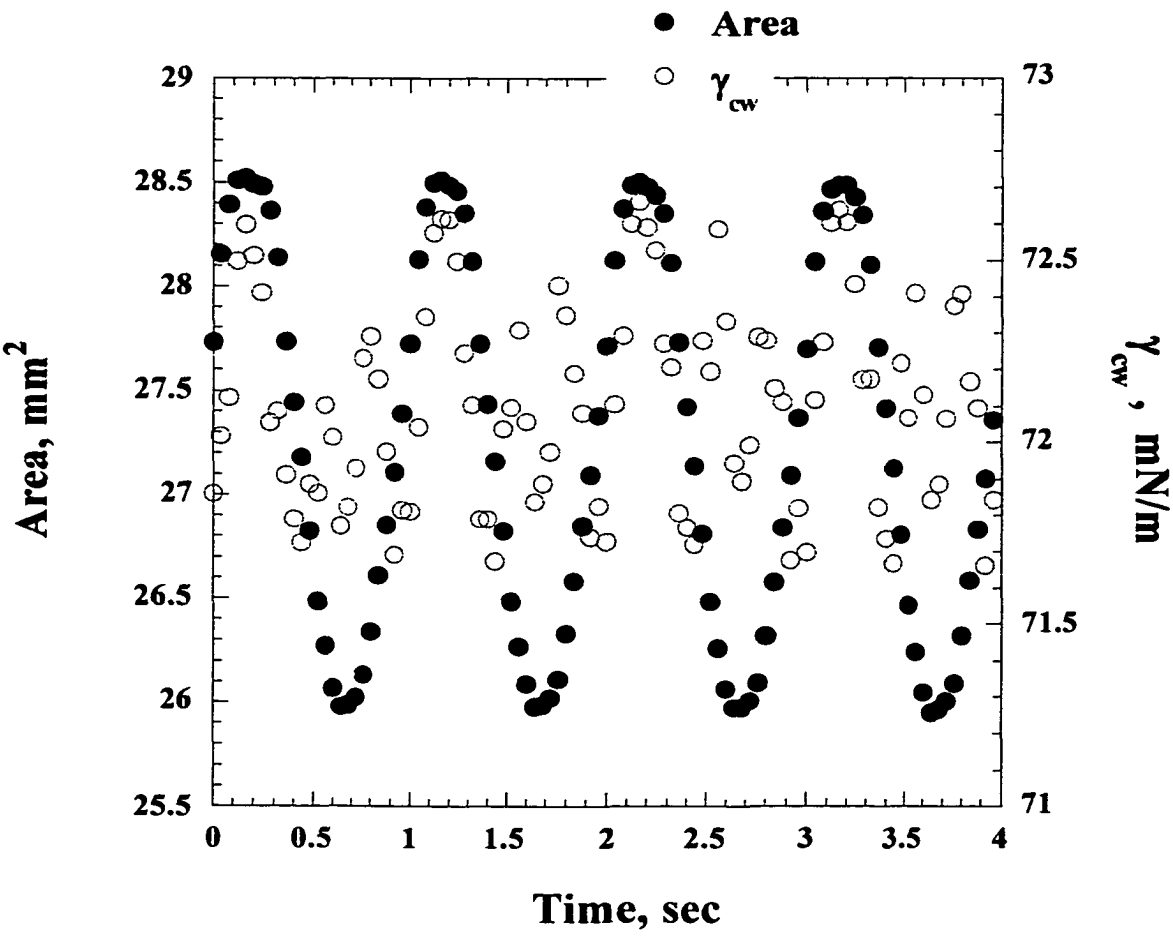

Fig. 5.3 Area and surface tension versus time of an oscillating clean water pendant drop at 1 Hz and 4.7 % change in area.

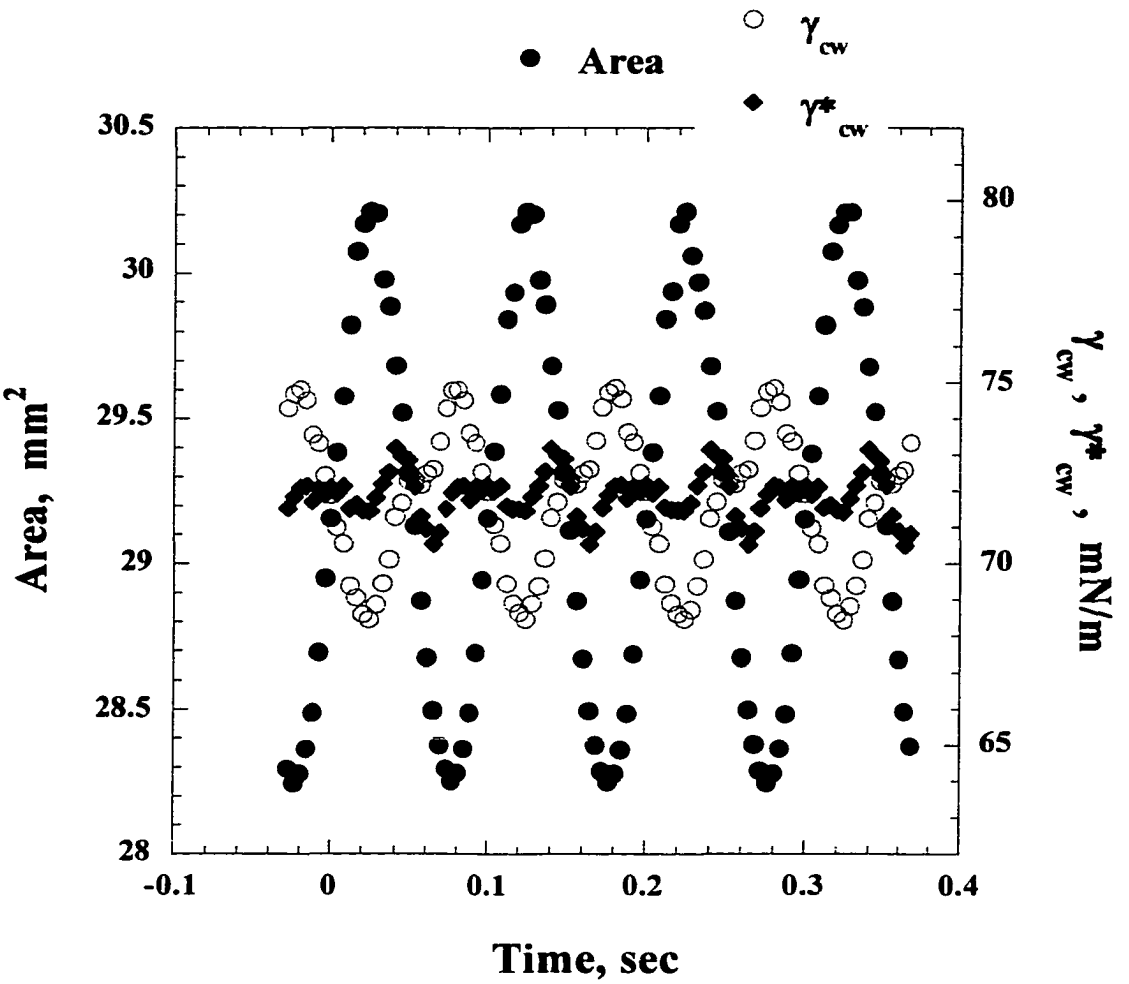

Fig. 5.4 A An oscillating clean water pendant drop at 10 Hz and 3.4 % change in area: area, Young-Laplace and corrected surface tensions versus time.

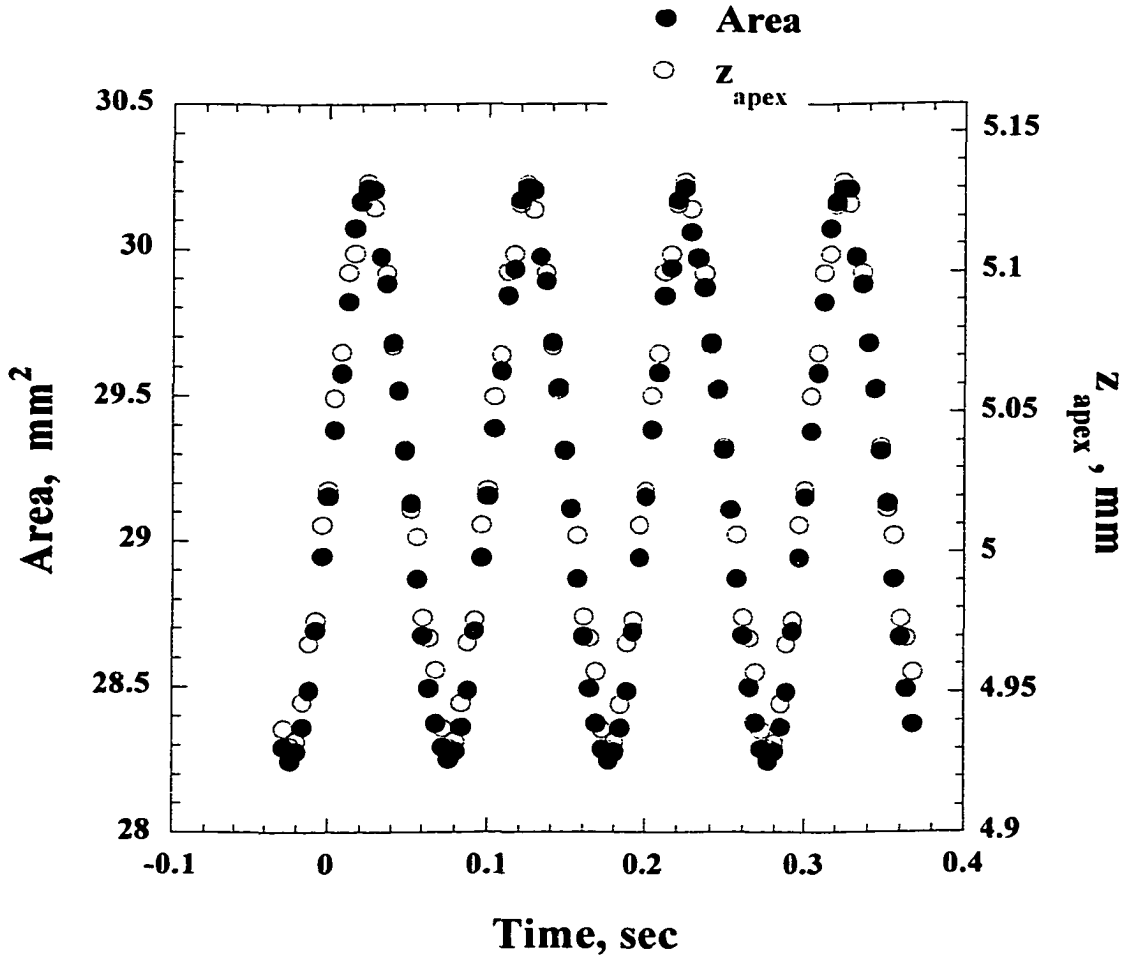

Fig. 5.4 B An oscillating clean water pendant drop at 10 Hz and 3.4 % change in area: area and vertical location of the apex versus time.

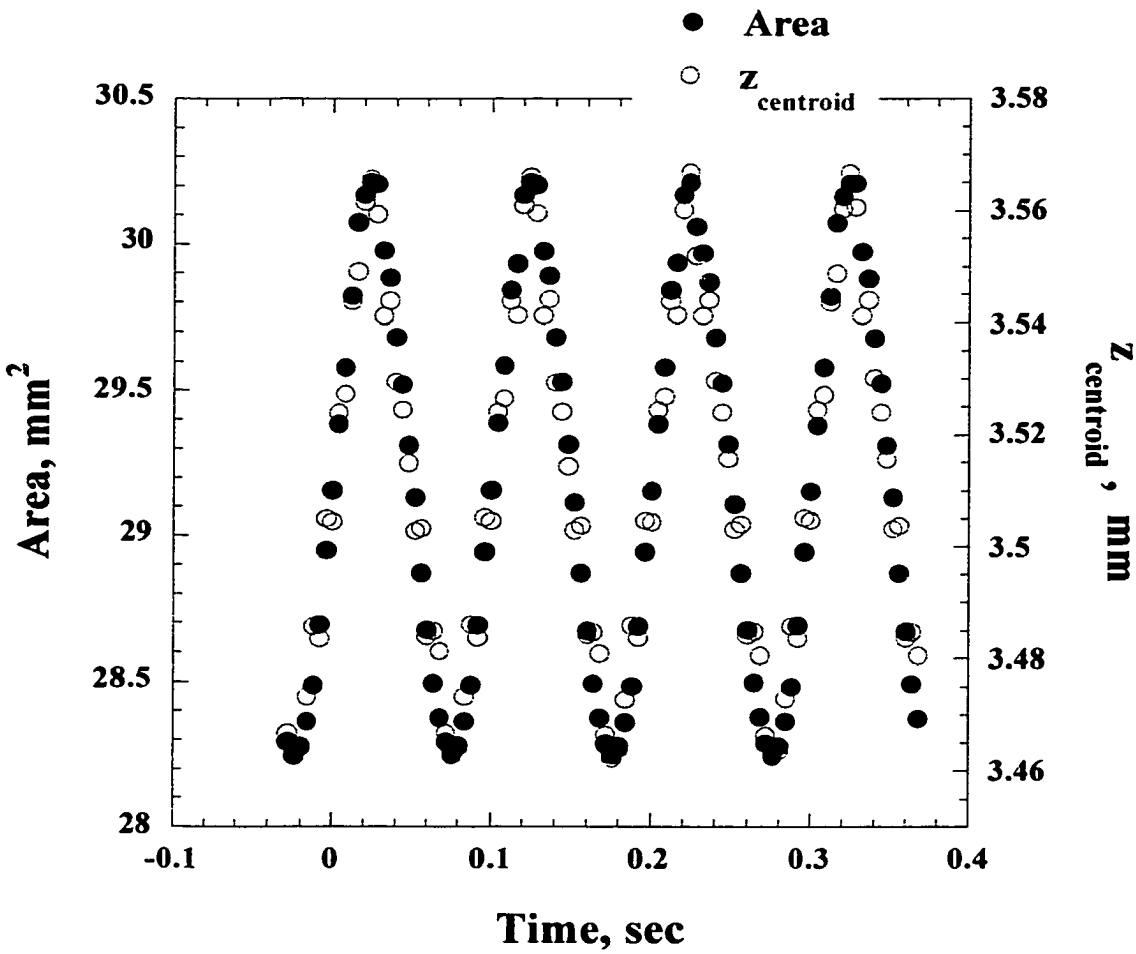

Fig. 5.4 C An oscillating clean water pendant drop at 10 Hz and 3.4 % change in area: area and vertical location of the centroid versus time

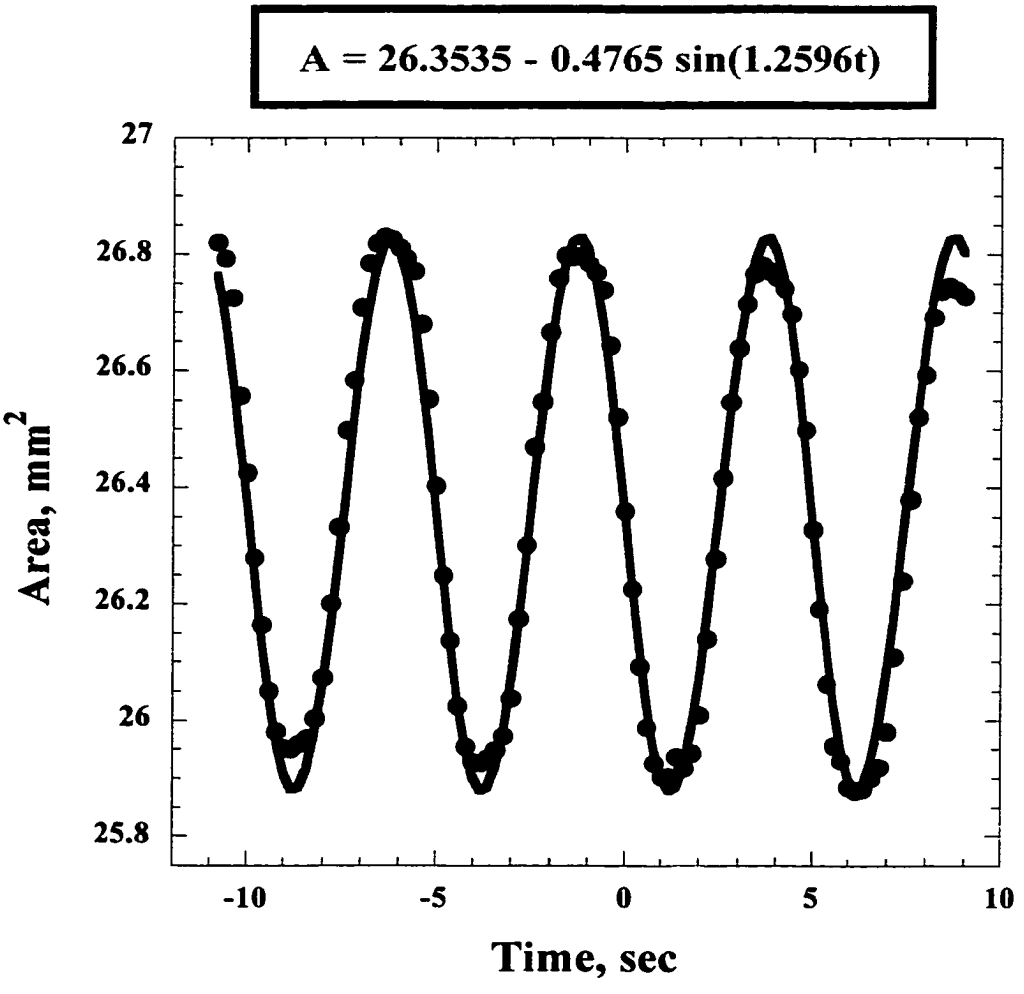

Fig. 5.5 A Oscillation of the liquid expanded phase of DPPC at 0.2 Hz and 1.8 % change in area: experimental and fitted areas versus time.

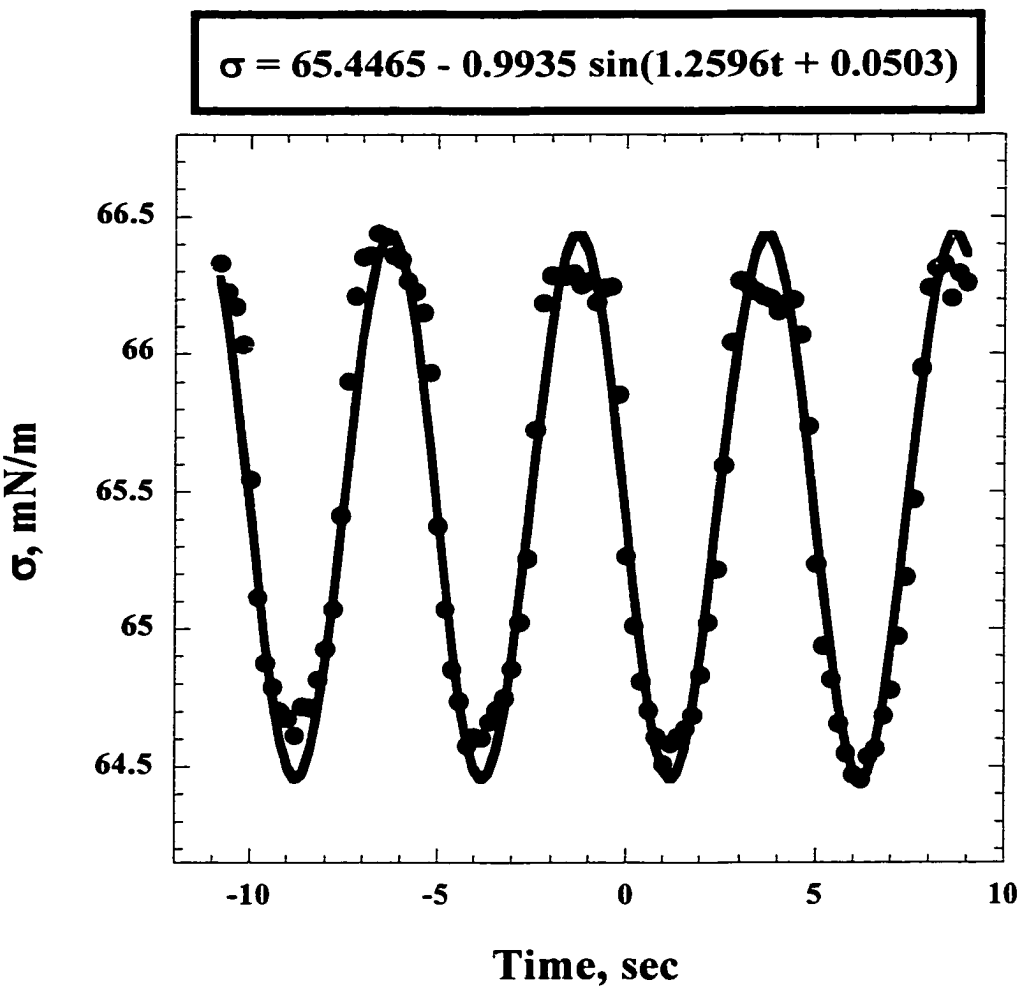

Fig. 5.5 B Oscillation of the liquid expanded phase of DPPC at 0.2 Hz and 1.8 % change in area: experimental and fitted compositional-dilatational surface tensions versus time.

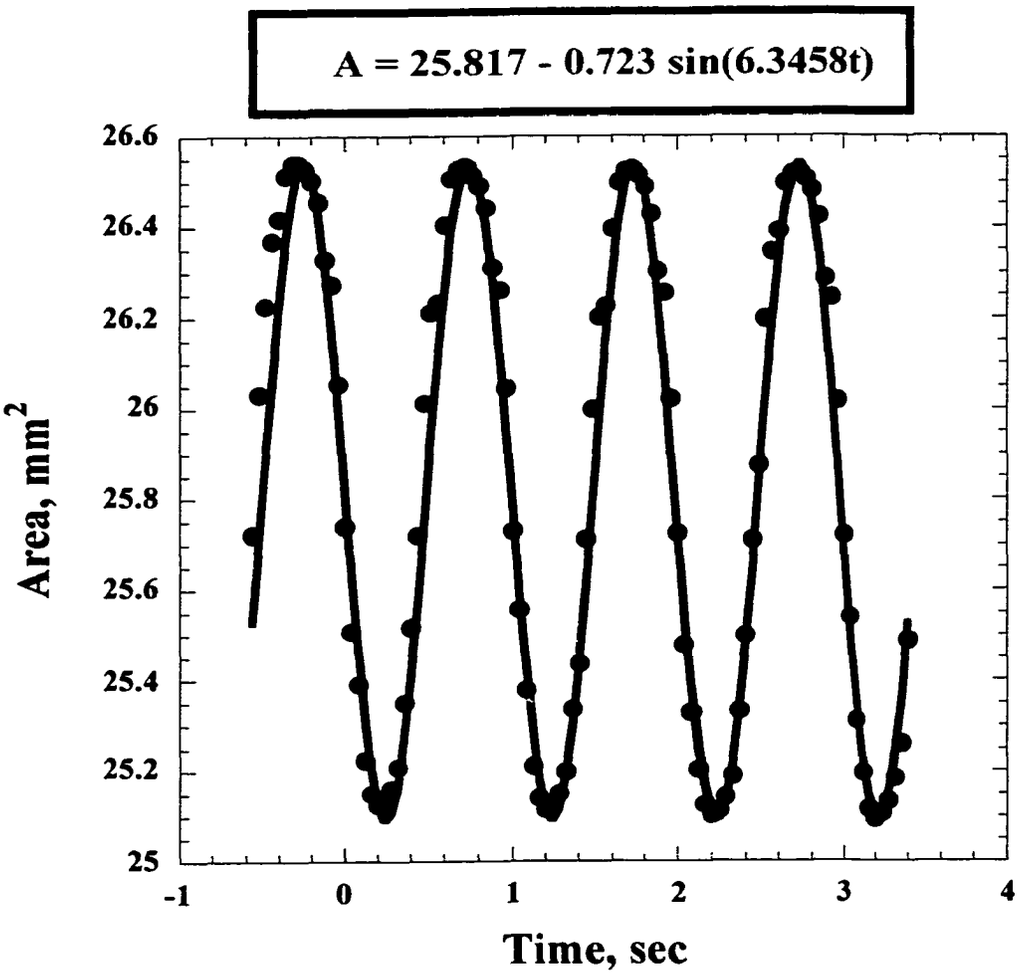

Fig. 5.6 A Oscillation in the liquid expanded phase of DPPC at 1 Hz and 2.8 % change in area: experimental and fitted areas versus time.

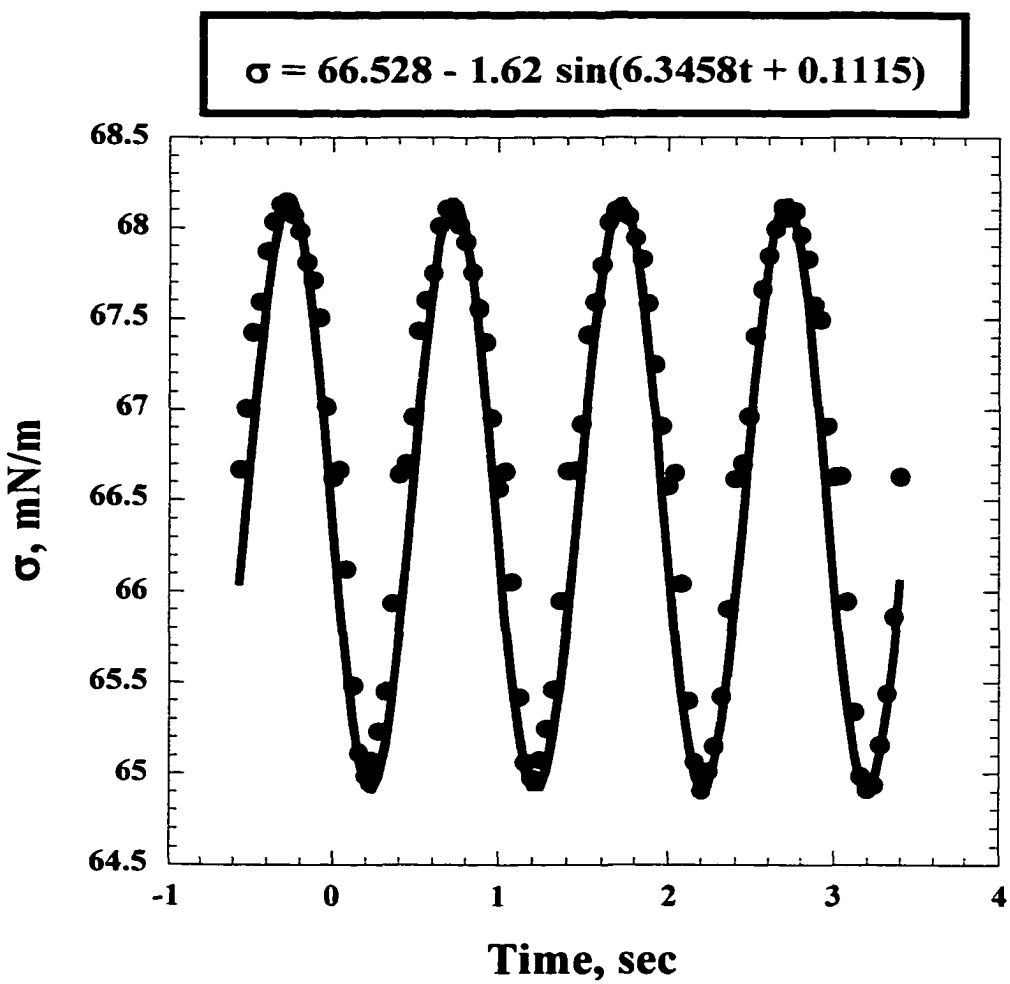

Fig. 5.6 B Oscillation in the liquid expanded phase of DPPC at 1 Hz and 2.8 % change in area: experimental and fitted compositional-dilatational surface tensions versus time.

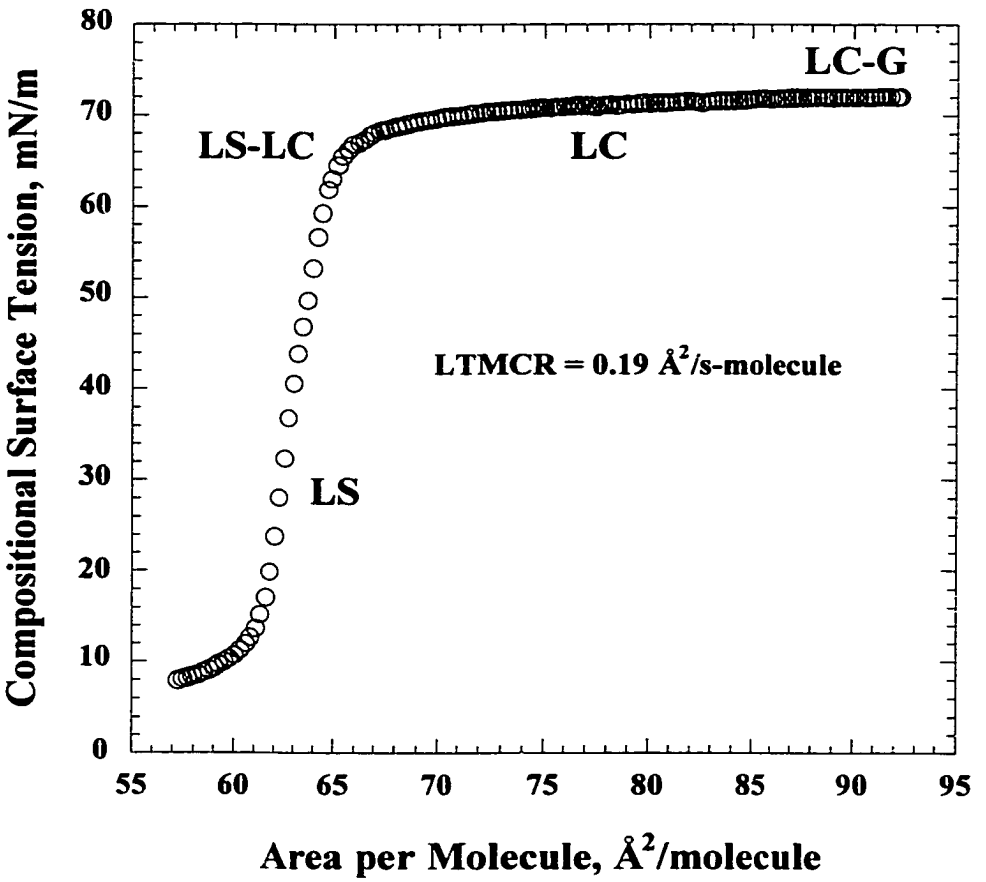

Fig. 5.7 Isotherm of tripalmitin measured at 25 ^{0}C and pH 5.5 obtained using a Langmuir trough surface balance: compositional surface tension versus area per molecule.

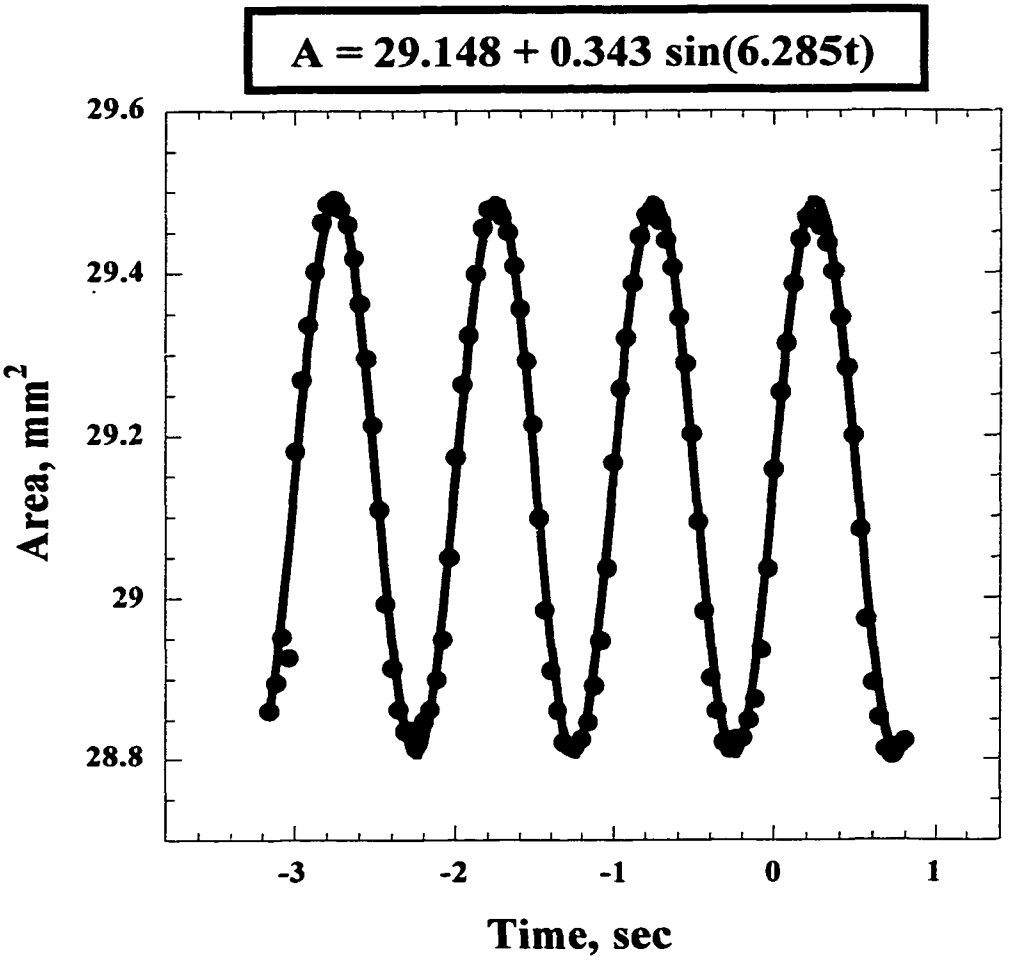

Fig. 5.8 A Oscillation of tripalmitin at 1 Hz and 1.2 % change in area: experimental and fitted areas versus time.

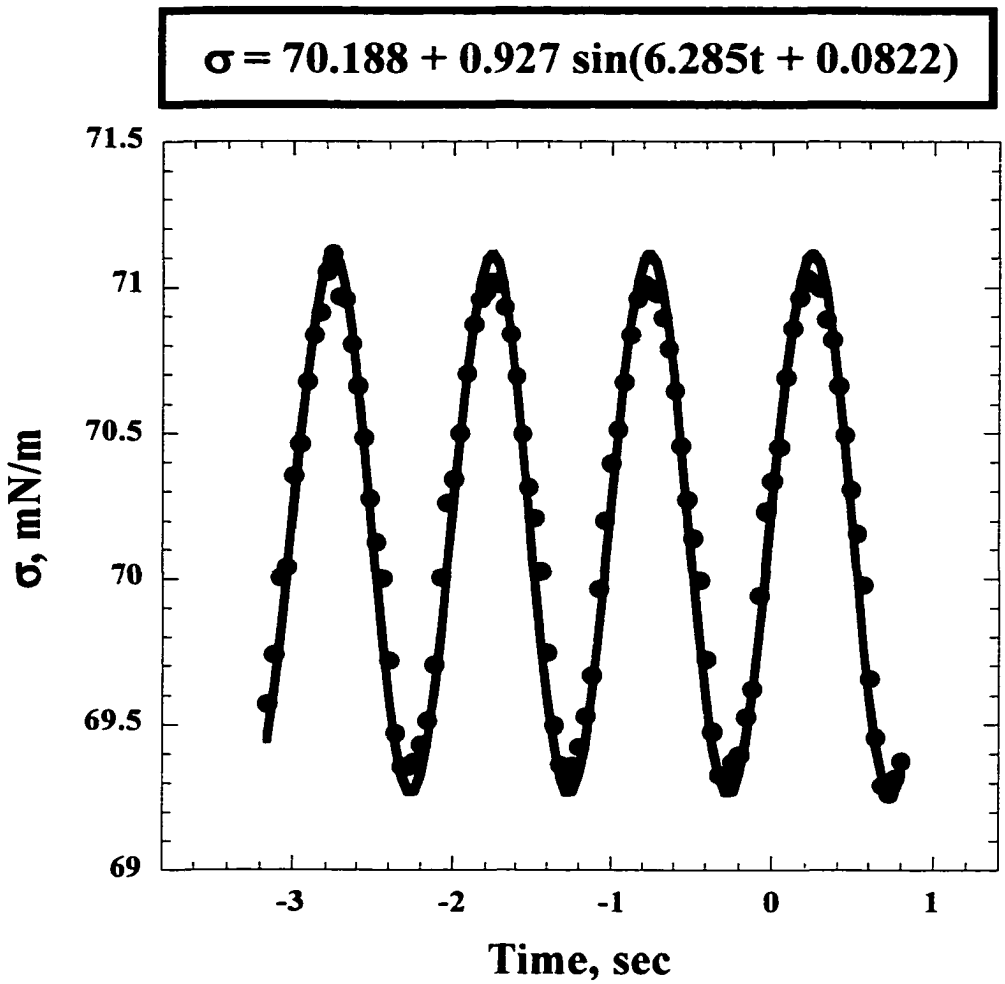

Fig. 5.8 B Oscillation of tripalmitin at 1 Hz and 1.2 % change in area: experimental and fitted compositional-dilatational surface tensions versus time.

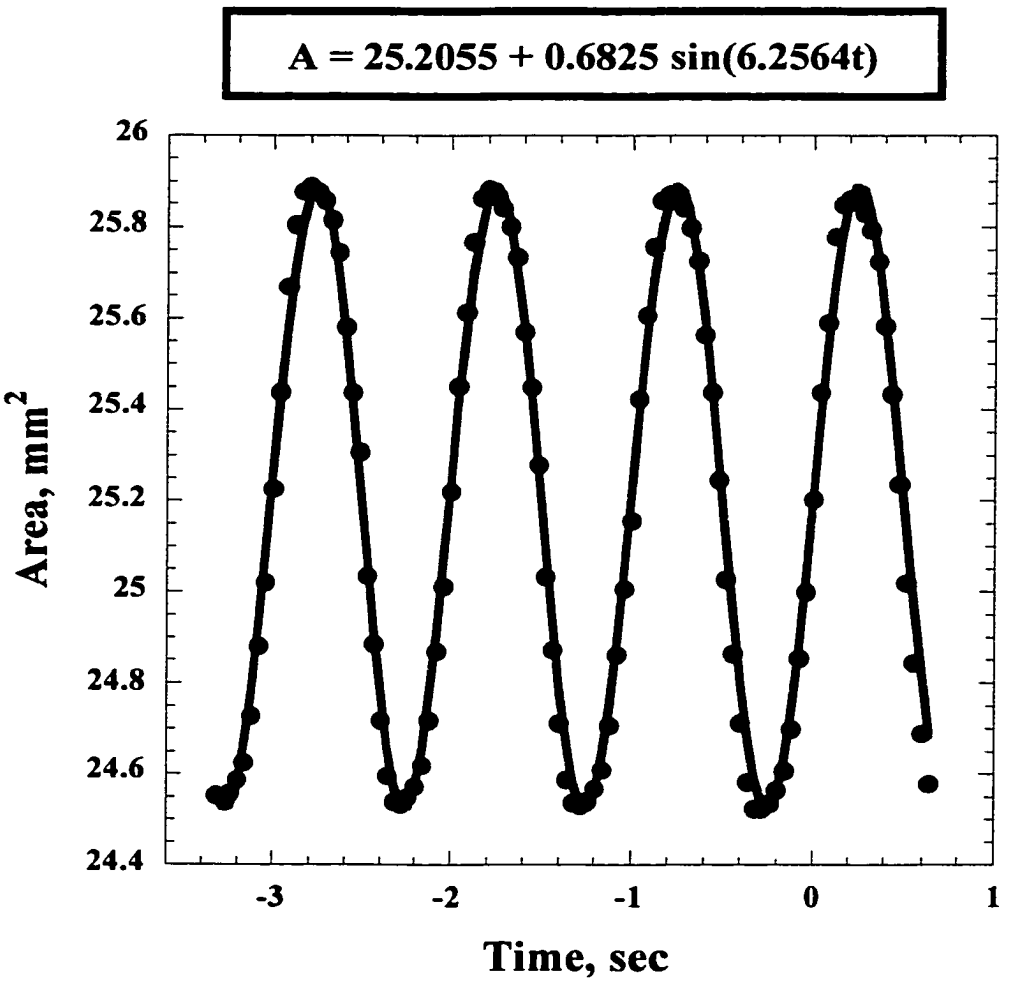

Fig. 5.9 A Oscillation of a mixed DPPC/OD monolayer in mole ratio 1:1 at 1 Hz and 2.7 % change in area: experimental and fitted areas versus time.

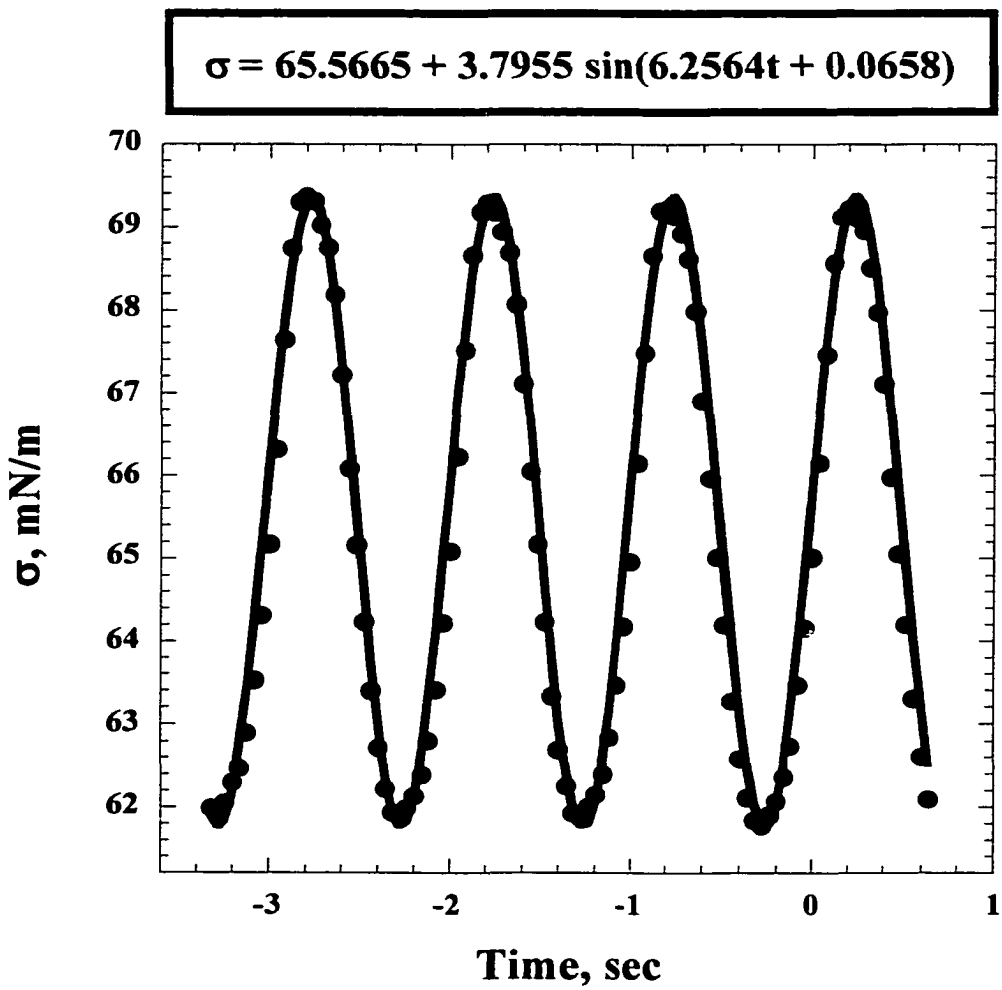

Fig. 5.9 B Oscillation of a mixed DPPC/OD monolayer in mole ratio 1:1 at 1 Hz and 2.7 % change in area: experimental and fitted compositional-dilatational surface tensions versus time.

Chapter 6

Conclusions and Recommendations for Future Research

6.1 Conclusions

In this study, we developed a surfactant hydrodynamic theory for measuring the surface dilatational viscosity from the experimental shape of an axisymmetrically deforming pendant water drop with an insoluble surfactant monolayer at the air-water interface for arbitrary types of area strain rates. We then tested our new equation experimentally and established a new technique for measuring the surface dilatational viscosity based on a constant rate of area change instead of an oscillatory rate of area change thereby obtaining the same results more economically. To conduct our surface dilatational viscosity measurements, we built a state of the art pendant drop apparatus. The results of our compression experiments show that the surface dilatational viscosity of the expanded phase of DPPC is approximately 1.3 mNs/m. This value agrees with the upper limit reported by Snik and collaborators.

We also extended the frequency range of the oscillatory axisymmetric drop shape analysis technique from 0.2-2 Hz to 0.2-20 Hz. This increment was possible due to a first order correction of the static Young-Laplace equation that we formulated and tested experimentally. To force the pendant drop to oscillate smoothly at high frequencies, we designed a piezoelectric syringe pump and added it to the pendant drop apparatus.

We designed the oscillatory experiments to allow us to directly measure the phase angles of simple surfactant monolayers for the first time owing only to surface dilatational

viscous effects. From our oscillatory experiments, we measured that the surface dilatational viscosity of DPPC is approximately 2.3 mNs/m at 0.2 Hz and 0.8 mNs/m at 1 Hz, and that the surface dilatational viscosity of TP is 1.0 mNs/m at 1 Hz as reported in Table 5.2. The values that we obtained for DPPC from compression and oscillatory experiments agree and reasonably comply with the upper limit reported by Snik and collaborators listed in Table 2.1. We could not make a comparison for TP or for the mixed DPPC/OD monolayers because their dilatational viscosities are not reported in the literature. We found good agreement between the Langmuir trough and pendant drop elasticities. Our results on the mixed monolayers indicate that the surface viscoelasticities of DPPC twice by the addition of octadecanol as shown in Table 5.3. Therefore, we learned how to control the surface dilatational viscosity by using a co-surfactant.

Finally, we expect that the pendant drop technique presented here will soon be used in the pharmaceutical industry to quantify and design the viscoelastic response of suspensions used to clinically treat the lungs. Several studies of protein and polymer films have been reported showing quite viscoelastic behavior resembling three-dimensional soft materials, and various rheological coefficients have been extracted from relaxation experiments of the films.

6.2 Recommendations for Future Research

The Langmuir trough and pendant drop isotherm of DPPC do not completely agree simply because the LE-LC first order phase transition plateau of the Langmuir trough isotherm is almost absent in the pendant drop isotherm, as shown in Fig. 4.10. It

was recently suggested [68] that the pendant drop curvature varies the domain shape and size during domain formation and growth and consequently does not allow the formation of the LE-LC phase transition of DPPC, if the transforming units have a small size they increase the slope of the isotherm. The verification of this prevailing hypothesis is important because there are many surfactant systems existing at curved interfaces rather than at flat interfaces. Dodecanol is partially soluble in water and undergoes the LE-LC phase transition and its pendant drop and Langmuir trough isotherms are identical [15]. Also, we must add that PDA undergoes the LE-LC phase transition and what is happening with DPPC is also happening with PDA. At flat interfaces of Langmuir troughs many studies of spread surfactant monolayers have identified various phases relating the compositional surface tension, surfactant surface concentration, and temperature. Phases of Langmuir surfactant monolayers at the air-water interface are generally studied using the Langmuir trough surface balance, x-ray diffraction, fluorescence microscopy, and Brewster angle microscopy. The microscopy techniques allow observing the phases and thus are very useful in understanding the monolayer phase behavior. For example, in fluorescence microscopy, an insoluble dye consisting of a non-polar chain and a fluorescing polar head is introduced on the surface. Phases are visualized by exciting the insoluble dye dissolved in the monolayer at a very low concentration. The polar head of the dye fluoresces in the LE phase and therefore illuminates this state and is quenched in the G phase since the fluorescing polar head is in contact with water, and is expelled from the LC phase which makes them appear dark. In summary, only the LE

phase appears bright and the G and LC are dark. Using the microscopy techniques the G-LE, G-LC and LE-LC have been shown to be first order since the coexisting states can be easily visualized and thus confirming the plateaus in surface tension measured simultaneously during the phase transitions.

Observing directly the phase behavior of a Langmuir monolayer at the air-water interface of a pendant drop is a convenient test of the hypothesis put forward. What we recommend for future work is to add a video recording florescence microscope to the pendant drop apparatus without interfering with the video recording of the drop shape needed for the surface tension measurement. The florescence microscope can be positioned 90 degree apart from the illumination system of the pendant drop apparatus. What must be proved experimentally is that the domain density and domain size of DPPC change just because of the curvature of the hosting interface. Recently, at the Chemical Engineering Department of the Johns Hopkins University Professor K. Stebe and her Ph.D. student Van Nguyen started investigating the phase behavior of a Langmuir isotherm of PDA at a curved interface of a sessile drop. So far, they observed using fluorescence microscopy how the bright LE domains disappear as the dark LC domains grow by video recording a sessile water drop evaporating with a spread monolayer of PDA.

Bibliography

1)Scriven, L. *Chem. Eng. Sci.* **1960**, *12*, 98.

2)Jiang, T.; Chen, J.; Slattery, J. *J. Colloid Interface Sci.* **1983**, *96*, 7-19.

3)Miller, R.; Wustneck, R.; Kragel, J.; and Kretzschmar, G. *Colloids Surf.* **1996**, *111*, 75.

4)Joly, M. *Rec. Progr. Surf. Sci.* **1964**, *1*, 1.

5)Edwards, D.; Brenner, H.; Wasan, D. *Interfacial Transport Processes and Rheology*; Butterworth-Heinemann: Boston, 1991.

6)Kragel, J.; Siegel, S.; Miller, R.; Born, M.; Schano, K. *Colloids Surfaces A: Physicochem. Eng. Asp* **1994**, *91*, 169-180.

7)Joly, M. *Surface and Colloid Science* **1972**, *5*, 1-77.

8)Joly, M. *Surface and Colloid Science* **1972**, *5*, 79-193.

9)Poskanzer, A.; Goodrich, F. *J. Colloid Interface Sci.* **1975**, *52*, 213.

10)Copeland, L.; Harkins, W.; Boyd, G. *J. Chem. Phys.* **1942**, *10*, 357.

11)Wasan, D.; Sampath, K.; Aderangi, N. *AIChE Symposium Series* **1980**, *76*, 93-96.

12)Poskanzer, A.; Goodrich, F. *Journal of Physical Chemistry* **1975**, *79*, 2122-2126.

13)Gupta, L.; Wasan, D. *Ind. Eng. Chem., Fundam.* **1974**, *13*, 26-32.

14)Pollar, M.; Pan, R.; Steiner, C.; Maldarelli, C. *Langmuir* **1998**, *14*, 7222-7234.

15)Subramanyan, R. ; City University of New York: New York City, 1999, pp 205.

16)Ting, L.; Wasan, T.; Miyano, K.; Xu, S. *J. Colloid Interface Sci.* **1984**, *102*, 248.

17)Kragel, J.; Kretzschmar, G.; Li, J.; Miller, R.; Mohwald, H. *Thin Solid Films* **1996**, *284*, 361.

18)Myrvold, R.; Hansen, F. *J. Colloid Interface Sci.* **1998**, *207*, 97.

19)Zhang, X.; Harris, M.; Basaran, O. *J. Colloid Interface Sci.* **1994**, *168*, 47-60.

20)Notter, R. *Lung Surfactants Basic Science and Clinical Applications*; Marcel Dekker, Inc.: New York, 2000; Vol. 149.

21)Vassilev, P.; Taneva, S.; Panaiotov, I.; Georgiev, G. *J. Colloid Interface Sci.* **1981**, *84*, 169.

22)Graham, D.; Phillips, M. *J. Colloid Interface Sci.* **1980**, *148*, 227.

23)Lucassen-Reynders, E.; Lucassen, J. *Colloids and Surfaces A: Physicochemical and Engineering Aspects* **1994**, *85*, 211-219.

24)Lucassen, J.; Van Den Tempel, M. *Chem. Eng. Sci.* **1972**, *27*, 1283.

25)Maru, H.; Wasan, D. *Chem. Eng. Sci.* **1979**, *34*, 1295.

26)Miyano, K.; Abraham, B.; Ting, L.; Wasan, T. *J. Colloid Interface Sci.* **1983**, *92*.

27)Lemaire, C.; Langevin, D. *Colloids Surf.* **1992**, *65*, 101.

28)Lucassen, J.; Giles, D. *J. Chem. Soc., Faraday Trans. I* **1975**, *71*, 217.

29)Kao, R.; Edwards, D.; Wasan, T.; Chen, E. *J. Colloid Interface Sci.* **1992**, *148*, 247.

30)Lucassen-Reynders, E.; Lucassen, J. *Advan. Colloid Interface Sci.* **1969**, *2*, 347.

31)Sohl, C.; Miyano, K.; Ketterson, J. *Rev. Sci. Instrum.* **1978**, *49*, 1464.

32)Jiang, Q.; Chiew, Y.; Valentini, J. *J. Colloid Interface Sci.* **1993**, *155*, 8.

33)Stenvot, C.; Langevin, D. *Langmuir* **1988**, *4*, 1179.

34)Manning-Benson, S.; Parker, S.; Bain, C.; Penfold, J. *Langmuir* **1998**, *14*, 990-996.

35)Tian, Y.; Holt, R.; Apfel, R. *J. Colloid Interface Sci.* **1997**, *187*, 1.

36)Chen, X.; Shi, T.; Tian, Y.; Jankovsky, J.; Holt, R.; Apfel, R. *J. Fluid Mech.* **1998**, *367*, 205.

37)Hard, S.; Neuman, R. *J. Colloid Interface Sci.* **1987**, *120*, 15.

38)Snik, A.; Kouijzer, W.; Kelltjens, J.; Houkes, Z. *J. Colloid Interface Sci.* **1983**, *93*, 301.

39)Hall, S.; Bermel, M.; Ko, Y.; Palmer, H.; Enhorning, G.; Notter, R. *J. Appl. Physiol.* **1993**, *75*, 468.

40)Snik, A.; Boonman, A.; Gieles, P.; Egberts, J. *Prog. Resp. Res.* **1984**, *18*, 24.

41)Hirsa, A.; Korenowski, G.; Logory, L.; Judd, C. *Langmuir* **1997**, *13*, 3813-3822.

42)Zhang, X. *J. Colloid Interface Sci.* **1999**, *212*, 107.

43)Pan, R.; Green, J.; Maldarelli, C. *J. Colloid Interface Sci.* **1998**, *205*, 213-230.

44)Wong, H.; Rumschitzki, D.; Maldarelli, C. *J. Fluid Mech.* **1999**, *379*, 279.

45)Richards, J.; Beris, A.; Lenhoff, A. *Phys. Fluids* **1993**, *A 5*, 1703.

46)Richards, J.; Lenhoff, A.; Beris, A. *Phys. Fluids* **1994**, *6*, 2640.

47)Richards, J.; Beris, A.; Lenhoff, A. *Phys. Fluids* **1995**, *7*, 2617.

48)Hirt, C.; Nichols, B. *J. Comput. Phys.* **1981**, *39*, 201.

49)Thompson, J.; Soni, B.; Weatherill, N. *Handbook of Grid Generation*; CRC Press:, 2000.

50)Aris, R. *Vectors, Tensors, and the Basic Equations of Fluid Dynamic*; Prentice Hall: New Jersey, 1962.

51)Benjamins, J.; Cagna, A.; Lucassen-Reynders, E. *Colloids and Surfaces* **1996**, *114*, 245-254.

52)Rotenberg, Y.; Boruvka, L.; Neumann, A. *J. Colloid Interface Sci.* **1983**, *93*, 169.

53)Faour, G.; Grimaldi, M.; Richou, J.; Bois, A. *J. Colloid Interface Sci.* **1996**, *181*, 385.

54)Slattery, J.; Chen, J.; Thomas, C.; Fleming III, P. *J. Colloid Interface Sci.* **1980**, *73*, 483-499.

55)Kwok, D.; Chiefalo, P.; Khorshiddoust, B.; Lahooti, S.; Cabrerizo-Vilchez, M.; del Rio, O.; Neumann, A. *Determination of Ultralow Interfacial Tension by Axisymmetric Drop Shape Analysis*; American Chemical Society, 1995.

56)Kwok, D.; Vollhardt, D.; Miller, R.; Li, D.; Neumann, A. *Colloids Surf.* **1994**, *88*, 51.

57)Li, J.; Miller, R.; Wustneck, R.; Mohwald, H.; Neumann, A. *J. Colloid Interface Sci.* **1995**, *96*, 295.

58)Lin, S.; McKeigue, K.; Maldarelli, C. *AIChE J.* **1990**, *36*, 1785.

59)Jyoti; Prokop, R.; Li, J.; Vollhardt, D.; Kwok, D.; Miller, R.; Mohwald, H.; Neumann, A. *Colloids Surf.* **1996**, *116*, 173.

60)Kwok, D.; Tadros, B.; Deol, H.; Vollhardt, D.; Miller, R.; Cabrerizo-Vilchez, M.; Neumann, A. *Langmuir* **1996**, *12*, 1851.

61)Susnar, S.; Chen, P.; del Rio, O.; Neumann, A. *Colloids Surf.* **1996**, *116*, 181.

62)McCracken, D.; Salmon, W. *Computing for Engineers and Scientists with FORTRAN 77*; Second ed.; John Wiley & Sons, Inc.: New York City, 1988.

63)Gerald, C.; Wheatley, P. *Applied Numerical Analysis*; Third ed.; Addison-Wesley Publishing Company: San Luis Obispo, 1985.

64)Press, W.; Flannery, B.; Teukolsky, S.; Vetterling, W. *Numerical Recipes the Art of Scientific Computing (FORTRAN Version)*; Cambridge University Press: Cambridge, 1990.

65)McConlogue, C.; Malamud, D.; Vanderlick, T. *Biochimica et Biophysica Acta* **1998**, *1372*, 124.

66)Ivanova, T.; Georgiev, G.; Ivanova, M.; Launois-Surpas, M.; Proust, J.; Puisieux, F. *Progr. Colloid Polym. Sci.* **1989**, *79*, 24.

67)Launois-Surpas, M.; Ivanova, T.; Panaiotov, I.; Proust, J.; Puisieux, F.; Georgiev, G. *Colloid Polym. Sci.* **1992**, *270*, 901.

68)Li, J.; Miller, R.; Mohwald, H. *Colloids Surfaces* **1996**, *114*, 123-130.

69)Djabbarah, N.; Wasan, D. *Chem. Engng. Sci.* **1982**, *37*, 175.